博士学位論文

The study on GTPase delivery mechanism of ribosomal P stalk during translation process

(翻訳過程におけるリボソーム P ストークの GTPase 運搬機構の解明)

北海道大学　大学院生命科学院

生命科学専攻　生命融合科学コース

2018.6

丹澤　豪人

INDEX

ABSTRACT

During translation process, the 3rd functional center of the large ribosomal subunit termed “GTPase-associated center” plays an essential part in the association and/or dissociation of GTPases for supplying the GTP hydrolysis energy continuously. The center contains a ribosomal protein complex known as the “ribosomal P stalk”, which is highly flexible and functionally conserved in three domains of life. This P stalk recruits several translational GTPases to the sarcin-ricin loop (SRL), a GTPase binding site on the large ribosomal subunit. Although several structures of ribosomes and the complex with translation factors, tRNAs, and mRNAs have been determined by X-ray crystallography and cryoelectron microscopy (cryo-EM) during past more than a decade, the P stalk could not be visible in detail because its flexibility. Therefore, the details of the recruitment mechanism are still unclear.

In archaea and eukaryotes, ribosomal P stalk consists of an anchor protein P0 and either P1 homodimer (archaea) or P1•P2 heterodimer (eukaryotes). The P stalk selectively recognizes specific GTPases such as initiation factor (IF5B), elongation factors (EF-2/EF-G and EF-1α/EF-Tu), and release factor (RF3), but no conserved binding regions exist in these GTPases. In this study, we investigated the interaction between P stalk and elongation factor 2 by structural analysis of *Pyrococcus horikoshii* EF-2 (*Pho*EF-2) in the Apo-form (*Pho*EF-2-Apo), GDP-form (*Pho*EF-2-D2-GDP), GMPPCP-form (*Pho*EF-2-GMPPCP) and GMPPCP-form in complex with the C-terminal 11 residues of P1 (P1C11) (*Pho*EF-2-GMPPCP-P1C11). The structure shows that helical structured P1C11 binds to a hydrophobic groove formed by domain G and subdomain G' of *Pho*EF-2. The P1-binding groove of *Pho*EF-2 is completely different from aEF-1α in

terms of both position and sequence, but hydrophobic shape of groove is uniform. Combining the *Pho*EF-2 mutants P1-binding assays, it was clear that three residues, M167 and F205 in domain G, and F226 in subdomain G' of *Pho*EF-2 are keys for the interaction with C-terminus of P1, especially, F226 pi-stacking interacted with F107 of P1. While three residues, L103, L106, and F107 of P1C11 involved in the interaction of *Pho*EF-2, G102 of P1C11 was first shown to contribute to the interaction.

Moreover, both binding assay of gel-mobility shift and SPR signal showed that the P1-binding affinity of *Pho*EF-2-GDP was comparable with that of *Pho*EF-2-GMPPCP, and they were slightly stronger than that of *Pho*EF-2-Apo. In order to clarify how *Pho*EF-2-GDP interacts with P1, we performed a molecular dynamics simulation to build a model of P1C11-bound GDP-form (*Pho*EF-2-GDP-P1C11). By structural comparison of current *Pho*EF-2 structures, we found the conformational changes of the P1C11-binding groove in each form. Taken all results together, we proposed that in response to the translation process, the groove has three states: closed, open, and release for recruiting and releasing GTPases. We also determined crystal structure of GDP-bound form of *Pho*EF-1α bound with P1C11 (*Pho*EF-1α-GDP-P1C11).

As P stalk binding translational GTPase, aIF5B shares domain G with aEF-2 and aEF-1α, but does not have subdomain G'. By superposing domain G, we found a hydrophobic groove in the opposite side of the GTP binding site of aIF5B domain G, which may relate to interact with aP1CTD. Additionally, eukaryotic P stalk also recruits of eukaryote-specific RIPs (ribosome inactivating protein) to ribosome, similar to translate GTPase. Considering the characteristics of partner-binding and their functions, it was indicated that P stalk possesses completely different recognition manner for translational GTPases

and RIPs, which is that, P stalk possesses a partner-function-dependent recognition mechanism.

INTRODUCTION

1. Protein synthesis on ribosome

Functions of proteins are, universally, essential to life-support activities and their proteins are synthesized on ribosomes existing in the cytoplasm of cells. The protein synthesis so-called "translation" is the final step of "central dogma" and the process of converting the information stored in the nucleotide sequence of messenger RNA (mRNA) into the sequence of amino acid in a polypeptide using GTP hydrolysis energy (Figure 1-1) (1, 2). A ribosome is conserved in all organisms and it is the molecular machine of a supermolecule complex (70S in bacteria and archaea, 80S in eukaryote), which is consisted of the large subunit (LSU: 50S in bacteria and archaea, 60S in eukaryote) (Figure 1-2A) and the small subunit (SSU: 30S in bacteria and archaea, 40S in eukaryote) (Figure 1-2B), including a large amount of ribosomal proteins and several ribosomal RNAs (rRNAs) (2-4). During the past more than a decade, three-dimensional structures of ribosome from archaea, bacteria and eukaryote were determined at high resolutions by

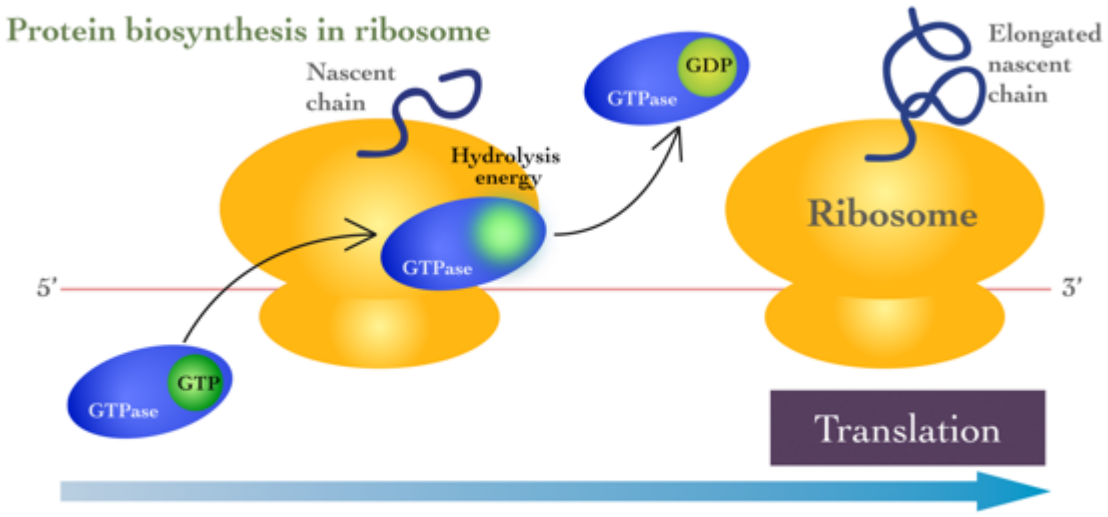

Figure 1-1. Protein biosynthesis on ribosome

X-ray crystallography and cryoelectron microscopy (cryo-EM) (Figure 1-2) (5-9). From these structures, the detailed mechanisms of the ribosomal functions have been revealed at the molecular level (1). The ribosome is mainly composed of rRNAs and ribosomal proteins almost contribute to the structural stabilities of rRNAs (3, 4). The ribosome direct related to translation should have, at least, two major parts: path of mRNA and transfer RNAs (tRNAs); and export tunnel of nascent polypeptide chains. The former exists on the interfaces between some rRNAs and some functional ribosomal proteins belonging to both of large and small subunits, and the latter penetrates the large subunit from its interface to the surface (Figure 1-3A). Additionally, it was also clarified that the former had three tRNA localization sites: aminoacylation-site (A-site), peptidyltransferase-site (P-site) and exit-site (E-site) (Figure 1-3A) (1, 5). Thus, the progress of the studies on translation science was remarkable and the great many things were clarified as described below.

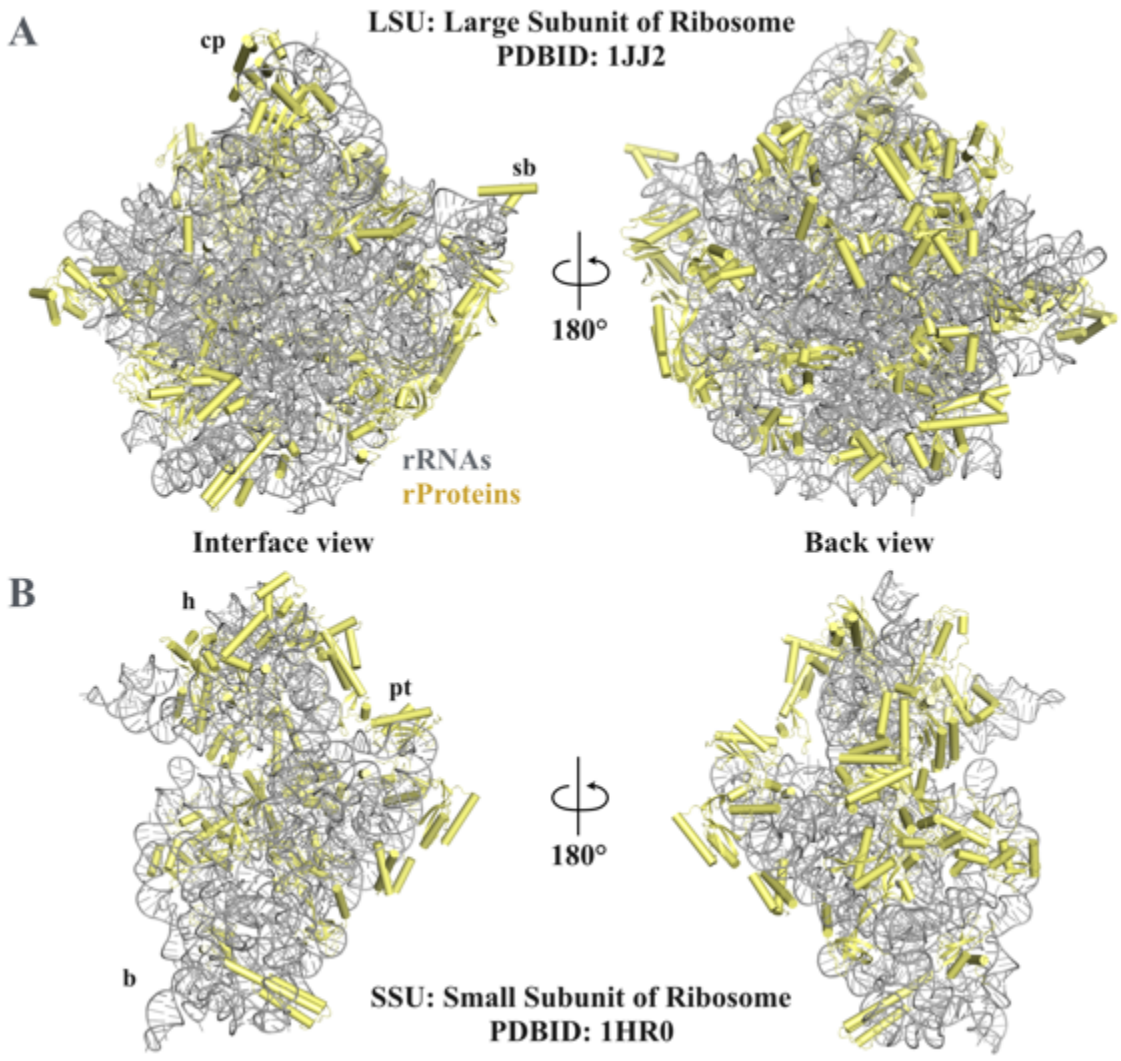

Figure 1-2. Crystal structures of large and small ribosomal subunits. The ribosomal RNAs and proteins are represented by ribbon models and colored gray and pale yellow, respectively. (**A**) The interface view (left) and the back view (right) of the structure of the large ribosomal subunit (LSU, PDBID: IJJ2) (5). (**B**) The interface (left) and back (right) view of the structure of the small ribosomal subunit (SSU, PDBID: 1HR0) (6).

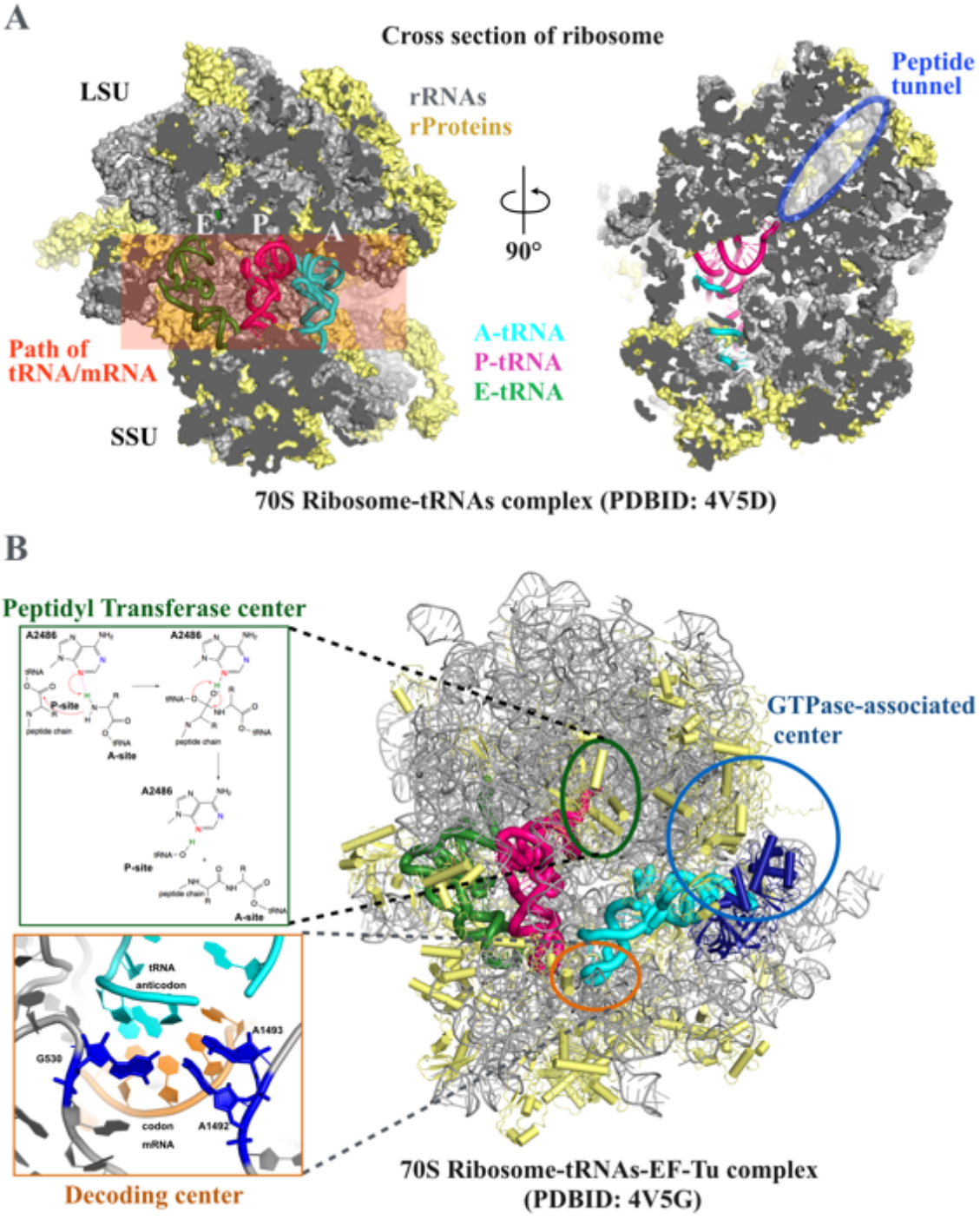

Figure 1-3. Ribosomal functions. The ribosomal RNAs and proteins are colored the same as using Figure 1-2. (**A**) The cross section of ribosome in complex with A-tRNA, P-tRNA, and E-tRNA (PDBID: 4V5D) (10). The color-coding of the cross

section is gray. A-tRNA, P-tRNA, and E-tRNA are represented by ribbon models and colored cyan, magenta, and green, respectively. The left structure shows the path of tRNAs and a mRNA (red mesh), and the right shows the peptide tunnel (blue circle and white mesh). (**B**) The ribosomal functional centers: the decoding center, the peptidyl transferase center, and GTPase-associated center on the structre of ribosome-EF-Tu-tRNA complex (PDBID: 4V5G) (11). They are shown in circles which are colored orange, green, and blue, respectively. The figure was referenced from the web site of the laboratory of Dr. Venki Ramakrishnan (http://www2.mrc-lmb.cam.ac.uk/groups/ribo/resources/videos/). The orange box (lower left) shows the closed view of the decoding center and the relationship among the codon of mRNA, the corresponding anticodon of tRNA, and rRNA (G530, A1492, and A1493) that recognizes minor groove formed by the codon-anticodon interaction. The nucleic acids: G530, A1492, and A1493 (18S rRNA of the small ribosomal subunit) which are essential for the decoding center, other rRNA, A/T-tRNA, and mRNA are colored blue, gray, cyan and orange, respectively. The green box (upper left) shows the reaction mechanism of the peptide bonding reaction at the peptidyl transferase center of the ribosome. A2486 is the ribozyme of 23S rRNA of the large ribosomal subunit.

2. Functional centers of ribosome through translation

Translation can almost be partitioned four stages into initiation, elongation, termination and ribosome recycling. From the atomic structures of ribosome, it does not replace functional regions or locations of the intra-molecule of ribosome during translation cycles, but several translation-related factors such as mRNA, tRNA and GTPases move and/or use some specific and integrated functional centers throughout translation. The ribosome has three key functional centers: 1) the decoding center, 2) the peptidyl transferase center and 3) the GTPase-associated center, for translation (4). The decoding center existing in the A-site of the small subunit recognizes both of the codon of the mRNA and its binding partner, the corresponding anticodon of tRNA. In bacteria, for example, three nucleotides: G530, A1492, and A1493 in 16S rRNA are known as key residues of the decoding center (Figure 1-3B, orange frame) (11). When an anticodon of aminoacylated tRNA (aa-tRNA) binds precisely to the codon of mRNA, related to the codon-anticodon interaction, of the A-site, the decoding center fixes the binding at the A-site (Figure 1-3B). Conversely, when any aa-tRNAs no-corresponding to a codon recruits to the ribosome, the dissociation of the aa-tRNAs from the ribosome are accelerated. This accurate recognition of a tRNA to the mRNA provides the opportunity to navigate to the next step, peptide-bonding reaction for elongating a nascent polypeptide chain. Its reaction occurs in the peptidyl transferase center at the large subunit (Figure 1-3B, green frame). In the case of bacteria, the nucleotide A2486 in this center is known as the active center of a ribozyme which catalyzes to form a peptide bond between the amide group in the amino acid with the tRNA at the A-site (A-tRNA) and the C-terminal carboxylate group of the nascent polypeptide chain binding to the tRNA at the P-site (P-tRNA) where is next to

the A-site. The detail of the reaction is shown in Figure 1-3B. Finally, the inherent guanosine triphosphate (GTP) bound translation factors (GTPases) that involve specificity in the individual stages during translation cycles bind to the "GTPase-associated center" of the large subunit and cause the GTP hydrolysis (Figure 1-3B, blue frame). This center is conserved and plays a crucial role in the continuous supply of the GTP hydrolysis energy that is needed for promoting the protein synthesis. However, from the crystal and cryo-EM structures of ribosome, it could not be visible in detail because its flexibility, therefore, the mechanism at molecular level is still unclear.

3. Ribosomal P stalk at GTPase-associated center

The GTPase-associated center can be divided two functional parts into the recruitment cycle of GTPases and the GTP hydrolysis (Figure 1-3B). In the former, a ribosomal protein complex termed "ribosomal stalk" that is highly flexible and lateral protuberance exists, and selectively recruits some specific GTPases such as initiation factor (IF5B), elongation factors (EF-1α/EF-Tu and EF-2/EF-G) and release factor (RF3) to Sarcin-Ricin Loop (SRL) which is the GTPase binding region of the large subunit of ribosome (Figure 1-4) (12). This stalk is functionally and architecturally conserved in all organisms and essential to promote the translational metabolic cycles. The stalk composes of an anchor protein (P0 in archaea and eukaryote, L10 in bacteria) and arm proteins, multiple copies of homodimer or heterodimers (P1 homodimer in archaea, P1-P2 heterodimer in eukaryote, L12 homodimer in bacteria), which are acidic ribosomal proteins (Figure 1-5). The architectures of both anchor proteins, P0 and L10 are similar that N-domain (rRNA-

anchoring domain) anchors the stalk at GTPase-associated center in the large subunit (Figure 1-5), while C-domain is a helical spine to bind multiple copies of stalk proteins that each monomer hands GTPase for recruiting/releasing them to/from the ribosome (13-15). Although the conformations of rRNA-anchoring domain between P0 and L10 are most similar, the helical spine of P0 has different structural characteristics from that of L10, indicating the structural difference between aP1 (P1/P2) and L12 (14).

In bacteria, the structure of stalk protein L12 forms three parts: an N-terminal domain (NTD) for dimerization and binding to helical spine of L10; a C-terminal domain (CTD) which consists of three α-helices and three β-strands, and hands GTPases; a hinge linker between two domains (Figure 1-6) (16). Previous studies showed that surface of L12CTD (Lys66-Ala68, Ile70, Gly80 and Lys82) interacted with the functional insertion domain termed subdomain G' of EF-G (Glu224 and Glu228) (17, 18). The structures of the ribosome complexed with elongation factor G (EF-G) by the X-ray crystallography also showed that the L12CTD bound to subdomain G' of EF-G directly (19, 20).

The archaeal stalk has three copies of aP1 homodimer, while the eukaryotic stalk has two sets of P1 and P2 heterodimer (14, 21). Based on sequence identity, P1 and P1/P2 can be considered to be evolutionally related. Similar to the L12, P1 is also composed of an N-terminal dimerization domain (NTD) for binding to P0, a C-terminal domain (CTD) for handing GTPases, and a flexible linker between two domains (Figure 1-6) (14, 21), but each domain is completely difference in both of sequence and structure between P1 and L12 (22). While the L12CTD is composed of about 70 amino acids, the P1CTD is formed by 25 amino acids predicted as two helices (Figure 1-6) (14). Such structural difference indicates that the interaction mechanisms between the stalk and GTPase in

archaea/eukaryote and bacteria are completely different, although the stalk proteins play same role to hand GTPases for recruiting them to the GTPase-associated center of the ribosome (13, 14). Moreover, it has been known that the C-terminal residues Leu (Leu103, Leu106) and Phe (Phe107) of P1CTD are essential to interact with GTPases and conserved through archaea and eukaryote (15).

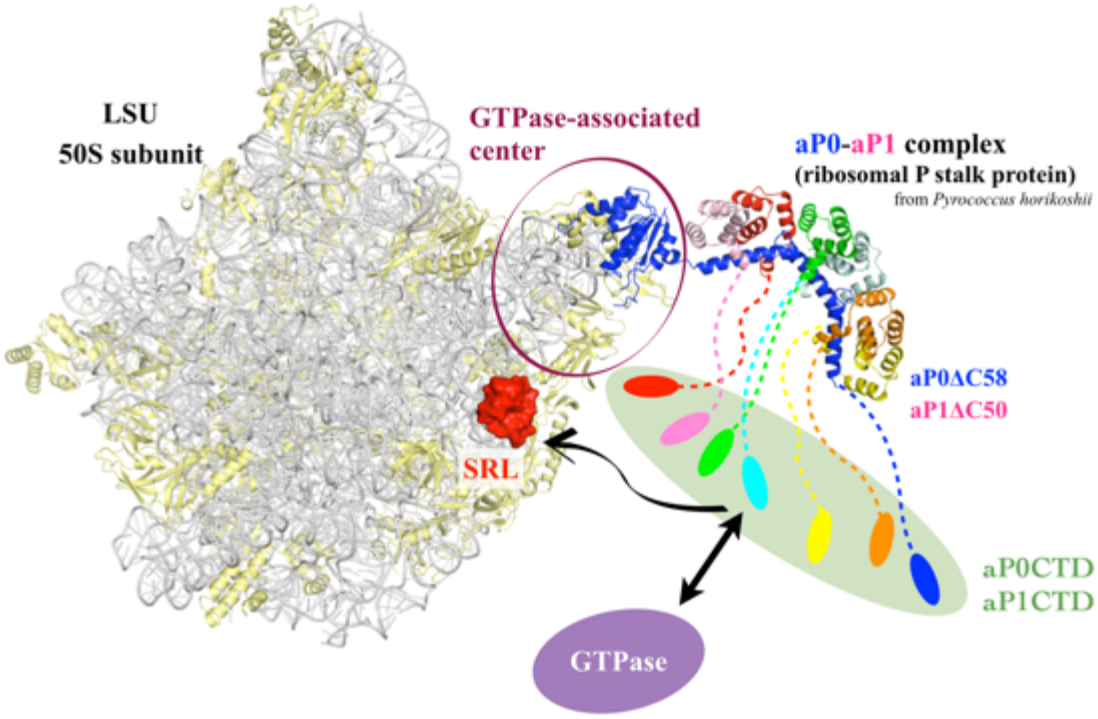

Figure 1-4. Model of the ribosomal P stalk on the large ribosomal subunit (PDBID: 2QA4) (23). The rRNAs and ribosomal proteins are represented by ribbon models and colored the same as Figure 1-2. The P stalk from *Pyrococcus horikoshii* (P0-$[P1]_2[P1]_2[P1]_2$, PDBID: 3A1Y) (14) is shown in ribbon model. P0 protein and six P1 proteins (three sets of P1 dimer) are colored blue, pale pink, red, green, cyan, orange, and yellow, respectively. The sarcin/ricin loop (SRL) that is the GTPase binding region of the ribosome is represented by surface model and colored red.

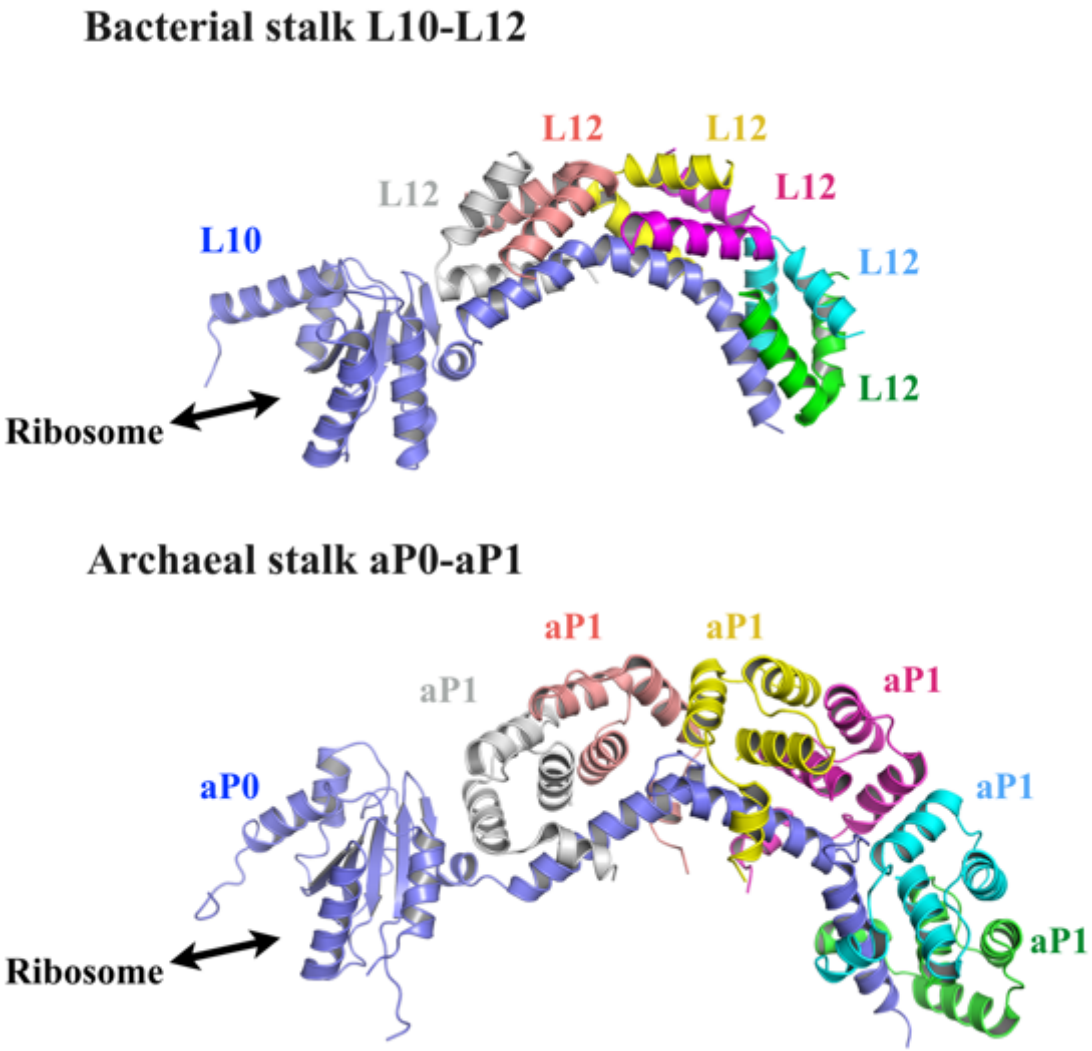

Figure 1-5. The backbone of the ribosomal stalk of bacteria and archaea. While bacterial stalk is composed of L10 protein and three sets of L12 dimer, archaeal ribosomal stalk is composed of aP0 and three sets of aP1 dimer. L10, L12, aP0, and aP1 proteins are labeled.

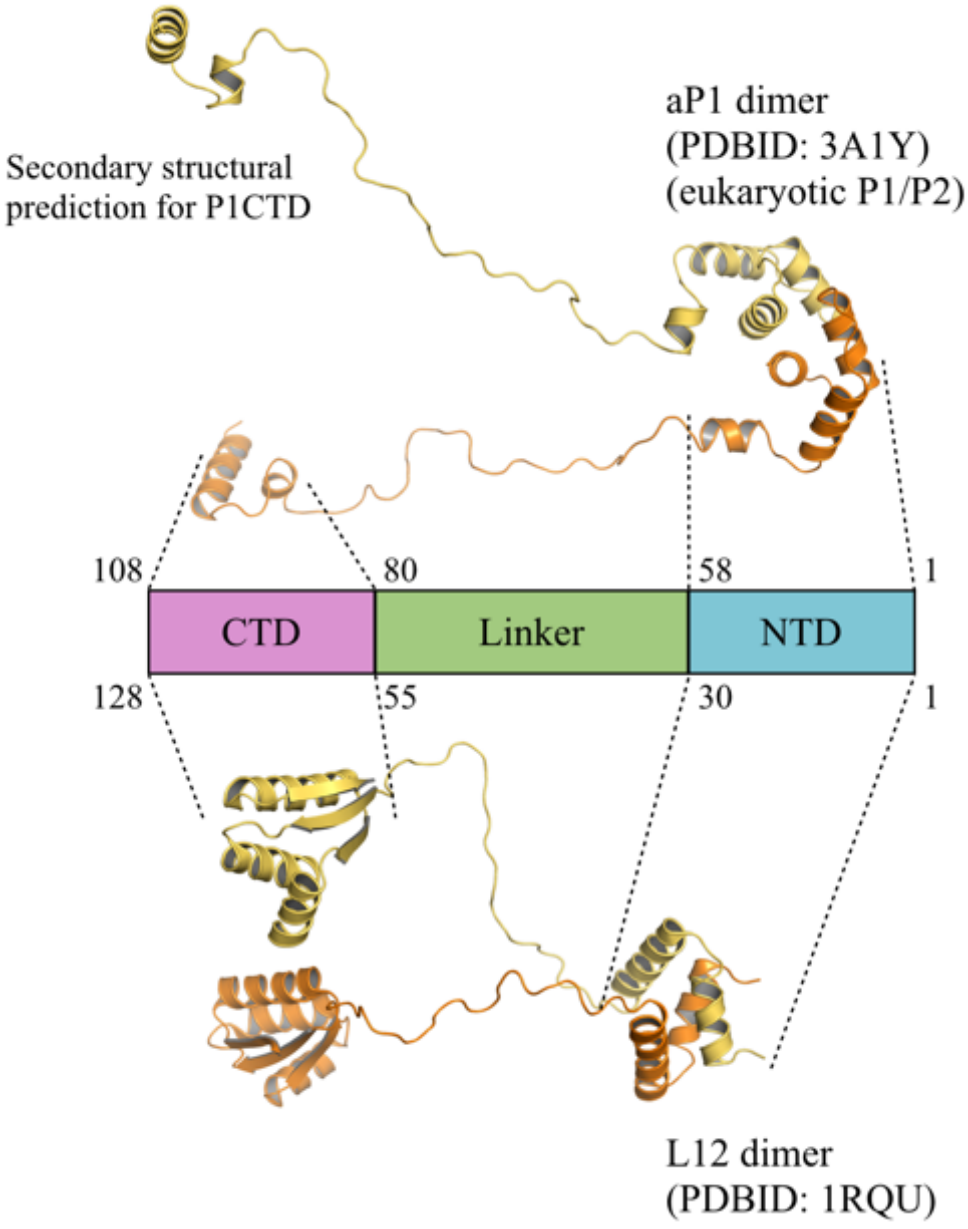

Figure 1-6. The domain constitution of archaeal P1 dimer (eukaryotic P1/P2 heterodimer) and bacterial L12 dimer. The N-terminal domain (NTD) of aP1 is used from P0-$[P1]_2[P1]_2[P1]_2$ (PDBID: 3A1Y) (14) and the C-terminal domain (CTD) and the linker are modeled by the secondary structural prediction using *Coot* (24). The full length of L12 homodimer determined (PDBID: 1RQU) (16).

4. Translation elongation factors

The translation elongation is a major part of the protein synthesis and the stepwise addition of amino acids to a polypeptide chain. During this stage, there are two major elongation factor GTPases that bind alternately to the GTPase binding region at the GTPase-associated center in their GTP-bound activated forms (11, 19). These factors of eukaryote and archaea are EF-1α and EF-2, which are bacterial homologues of EF-Tu and EF-G, respectively. Firstly, GTP-bound EF-1α (EF-1α-GTP) recognizes an aa-tRNA, and the P stalk delivers the complex of EF-1α-GTP-aa-tRNA to the ribosomal GTPase binding region which is Sarcin/Ricin loop (SRL) (Figures 1-3B and 1-4). By the GTP hydrolysis of EF-1α-GTP at the GTPase-associated center of the ribosome, GDP-bound EF-1α (EF-1α-GDP, inactivated form) that has a large conformational change from EF-1α-GTP releases the aa-tRNA, which is fixed the A-site of the ribosome (Figures 1-3A and 1-3B), finally, dissociates from the ribosome by the P stalk. In the case of archaea, EF-1α is also known to work in the release state of translation. EF-1α, instead of RF3 which is the release factor GTPase in eukaryote and bacteria (25, 26), delivers RF1, which is a tRNA mimic protein and recognizes the stop codon (27, 28), to the A-site of the ribosome to stop the translation (29). On the other hand, as well as EF-1α-GTP-aa-tRNA, GTP-bound EF-2 (EF-2-GTP) which is a translocational enzyme is recruited to the GTPase-associated center of the hybrid state of the ribosome by the P stalk and plays an important role in the ratchet in order not to return the classical state of the ribosome (20, 30). After the GTP hydrolysis, the domains III-V of the GDP-bound EF-2 (EF-2-GDP) rotates considerably at the angle of ~60° and tRNAs in the ribosome push relatively into

the next site for vacating A-site and preparing for recruiting new tRNA with EF-1α-GTP (19).

5. Relationship between P stalk and various translational GTPases

Bacterial translational GTPases such as IF2, EF-Tu, EF-G, and RF3 are known to interact with the stalk L12CTD (12). On the other hand, in archaea, the aP1CTD recognizes GTPases such as aIF5B, aEF-1α and aEF-2 yet not aIF2γ (Figure 1-7) from previous results of the gel-mobility shift assays, although they all uniformly share the structure of domain G which is the GTP binding domain. It is indicated that the P stalk has the recognition-specificity (15). Similar to EF-G, aEF-2 also has subdomain G', however, aIF5B and aEF-1α do not have subdomain G'. In the case of aEF-1α, previous structural and functional studies showed that the groove formed by the domains G and III of GDP bound aEF-1α interacts with aP1CTD. Taken all together, these findings indicate that aP1CTD has substrate-recognition specificity with a broad substrate-recognition ability. To recognize various translational GTPases, the aP1CTD needs to adapt to the different sequences and structures of its binding partners. Therefore, it is indispensable to investigate the details of interaction between individual translational GTPases and P1CTD by structural analysis.

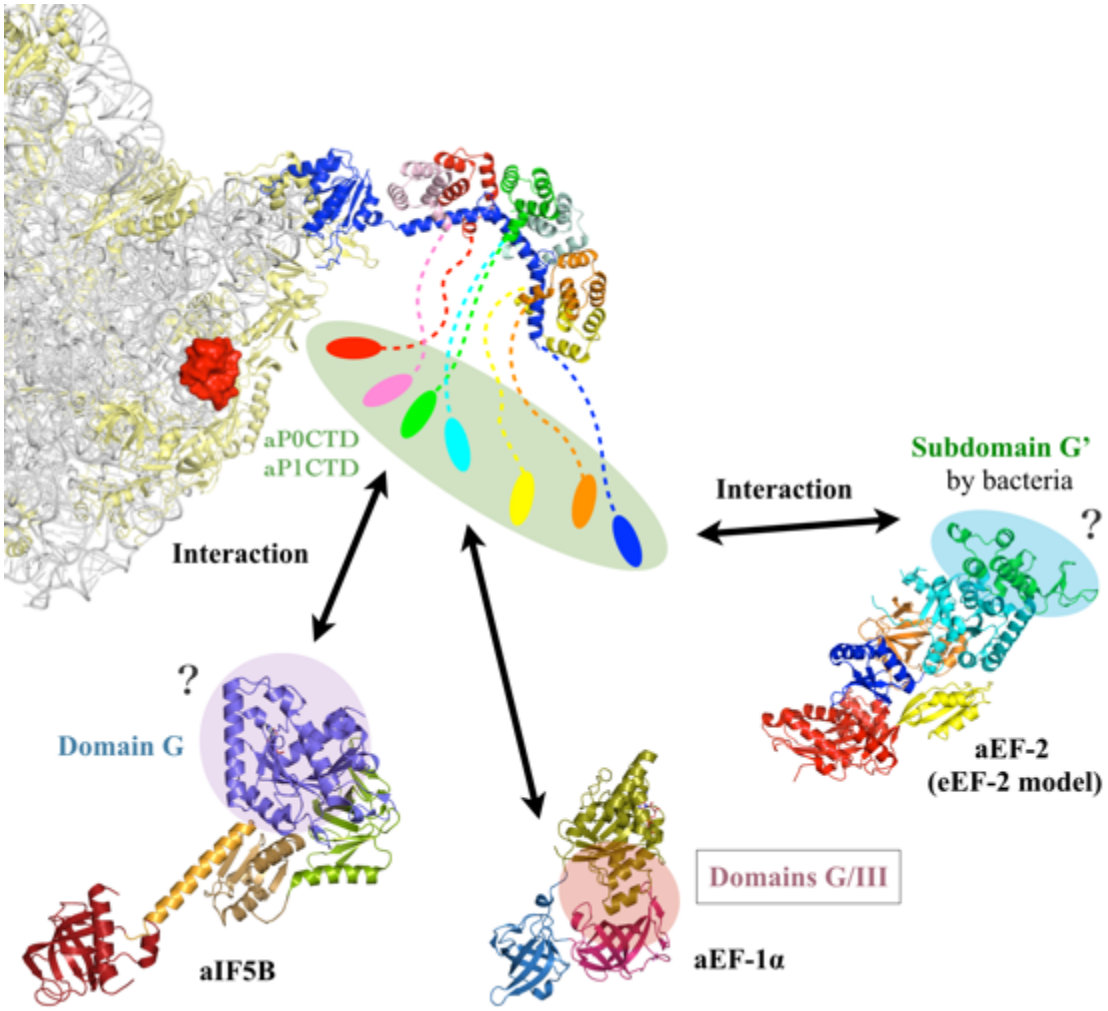

Figure 1-7. Relationship between the ribosomal P stalk and various translational GTPases, such as aIF5B, aEF-1α and aEF-2. The model of the P stalk on the ribosome is the same as using Figure 1-4. aIF5B (PDBID:) (31), aEF-1α (PDBID: 1SKQ) (32), and eEF-2 (PDBID: 1N0V) (33) are represented by ribbon models and their colors are divided into each domain, especially, the domain G of aIF5B, the domains G and III of aEF-1α, the subdomain G' of eEF-2 are colored purple, olive, raspberry, and green, respectively. Circular meshes colored salmon of aEF-1α is the aP1CTD binding region, and those colored purple and cyan are the estimated region of aP1CTD binding.

6. Target of research

In order to completely understand the GTPase recognition mechanism of P1CTD, we determined the crystal structures of *Pyrococcus horikoshii* aEF-2 in Apo-form, GDP-form, GTP-form and GTP-form in complex with P1CTD peptide fragment (11 C-terminal residues of P1, P1C11). The structures of aEF-2 show that P1CTD was located on a hydrophobic groove formed by the domain G and the subdomain G' of aEF-2 with conformational changes around P1CTD binding region of aEF-2. In addition, a model of aEF-2-GDP complexed with P1CTD was built by molecular dynamics simulation based on the structures of GDP-form and GTP-form in presence of aP1CTD. Combining the gel-mobility shift assay and quantitative binding assays between aP1 and aEF-2 variants with previous results of aP1 mutant analyses, we propose a structural basis for aEF-2 recognition mechanism of aP1CTD when P stalk recruits aEF-2 to the GTPase-associated center of the ribosome during the elongation process.

In order to further understand the other GTPase, aEF-1α recognition mechanism of P1CTD, we also determined the crystal structure of aEF-1α-GDP in complex with P1CTD (P1C11). Compared to previous aEF-1α-GDP-P1CTD which the peptide was longer than P1C11, the interaction between aEF-1α and P1CTD was slightly different, and combining the gel-mobility shift assay between P1 and aEF-1α-GDP mutant, we newly identified a P1 binding residue of aEF-1α. Moreover, from the competition experiment between aEF-2 and aEF-1α for P1, and we suggest the strength of the interactions of aEF-2-P1 and aEF-1α-P1.

MATERIAL & METHODS

1. Plasmid Construct

The full length (735 residues) of *P. horikoshii* aEF-2 (*Pho*EF-2) was expressed in *E. coli*. The gene encoding *Pho*EF-2 was cloned with a C-terminal hexahistidine tag (His_6) into the pET-26M vector. The plasmids of all *Pho*EF-2 mutants (Table 1) and truncated *Pho*EF-2 which was constructed by domain G, subdomain G' and domain II (amino acids: 1-389 and hereafter refer as *Pho*EF-2-D2) were constructed by QuikChange methods. Resulted plasmids were transformed into *Escherichia coli* B834(DE3)-pRARE2. Cells were cultivated in 30 mg/mL Luria-Broth (1.2×LB) medium (Miller, sigma) containing 15 μg/mL kanamycin, 34 μg/mL chloramphenicol, 1 % glucose at 37°C until the optical density at 600 nm (OD_{600}) reached 0.4-0.6. Isopropyl-D-1-thiogalactopyranoside (IPTG) was then added to a final concentration of 1 mM to induce gene expression and cultivation was continued for 20 h at 25°C. The plasmid of the full length (428 residues) of *P. horikoshii* aEF-1α (*Pho*EF-1α) was expressed in *E. coli*. The gene encoding *Pho*EF-1α was cloned with a C-terminal hexahistidine tag (His_6) into the pET-26M vector. The plasmid of *Pho*EF-1α mutant (*Pho*EF-1α I369S) was constructed by QuikChange method. Resulted plasmids were transformed into *E. coli* B834(DE3)-pRARE2. Cells were cultivated in 25 mg/mL LB medium containing 15 μg/mL kanamycin, 34 μg/mL chloramphenicol at 37°C until the optical density at 600 nm (OD_{600}) reached 0.4-0.6. IPTG was then added to a final concentration of 1 mM to induce gene expression and cultivation was continued for 20 h at 25°C. The plasmid of the full length (108 residues) of *Pyrococcus horikoshii* aP1 was cloned without any tags into the pET-3a vector by our collaborator, Dr. Uchiumi group at Niigata University, and was expressed in *E. coli*

BL21(DE3) codon plus RIL (Stratagene) (15). The plasmids of all P1 mutants (a part of Table 2) were constructed by QuikChange methods and was expressed in *Escherichia coli* B834(DE3)-pRARE2. Cells were cultivated in 25 mg/mL LB medium containing 100 μg/mL ampicillin, 34 μg/mL chloramphenicol, 1 % glucose at 37°C until the optical density at 600 nm (OD_{600}) reached 0.4-0.6. IPTG was then added to a final concentration of 1 mM to induce gene expression and cultivation was continued for 20 h at 25°C (15).

2. Purifications of Proteins and a Peptide of C-terminal P1

The harvested recombinant cells expressing P1 was disrupted with DNase I, 0.75 mg/mL Lysozyme and buffer A [50 mM Tris-HCl pH 8.0, 100 mM NaCl, 1 mM EDTA, 2 mM DTT] by sonication at 4°C and centrifuged at 10°C, 40,000g for 30 min. After heat-treatment at 70°C for 30 min with centrifugation at 4°C, 10,000g for 20 min, the supernatant was subjected to 10 mL HiTrap Q-Sepharose XL (GE Healthcare) and eluted with a gradient of 100-500 mM NaCl in buffer B [20 mM Tris-HCl pH 8.0, 1 mM EDTA, 1 mM DTT], and then, purified using Superdex 75 pg 26/60 gel-filteration column (GE Healthcare) equilibrated with buffer C [20 mM Tris-HCl pH 8.0, 100 mM NaCl, 1 mM EDTA, 1 mM DTT]. The eluted sample was purified using RESOURCE Q anion-exchange column (GE Healthcare) and eluted with a gradient 100-1000 mM NaCl in buffer B. The collected fractions were dialyzed in buffer D [20 mM Tris-HCl pH 7.5, 100 mM KCl, 1 mM DTT] (15). P1 was concentrated to 65 mg/mL.

The harvested recombinant cells expressing *Pho*EF-2, its mutants or *Pho*EF-2-D2 were disrupted with DNase I, 0.75 mg/mL Lysozyme and buffer E [50 mM Tris-HCl pH 8.0,

10 mM $MgCl_2$, 10 % Glycerol, 1 mM PMSF, 1 mM β-mercaptoethanol] by sonication at 4°C and centrifuged 10°C, 40,000g for 30 min. After heat-treatment at 70°C for 30 min with centrifugation at 10,000g for 30 min, the supernatant was subjected to 5 mL HisTrap HP (GE Healthcare) and eluted with a gradient of 50-250 mM imidazole in buffer F [20 mM Tris-HCl pH 8.0, 100 mM KCl, 1 mM β-mercaptoethanol], and then, purified using Superdex 200 pg 26/60 gel-filteration column (GE Healthcare) equilibrated with buffer G [20 mM Tris-HCl pH 7.5, 100 mM KCl, 10 mM $MgCl_2$, 1 mM DTT]. The eluted fractions containing the target were mixtures of two different samples; GDP-bound form and nucleotide-free Apo form. For obtaining nucleotide-free form (Apo form), the sample was purified twice using RESOURCE Q anion-exchange column (GE Healthcare), after heat-treating at 70°C for 10 min. Firstly, the sample was injected to the column and eluted with a gradient 5-500 mM KCl in buffer H [20 mM Tris-HCl pH 8.0, 5 mM KCl, 1 mM DTT]. The collected fractions were dialyzed in buffer I [20 mM Tris-HCl pH 8.0, 100 mM KCl, 1 mM DTT]. Then, the sample was again applied to RESOURCE Q anion-exchange column using same protocol as above. Purified nucleotide-free *Pho*EF-2 was confirmed by mass spectrometry analysis (Figure 2-1). The purification of *Pho*EF-2-D2 was performed by same protocol of *Pho*EF-2 except for the last two steps of nucleotide-free *Pho*EF-2. All purification experiments were carried at room temperature. Nucleotide-free *Pho*EF-2 and *Pho*EF-2-D2 were concentrated to 17 and 13 mg/mL, respectively.

The harvested recombinant cells expressing *Pho*EF-1α and its mutant were disrupted with DNase I, 0.75 mg/mL lysozyme and buffer E by sonication and centrifuged at 4°C, 10°C, 40,000g for 30 min. After heat-treatment at 70°C for 30 min with centrifugation at

10,000g for 30 min, the supernatant was subjected to 5 mL HisTrap HP (GE Healthcare) and eluted with a gradient of 50-250 mM imidazole in buffer F, and then, purified using Superdex 200 pg 26/60 gel-filteration column (GE Healthcare) equilibrated with buffer G as well as the purification of *Pho*EF-2. *Pho*EF-1α and its mutant were concentrated to 24 mg/mL.

In previous studies, P1-binding affinity analysis of 10 mutants for 12 C-terminal residues (99-108aa) of P1 (1-108aa) were performed (15). The results showed that among them, F107S, L106S, L103S lose GTPase-binding affinity. Moreover, the structure of *Pho*EF-1α complexed with P1 C-terminus also showed long peptide of P1C may induce effects from crystal packing. Therefore, we designed to use a short fragment of P1CTD. The peptide of 11 C-terminal amino acids of P1 (hereafter referred as P1C11), residues E98-G108 (EALAGLSALFG) (Table 2), was synthesized and purified by Sigma Aldrich Japan.

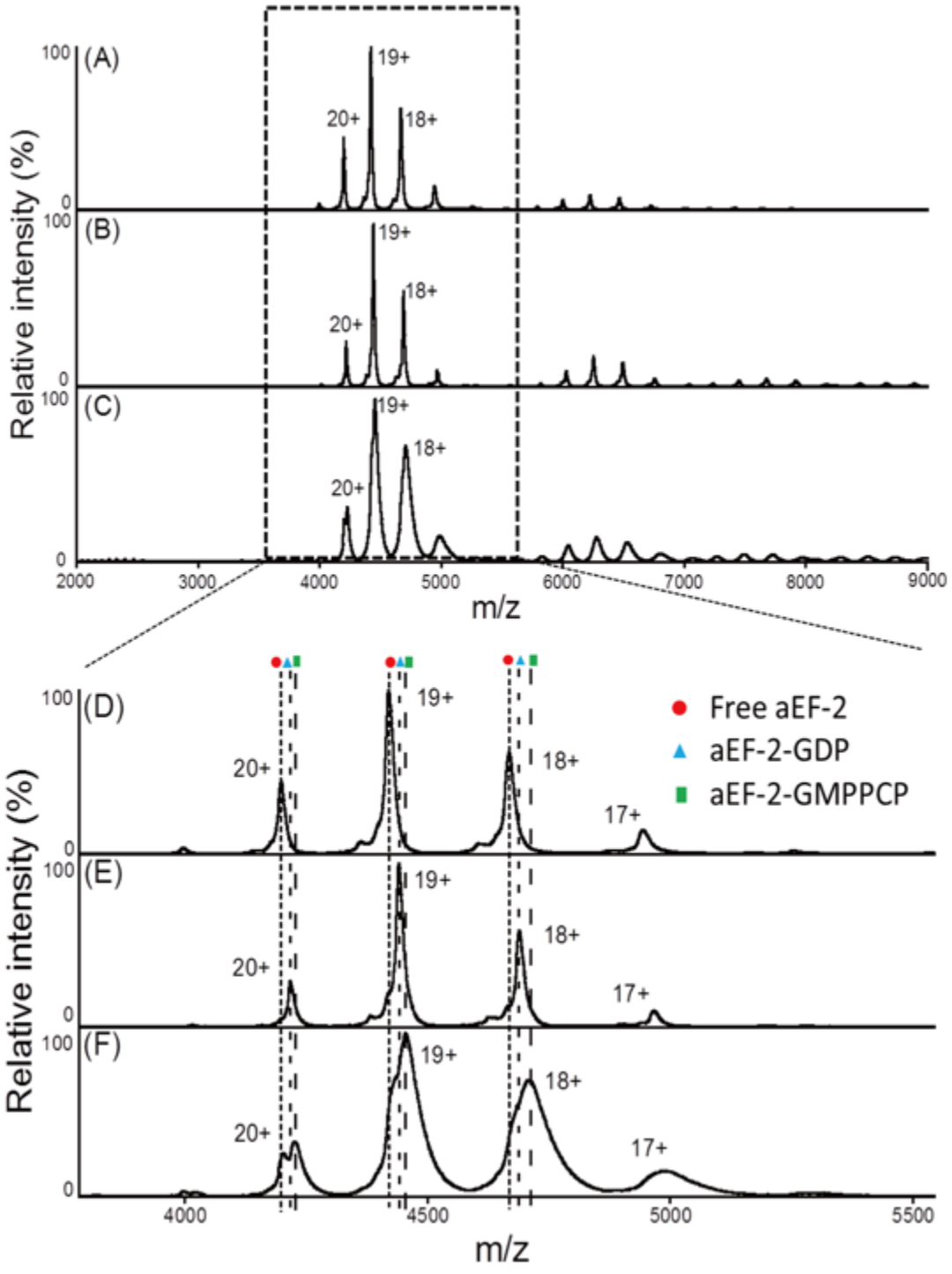

Figure 2-1. Mass spectrometry under nondenaturing conditions of elongation factor *Pho*EF-2 or *Pho*EF-2 associated with GMPPCP (guanylyl 5'-[β,γ-methylene-di-phosphonate]) or GDP. Purified *Pho*EF-2 (20 μM) was incubated

without any nucleotide (**A**) and (**D**), or with 2 mM GDP (B) and (E) or 2 mM GMPPCP (**C**) and (**F**) at 70 °C. After the solution had been diluted to 10 mM, the buffer was exchanged quickly, and the sample subjected to MS under nondenaturing conditions.

Table 1. The list of *Pho*EF-2 mutants for binding assays.

Construct	Residue	Domain	Function	Mutation	Interaction
*Pho*EF-2-GMPPCP	Pro164	Domain G	P1-binding	P164S	++
	Met167			M167S	+
	Met168			M168S	++
	Phe171			F171S	++
	Val198			V198S	++
	Phe205			F205S	+
	Leu214	Subdomain G'		L214S-V216S	++
	Val216				
	Met219			M219S	++
	Lys225			K225S	++
	Phe226			F226S	-
	Asn227			N227S	++

++: The binding ability is comparable to wild type.

+: The binding ability is less similar to the wild type.

–: The binding ability is undetectable.

Table 2. The list of P1 mutants for binding assays.

Construct	Residue	Domain	Function	Mutation	Interaction
P1	Glu97	C-terminal domain (CTD)	EF-2-binding	E97L	++
	Glu98			E98L	++
	Ala99			A99S	++
	Leu100			L100S	+
	Ala101			A101S	++
	Gly102			G102S	-
	Leu103			L103S	-
	Ala105			A105S	++
	Leu106			L106S	-
	Phe107			F107S	-
	Gly108			G108D	++
				G108A	++
				ΔC1	++

++: The binding ability is comparable to wild type.

+: The binding ability is less similar to the wild type.

–: The binding ability is undetectable.

Except for G102S, G108A, and ΔC1, the mutant experiments were demonstrated as described previously (15).

Red flame in the column is the components of P1C11 peptide.

3. Crystallization and Data collection

To obtain GTP-bound *Pho*EF-2, an analogue of GTP, GMPPCP was added to purified and concentrated nucleotide-free *Pho*EF-2 in the ratio 25:1 Mol of GMPPCP: *Pho*EF-2 (hereafter refer as *Pho*EF-2-GMPPCP) and then heat-treated at 50°C for 30 min (15). Moreover, in order to construct *Pho*EF-2-GMPPCP in complex with P1C11 (hereafter refer as *Pho*EF-2-GMPPCP-P1C11), *Pho*EF-2-GMPPCP samples were added 0.4 mg powder of P1C11 in the ratio 1:20 of *Pho*EF-2-GMPPCP:P1C11, subsequently heat-treated at 50°C for 30 min, and then centrifuged at 13,000g for 5 min. The *Pho*EF-2-D2 sample was also heat-treated at 50°C for 30 min before crystallization. The initial crystallization screening of *Pho*EF-2-GMPPCP, *Pho*EF-2-GMPPCP-P1C11 and *Pho*EF-2-D2 was carried out by using sitting-drop method in small scale (96-well plate) with our manufacturing PEG (polyethylene glycol) cocktail containing 10 % or 20 % (wt/vol) of PEG400-10000 and 0.1 M buffers in pH range of 5.0-8.0 (Table 3).

Table 3. The list of PEG cocktail initial screening kit: PEG Grid No Salt

		1	2	3	4	5	6	7	8
		10%	20%	10%	20%	10%	20%	10%	20%
A	0.1 M	PEG400		PEG1000		PEG400		PEG1000	
		Citric acid pH 5.0				MES pH 6.0			
B		PEG400		PEG1000		PEG400		PEG1000	
		HEPES pH 7.0				Tris pH 8.0			
C		PEG2000MME		PEG3350		PEG2000MME		PEG3350	
		Citric acid pH 5.0				MES pH 6.0			
D		PEG2000MME		PEG3350		PEG2000MME		PEG3350	
		HEPES pH 7.0				Tris pH 8.0			
E		PEG4000		PEG6000		PEG4000		PEG6000	
		Citric acid pH 5.0				MES pH 6.0			
F		PEG4000		PEG6000		PEG4000		PEG6000	
		HEPES pH 7.0				Tris pH 8.0			
G		PEG8000		PEG10000		PEG8000		PEG10000	
		Citric acid pH 5.0				MES pH 6.0			
H		PEG8000		PEG10000		PEG8000		PEG10000	
		HEPES pH 7.0				Tris pH 8.0			

The initial crystals of *Pho*EF-2-GMPPCP appeared about 2-3 weeks at 20°C under several conditions containing (1) 10 % PEG6000 and 0.1 M MES-NaOH pH 6.0; (2) 10 % PEG3350 and 0.1 M MES-NaOH pH 6.0; (3) 10 % PEG8000 and 0.1 M Citric acids pH 5.0, however, the appeared crystals of the condition (3) decayed within 2 weeks (Figure 2-2A). After optimized crystallization conditions, the diffraction-quality crystals of *Pho*EF-2-GMPPCP were grown up with reservoir solution containing 6-12 % PEG6000 or PEG3350 and 0.1 M MES-NaOH pH 5.8-6.4 by the sitting-drop method in large scale (Figure 2-2B). For the X-ray diffraction experiment, the crystal of *Pho*EF-2-GMPPCP was rapidly soaked through two cryoprotectants of reservoir solution containing 5 % Glycerol and Paratone-N before flash-cooling under a cryostream. The diffraction data was collected at beamline AR-NW12A of Photon Factory (PF), Tsukuba, Japan.

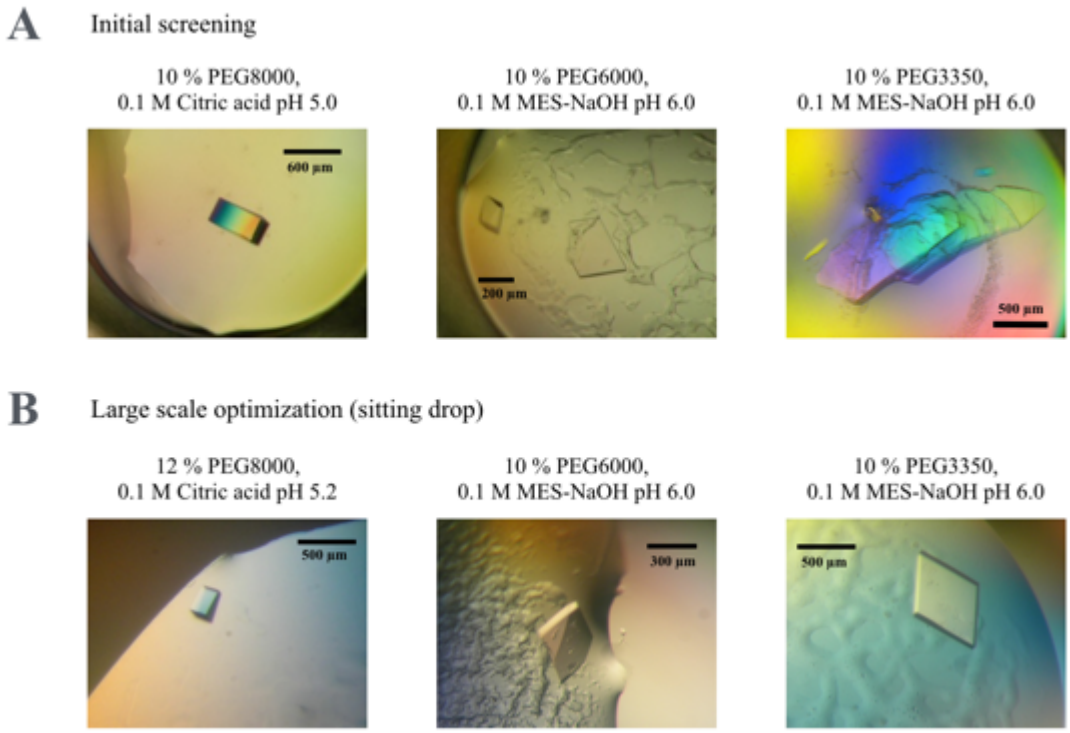

Figure 2-2. Crystallization conditions of GMPPCP-bound form of *Pho*EF-2 (*Pho*EF-2-GMPPCP) and the corresponding crystals. (**A**) Initial crystals of *Pho*EF-2-GMPPCP under several conditions containing 1) 10 % PEG8000 and 0.1 M Citric acids pH 5.0 2) 10 % PEG6000 and 0.1 M MES-NaOH pH 6.0; 3) 10 % PEG3350 and 0.1 M MES-NaOH pH 6.0; of our manufacturing screening kit PEG Grid No Salt as shown Table 3. (**B**) Crystals under optimized crystallization conditions containing 1) 12 % PEG8000 and 0.1 M Citric acids pH 5.2 2) 10 % PEG6000 and 0.1 M MES-NaOH pH 6.0; 3) 10 % PEG3350 and 0.1 M MES-NaOH pH 6.0; of the initial screening of (A).

The initial crystals of *Pho*EF-2-GMPPCP-P1C11 appeared in a week with reservoir solution containing (1) 10 % PEG8000 and 0.1 M MES-NaOH pH 6.0; (2) 10 % PEG10000 and 0.1 M MES-NaOH pH 6.0; (3) 10 % PEG8000 and 0.1 M HEPES-NaOH pH 7.0; (4) 20 % PEG10000 and 0.1 M HEPES-NaOH pH 7.0 but nearly all of these were multi-crystals (Figure 2-3). For obtain the high quality single crystals, we tried to crystallize using a salt screening kit (NeXtal Stock Kit Salt of QIAGEN) as the additive reagents, and use several crystallization techniques (Figures 2-4A and 2-4B). As the result, the single crystals of *Pho*EF-2-GMPPCP-P1C11 were grown up within one day by the micro-seeding technique that drop was set up in a ratio 0.1:1:1 of micro-seeds solution: protein: reservoir solution (10 % PEG10000, 0.1 M MES pH 6.0, 0.5 M Lithium acetate dehydrate) by micro batch method (Figure 2-4C). A diffraction data set of *Pho*EF-2-GMPPCP-P1C11 was collected at beamline BL44XU of SPring-8 (Harima, Japan) under a stream of nitrogen gas, after soaking through cryoprotectants of reservoir solution containing 3.5-14 % Sucrose (3.5 % stepwise) and Paratone-N.

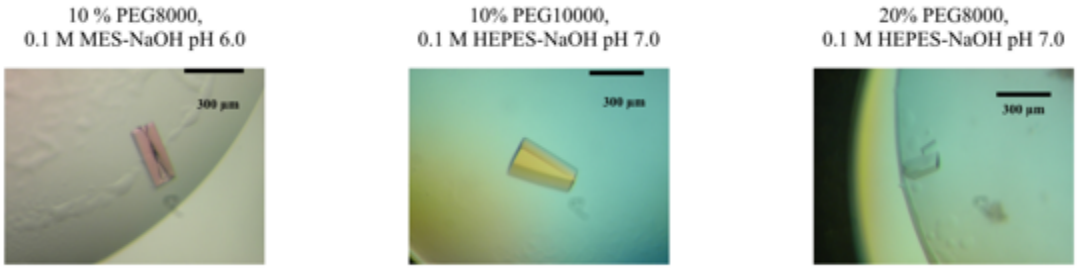

Figure 2-3. Crystallization conditions of *Pho*EF-2-GMPPCP in presence of P1C11 peptide (*Pho*EF-2-GMPPCP-P1C11) and its corresponding crystals. Initial crystals of *Pho*EF-2-GMPPCP-P1C11 under several conditions containing 1) 10 % PEG8000 and 0.1 M MES-NaOH pH 6.0 2) 10 % PEG10000 and 0.1 M HEPES-NaOH pH 7.0; 3) 20 % PEG8000 and 0.1 M HEPES-NaOH pH 7.0; of our manufacturing screening kit PEG Grid No Salt as shown Table 3.

A 10 % PEG8000, 0.1 M MES-NaOH pH 6.0

+ Potassium nitrate

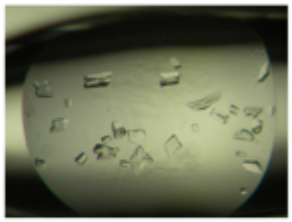

+ di-Ammonium hydrogen citrate

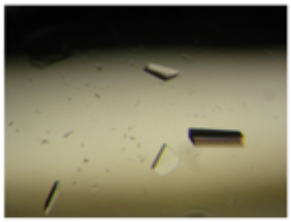

+ Lithium acetate dihydrate

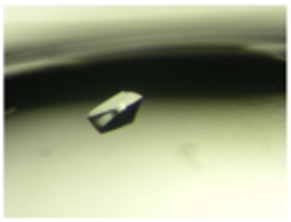

+ Lithium nitrate

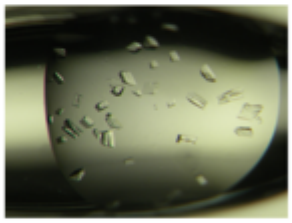

+ Jeffamine M-600 pH 7.0

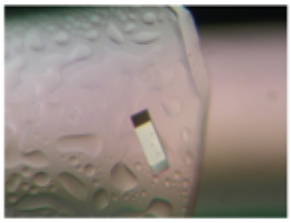

10 % PEG10000, 0.1 M MES-NaOH pH 6.0

+ tri-Sodium citrate dihydrate

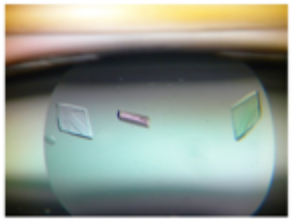

+ Potassium dihydrogen phosphate

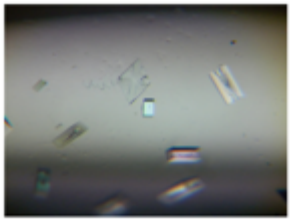

+ Calcium acetate hydrate

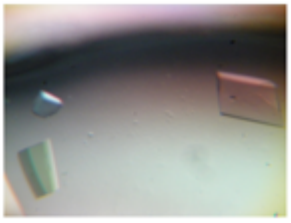

B 10 % PEG10000, 0.1 M MES-NaOH pH 6.0 + 0.5 M Lithium acetate dihydrate

small scale method (96 well)

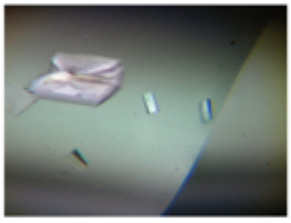

large scale method (Sitting drop)

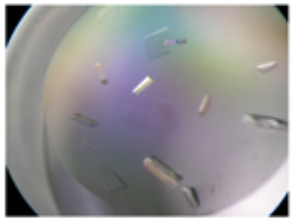

large scale method (Hanging drop)

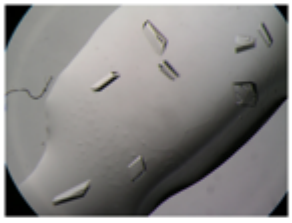

C micro-seeding + micro batch method

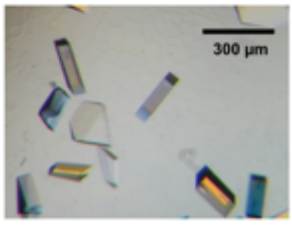

Figure 2-4. Crystallization optimization of *Pho*EF-2-GMPPCP-P1C11 using salt screening kit and its corresponding crystals. (**A**) Optimized crystals of two initial crystallization conditions containing 1) 10 % PEG8000 and 0.1 M MES-NaOH pH 6.0 and 2) 10 % PEG10000 and 0.1 M MES-NaOH pH 6.0 using a salt screening kit (NeXtal Stock Kit Salt of QIAGEN) as the additive reagents (Potassium nitrate, di-Ammonium hydrogen citrate, Lithium acetate dihydrate, Lithium nitrate, and Jeffamine M-600 pH 7.0 in (1) condition and tri-Sodium citrate dihydrate, Potassium dihydrogen phosphate, and Calcium acetate hydrate in (2) condition). (**B**)-(**C**) Crystals of the condition containing 10 % PEG10000, 0.1 M MES-NaOH pH 6.0, 0.5 M Lithium acetate dihydrate using several crystallization techniques sitting-drop method in small scale (96-well plate) and large scale (24-well plate), hanging-drop method in large scale (24-well plate) (**B**), and micro-seeding and micro-batch method (**C**).

The rodlike-octahedral crystals of *Pho*EF-2-D2 were grown up in a couple of days with reservoir condition containing 10 % PEG1000 (produced by Hampton), 0.1 M MES-NaOH pH 6.0 (Figure 2-5). We optimized crystallization by the sitting-drop methods in small scale. The octahedral crystals appeared within a couple of days at 293 K with a reservoir containing 10 % (wt/vol) PEG1000 (produced by QIAGEN) and 0.1 M MES-NaOH pH 6.0 (Figure 2-5). After the crystal of *Pho*EF-2-D2 was rapidly soaked through the reservoir containing 25 % Glycerol, the diffraction data was collected to 1.6 Å resolution at beamline BL-5A of PF.

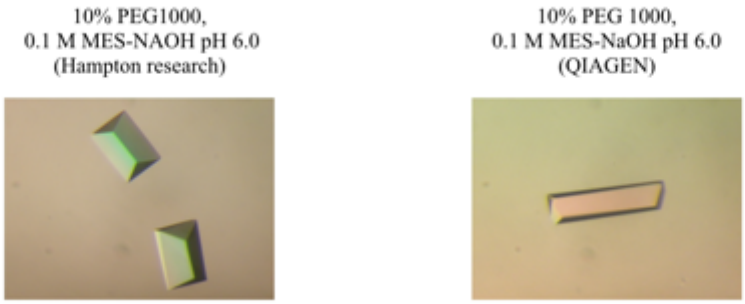

Figure 2-5. Crystallization conditions of GDP-bound form of the truncated mutant of *Pho*EF-2 domain G, subdomain G' and domain II (*Pho*EF-2-D2-GDP) and its corresponding crystals.Crystals of *Pho*EF-2-D2-GDP under one condition containing 1) 10 % PEG1000 (Hampton research) and 0.1 M MES-NaOH pH 6.0 (left figure) 2) 10 % PEG1000 (QIAGEN) and 0.1 M MES-NaOH pH 6.0 (right figure); based on our manufacturing screening kit PEG Grid No Salt as shown Table 3.

To construct *Pho*EF-1α in complex with P1C11 (hereafter refer as *Pho*EF-1α-P1C11), firstly, *Pho*EF-1α was diluted to 8 mg/mL with buffer J [20 mM Tris-HCl pH 9.0, 100 mM KCl] and then, GMPPCP was added to purified and concentrated *Pho*EF-1α in the ratio 25:1 Mol of GMPPCP:*Pho*EF-1α and then heat-treated at 50°C for 30 min. *Pho*EF-1α samples were added 0.4 mg powder of P1C11 in the ratio 1:20 of *Pho*EF-1α:P1C11, subsequently heat-treated at 50°C for 30 min, and then centrifuged at 13,000g for 5 min. The initial crystallization screening of *Pho*EF-1α was carried out by using sitting-drop method in small scale (96-well plate) with our manufacturing kit (Table 3).

The initial crystals of *Pho*EF-1α appeared in one week with reservoir solution containing (1) 20 % PEG2000MME, 0.1 M Tris-HCl pH 8.0, (2) 10 % PEG3350, 0.1 M MES-NaOH pH 6.0 but all of these were multi-crystals although the quantities of the reservoir solution were changed (Figures 2-6A and 2-6B). In order to obtain the high quality single crystals, the mixture of *Pho*EF-1α-P1C11 was heat-treated at 50°C for 2.5 hours, and then centrifuged at 13,000g for 5 min before the initial crystallization screening. As the result of this alteration, the single crystals of *Pho*EF-1α-P1C11 were grown up in one week with reservoir containing 20 % PEG2000MME, 0.1 M Tris-HCl pH 8.0 (Figure 2-6C). After the crystal of *Pho*EF-1α was rapidly soaked through the cryoprotectants of reservoir solution containing 15 % Glycerol and Paratone-N before flash-cooling under a cryostream, the diffraction data was collected to 2.4 Å resolution at BL-5A.

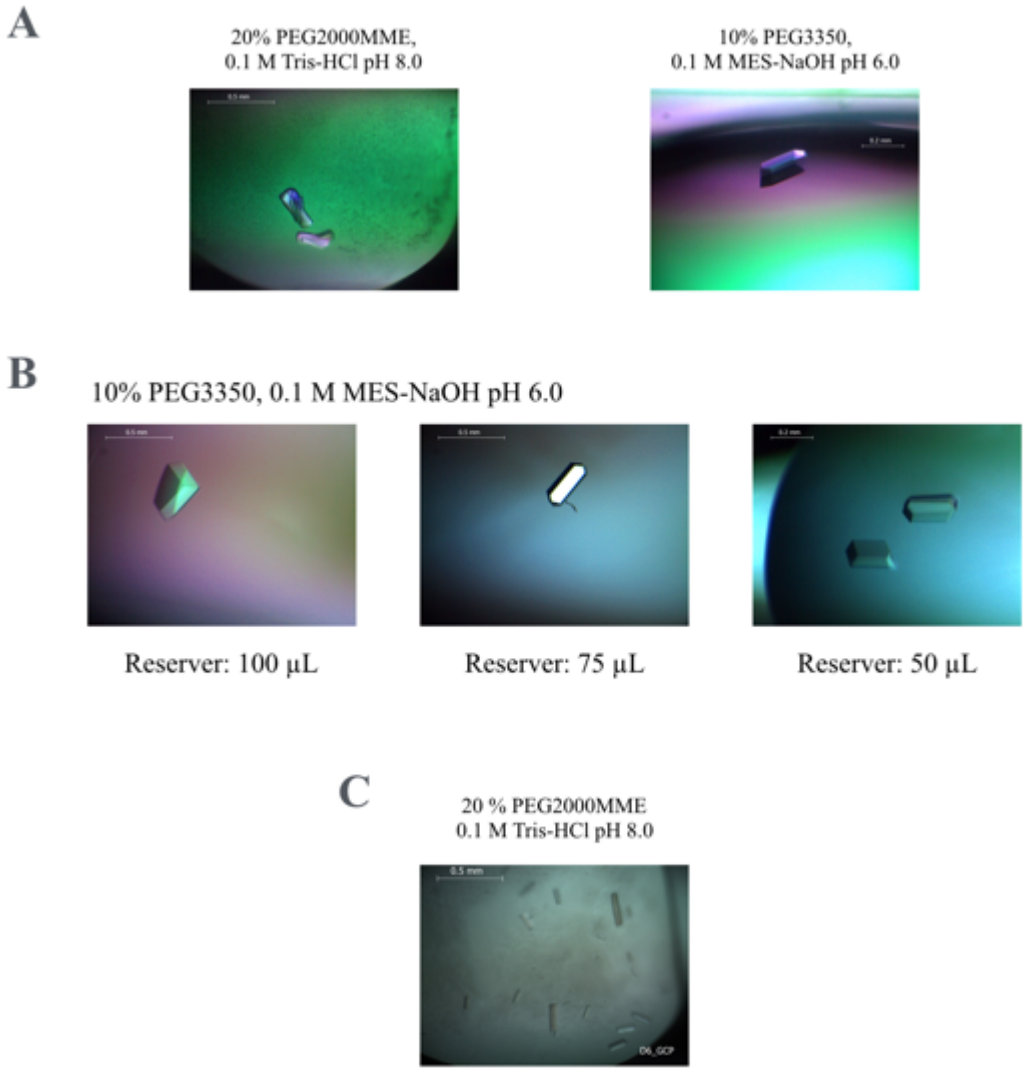

Figure 2-6. Crystallization conditions of GDP-bound form of *Pho*EF-1α in complex with P1C11 (*Pho*EF-1α-GDP-P1C11) and its corresponding crystals. (**A**) Initial crystals of *Pho*EF-1α-GDP-P1C11 under several conditions containing 1) 10 % PEG2000MME and 0.1 M Tris-HCl pH 8.0 and 2) 10 % PEG3350 and 0.1 M MES-NaOH pH 6.0 of our manufacturing screening kit PEG Grid No Salt as shown Table 3. (**B**) Crystals of *Pho*EF-1α-GDP-P1C11 under the condition containing 10 % PEG3350 and 0.1 M MES-NaOH pH 6.0 by several different

volumes of the reservoir. (**C**) Crystals of *Pho*EF-1α-GDP-P1C11 under the condition containing 10 % PEG2000MME and 0.1 M Tris-HCl pH 8.0 with the optimization of sample preparation.

All data sets were indexed, integrated, scaled, and merged by using the program *XDS* package (34). These crystals of *Pho*EF-2-GMPPCP, *Pho*EF-2-GMPPCP-P1C11, *Pho*EF-2-D2, and *Pho*EF-1α-P1C11 belong to the same space groups, $P2_12_12_1$ with different cell parameters of $a = 84.2$, $b = 116.1$, $c = 189.2$ Å, $a = 79.8$, $b = 121.9$, $c = 199.3$ Å, $a = 50.2$, $b = 85.6$, $c = 114.4$ Å, and $a = 54.7$, $b = 77.8$, $c = 103.5$ Å, respectively. The statistics of data process of the three types of *Pho*EF-2 are summarized in Table 4 and that of *Pho*EF-1α-P1C11 is summarized in Table 5.

Table 4. Data collection and refinement statistics

	***Pho*EF-2-GMPPCP/-Apo**	***Pho*EF-2-D2-GDP**	***Pho*EF-2-GMPPCP-P1C11**
PDB ID	5H7J	5H7K	5H7L
Data Collection			
Beamline	PF AR-NW12A	PF BL-5A	SPring-8 BL44XU
Wavelength (Å)	1.0000	1.0000	1.0000
Resolution range (Å)	39.59–2.30 (2.44–2.30)[a]	47.56–1.60 (1.70–1.60)	48.43–3.10 (3.27–3.10)
Space group	$P2_12_12_1$	$P2_12_12_1$	$P2_12_12_1$
Unit-cell parameters (Å)	a = 84.22	a = 50.16	a = 79.77
	b = 116.13	b = 85.56	b = 121.90
	c = 189.17	c = 114.42	c = 199.26
No. of reflections	423608 (67515)	476998 (75882)	207742 (32208)
No. unique reflections	82481 (13105)	65800 (10475)	36125 (5630)
Completeness (%)	99.2 (98.7)	99.9 (99.7)	99.0 (98.0)
Redundancy	5.14 (5.15)	7.25 (7.24)	5.75 (5.72)
Average I/σ(I)	20.23 (3.80)	19.07 (2.52)	15.69 (2.86)
R_{merge}[b]	0.05 (0.389)	0.077 (0.729)	0.07 (0.598)
Molecules/ asymmetric unit	2	1	2
Refinement			
Used reflections	82476	65789	35821
R_{work}/R_{free} **(%)**[c]	21.51/25.67	17.12/19.79	23.02/28.54
Atoms			
Amino acid residues	10880	3003	11052
Water molecules	205	408	0
Ligands	32	28	64
RMSD from ideality			
Bond length (Å)	0.010	0.007	0.011
Torsion angle (°)	1.320	1.131	1.644
Ramachandran plot (%)			
Favoured	96.85	98.67	93.59
Allowed	2.49	1.33	6.12
Outliers	0.66	0.00	0.29

[a]Values in parentheses are for the highest resolution shell.

[b]$R_{merge} = \sum_{hkl}\sum_i |I_i(hkl) - \langle I_i(hkl) \rangle| / \sum_{hkl}\sum_i I_i(hkl)$, where i is the number of observations of a given reflection and $I(hkl)$ is the average intensity of the i observations. R_{free} was calculated with a 5% fraction of randomly selected reflections evaluated from refinement. The highest resolution shell is shown in parentheses.

[c]$R_{work} = \sum_{hkl}||F_{obs}|-|F_{calc}||/\sum_{hkl}|F_{obs}|$, R_{free} was calculated for 5% randomly selected test sets that were not used in the refinement.

Table 5. Data collection and refinement statistics

	***Pho*EF-1α-GDP-P1C11**
Data Collection	
Beamline	PF BL-5A
Wavelength (Å)	1.0000
Resolution range (Å)	50.0–2.40 (2.55–2.40)[a]
Space group	$P2_12_12_1$
Unit-cell parameters (Å)	a = 54.74
	b = 77.82
	c = 103.45
No. of reflections	
No. unique reflections	
Completeness (%)	96.7 (88.7)
Redundancy	2.23 (2.53)
Average I/σ(I)	39.0 (3.10)
R_{merge}[b]	0.05 (0.31)
Molecules/ asymmetric unit	1
Refinement	
Used reflections	
R_{work}/R_{free} **(%)**[c]	18.48/23.32

All statistics values are calculated the same methods of Table 4.

4. Structure determination and refinement

The structure of *Pho*EF-2-GMPPCP was solved at 2.3 Å resolution by molecular replacement using *Molrep* of the *CCP4* suite (35). The structure of *S. cerevisiae* eEF-2 Apo-form (PDB ID: 3B78) (36) was used as a search model. The structure was refined using *Phenix.refine* (37) and modified manually using *Coot* (24). After rigid body refinement and several cycles of restrained refinement, we found the electron density maps (Fo-Fc and 2Fo-Fc) of GMPPCP in the GTP binding site. Finally, R and R_{free} factors of EF-2-GMPPCP structure were converged to 21.65 % and 25.47 %, respectively.

3.1 Å resolution structure of *Pho*EF-2-GMPPCP-P1C11 was solved by molecular replacement using *Molrep* in the *CCP4* suite (35), with the refined structure of the *Pho*EF-2-GMPPCP as a search model. After several cycles of restrained refinement, both 2Fo-Fc and Fo-Fc maps of the P1C11 were shown, and model of P1C11 was built manually using *Coot* program (24). The structure of *Pho*EF-2-GMPPCP-P1C11 was refined using *Phenix.refine* (37) following manual modification using *Coot* (24). Finally, R and R_{free} factors were converged to 23.02 % and 28.54 %, respectively.

In addition, the structure of aEF-2-D2 was solved by molecular replacement using *Phaser* of *Phenix* package (38) with the structure of domain G, subdomain G' and domain II of the *Pho*EF-2-GMPPCP-P1C11 (residues 12-386 without GMPPCP and P1C11) as a search model. Similar to that of *Pho*EF-2-GMPPCP and *Pho*EF-2-GMPPCP-P1C11, after rigid body refinement and several cycles of restrained refinement using *Phenix.refine*, the map of GDP was shown in both of 2Fo-Fc and Fo-Fc map at GTP binding site (hereafter refer as *Pho*EF-2-D2-GDP). The structure of *Pho*EF-2-D2 was refined using the same

method as above. Finally, R and R_{free} factors were converged to 17.04 % and 19.77 %, respectively. The summaries of refinement are presented in Table 4. All structure figures were generated by PyMOL (The PyMOL Molecular Graphics System, Version 1.3 Schrödinger, LLC). Figures for surface potentials were produced by APBS (39). Sequence alignments was performed by CLUSTALW (40).

2.4 Å resolution structure of *Pho*EF-1α-P1C11 was solved by molecular replacement using *Phaser* of *Phenix* package (38) with the structure of *Pho*EF-1α (PDBID: 3WYA) as a search model. Similar to that of others, after rigid body refinement and several cycles of restrained refinement using *Phenix.refine*, the maps of GDP and P1C11 were shown in both of 2Fo-Fc and Fo-Fc map at GTP binding site (hereafter refer as *Pho*EF-1α-GDP-P1C11). The structure of *Pho*EF-1α-GDP-P1C11 was refined using the same method as above. Finally, R and R_{free} factors were converged to 18.48 % and 23.32 %, respectively. The summaries of refinement are presented in Table 5.

5. Molecular dynamics simulation (collaborator's work)

5-1. All-atom model construction

In order to investigate how P1CTD binds to GDP-form of *Pho*EF-2, molecular dynamics simulation was carried out based on the structures of *Pho*EF-2-GTP-P1C11 and *Pho*EF-2-GDP. Before modeling *Pho*EF-2-GDP-P1C11, all-atom models of *Pho*EF-2, P1C11, GTP and GDP were constructed from the coordinates derived from *Pho*EF-2-GMPPCP-P1C11 and *Pho*EF-2-D2-GDP as described previously (41, 42). The full length structures of *Pho*EF-2-GMPPCP-P1C11 and *Pho*EF-2-GDP were modeled by added missing parts:

1) Mg^{2+} ion with coordinating water molecules form structure of *Taq*EF-Tu (PDB ID: 1EFT) based on structural alignment with VMD (43, 44); 2) Switch I from the structure of *Tth*EF-G (PDB ID: 4V90) using the SWISS-MODEL server (30, 45); 3) Residues 305-310 of the *Pho*EF-2-GMPPCP-P1C11 from the *Pho*EF-2-D2-GDP structure; 4) C-terminal residues (387-735) of *Pho*EF-2-GDP from the *Pho*EF-2-Apo structure. The GMPPCP in *Pho*EF-2-GMPPCP-P1C11 was manually modified to GTP. Hydrogen atoms were added with the psfgen package in the NAMD software and the side chains of His were protonated at the ε-nitrogen (46). Water molecules were added to the models using the Solvate package in VMD to generate a water box of TIP3 extending 10 Å from the protein structure in every direction (44). The energy of the solvated system was minimized using an iterative process of minimizing the energy of the [water, protein]^2 each for 10^4 steps followed by a system minimization of 10^5 steps using the NAMD software (46). After minimization, Na^+ ions were added using the Autoionize package in VMD. A final minimization of 10^5 steps on the entire system was performed.

5-2. *Pho*EF-2-GDP-P1C11 model construction

The complex of *Pho*EF-2-GDP-P1C11 was modeled using the coordinates of P1C11 of *Pho*EF-2-GTP-P1C11 and *Pho*EF-2-GDP after 10 ns of production time described above. To position P1C11, the structure of *Pho*EF-2-GDP and *Pho*EF-2-GTP-P1C11 were aligned, and the system was then solvated with the VMD as described above. The added water molecules were minimized for 10^5 steps followed by a 10^5 step minimization of *Pho*EF-2-GDP. The *Pho*EF-2-GDP-P1C11 system was then minimized, ionized, equilibrated and simulated for 50 ns as described below.

5-3. Simulation parameters

All equilibrated molecular dynamics simulations were performed using NAMD 2.9 with CHARMM 27 parameters (46, 47). Each simulation used periodic boundary conditions in an NPT ensemble with a time step of 2 fs. The temperature was controlled with Langevin dynamics and the pressure was maintained at 1 atmosphere with a Nosé-Hoover Langevin piston. A cut-off distance of 12 Å and a switching distance of 10 Å were used. Short-range (Van der Waals) and long-range electrostatic interactions were computed every 2 fs. Each model was equilibrated at 27°C and 77°C for 150 ps. The equilibrations were then cooled to 27°C by applying the velocities of the 27°C system to the coordinates of the 77°C system, and 50-ns production runs were performed after system cooling.

5-4. Analysis of molecular dynamics simulations

Snapshots of the *Pho*EF-2-GTP-P1C11 and *Pho*EF-2-GDP simulations were saved every 2 fs and were then compiled using Carma software to remove water molecules as well as movements of the protein's center of mass (48). The root mean square deviation (RMSD), dihedral angles, and atom distance calculations were performed using our scripts and invoked with the VMD software package (44). Dihedral angles and atom distances were plotted on a histogram with bin sizes of 2° and 0.2 Å respectively. Histograms were fit with a one or two Gaussian terms using equation 1 and 2

$$\text{counts} = Ae^{\frac{-(x-\bar{x}_a)}{2\sigma_a^2}} \quad (1)$$

$$\text{counts} = Ae^{\frac{-(x-\bar{x}_a)}{2\sigma_a^2}} + Be^{\frac{-(x-\bar{x}_b)}{2\sigma_b^2}} \quad (2)$$

where A and B represent the maximum value of the populations, $\bar{x}_a$ and $\bar{x}_b$, and σ_a and σ_b are the averages and standard deviations for populations A and B respectively.

6. Gel mobility shift assay

Binding assay between P1 and *Pho*EF-2 was examined by gel mobility shift assay using Native-PAGE under the condition that P1 was mixed in concentration of 100 pmol with increasing concentrations of 100 to 400 pmol of individual *Pho*EF-2 mutants (Table 1 and Figure 2-5). The binding buffer contained 20 mM Tris-HCl pH 7.5, 20 mM KCl, and 10 mM $MgCl_2$. Each mutants was mixed with GMPPCP or GDP in the ratio 25:1 of GMPPCP:protein or GDP:protein, and then, heat-treated at 70°C for 10 min before binding assays. Then, each mutant with buffer K [20 mM Tris-HCl pH 8.0, 100 mM KCl, 1 mM DTT] termed TMK buffer was added to P1 and the binding buffer (Table 6A), and the mixture was incubated at 70°C for 10 min again. After the incubation, each sample was applied to Native-PAGE gel electrophoresis using 5% polyacrylamide (acryalamide/bisacrylamide ratio 39⁄1) at 12.5 V⁄cm with a 192 mM glycine and 25 mM Tris buffer system for 1 h at room temperature. The gels were stained with Coomassie brilliant blue R-250 (15). Binding assay between P0-$[P1]_2[P1]_2[P1]_2$ and *Pho*EF-2 was examined by Native-PAGE under the condition that the heptameric complex of P0-P1 which the buffer contained 20 mM Tris-HCl pH 7.5, 100 mM KCl, 1 mM DTT, 0.01 % Triton-X 100, was mixed in concentration of 2.5 pmol with increasing concentrations of

2.5 to 37.5 pmol of individual GMPPCP-bound, GDP-bound, or Apo forms of *Pho*EF-2. The method of the gel-mobility shift assays was the same as described above (Table 6B).

Binding assay between P1 and GDP-bound form of *Pho*EF-1α (Table 6C), was also examined using the same as described above. The competition experiment between P1 and *Pho*EF-1α and/or *Pho*EF-2 was examined by Native-PAGE under the same condition and method basically (Table 6D).

Table 6. Native-PAGE sample preparation lists

A Binding assays between *Pho*EF-2 and P1

P1:*Pho*EF-2	P1	*Pho*EF-2/*Pho*EF-1α	10×TMK	D.W
P1 only	1 µl	-	1 µl	8 µl
1:1	1 µl	1 µl 200 pmol/µl	1 µl	7 µl
1:2	1 µl	2 µl	1 µl	6 µl
1:3	1 µl	3 µl	1 µl	5 µl
1:4	1 µl	4 µl	1 µl	4 µl
*Pho*EF-2 only	-	1 µl	1 µl	8 µl

B Binding assays between *Pho*EF-2 and P0-P1

P0-P1:*Pho*EF-2	P0-P1	*Pho*EF-2	10×TMK	D.W
P0-P1 only	1 µl	-	1 µl	8 µl
1:1	1 µl	1 µl 25 pmol/µl	1 µl	7 µl
1:2	1 µl	2 µl	1 µl	6 µl
1:4	1 µl	4 µl	1 µl	4 µl
1:8	1 µl	200 pmol/µl 1 µl	1 µl	7 µl
1:10	1 µl	1.25 µl	1 µl	6.7 µl
1:15	1 µl	1.88 µl	1 µl	6.1 µl
*Pho*EF-2 only	-	1 µl	1 µl	8 µl

C Binding assays between *Pho*EF-1α and P1

P1:*Pho*EF-1α	P1	*Pho*EF-1α	10×TMK	D.W
P1 only	1 μl	-	1 μl	8 μl
1:1	1 μl	1 μl 200 pmol/μl	1 μl	7 μl
1:2	1 μl	2 μl	1 μl	6 μl
1:3	1 μl	3 μl	1 μl	5 μl
1:4	1 μl	4 μl	1 μl	4 μl
*Pho*EF-2 only	-	1 μl	1 μl	8 μl

D Competition experiments between *Pho*EF-1α and/or *Pho*EF-2 and P1

P1:*Pho*EF-1α:*Pho*EF-2	P1	*Pho*EF-1α	*Pho*EF-2	10×TMK	D.W
P1 only	1 μl	-	-	1 μl	8 μl
1:1:0	1 μl	1 μl	-	1 μl	7 μl
1:2:0	1 μl	2 μl	-	1 μl	6 μl
1:2:1	1 μl	2 μl	1 μl	1 μl	5 μl
1:2:2	1 μl	2 μl	2 μl	1 μl	4 μl
1:2:3	1 μl	2 μl	3 μl	1 μl	3 μl
1:2:4	1 μl	2 μl	4 μl	1 μl	2 μl
*Pho*EF-1α only	-	1 μl	-	1 μl	8 μl
*Pho*EF-2 only	-	-	-	1 μl	8 μl

7. Circular dichroism (CD) spectrometery

Circular dichroism (CD) spectra were collected on a J-805 spectropolarimeter (JASCO, Japan) under an atmosphere of N_2 at room temperature in a quartz cell with a path length of 1 mm. The protein samples were dialyzed in a buffer E [20 mM Tris-HCl, pH 8.0, 10 mM KCl, 1 mM DTT]. The concentration of *Pho*EF-2 and the its mutants; F226S, L214S/V216S, V198S/L214S/V216S were estimated to 0.1, 0.25, 0.2, and 0.1 mg/mL, respectively by using absorption. The CD spectra were obtained from a wavelength region of 190–300 nm by taking the average of four scans. The molar ellipticity per residues was calculated by $(h) = h / (10n/cl)$. Here, h is the CD signal in mdeg, n is the number of residues, c is the concentration in mol L^{-1}, and l is the length of the cuvette path (cm).

8. Surface plasmon resonance

The real time measurement of the interaction between P1 and *Pho*EF-2-GMPPCP or *Pho*EF-2-GDP was performed using a BIACORE 3000 biosensor system (GE Healthcare) at 37 °C. Firstly, all samples were dialyzed by a buffer F [10 mM HEPES, 150 mM NaCl, 100 μM $MgCl_2$, 0.005 % polyoxyethylene sorbitan monolaurate, pH 7.4] and the buffer was used as the running buffer at the flow rate of 50 μL/min. Biotinylation using NHS-amine coupling on amino group of P1 via PEG linker was carried out using EZ-Link NHS-PEG_4-Biotin (Thermo Scientific). A sensor chip CAP (GE healthcare) was used for the immobilization of biotinylated P1. *Pho*EF-2-GMPPCP and *Pho*EF-2-GDP was injected over the immobilized P1. The binding response at each concentration was

calculated by subtracting the equilibrium response measured in the control flow cell from that in the P1 flow cell. Beta- 2-microglobulin was used as negative control. Each resonance unit was fitted to simple 1:1 Langmuir binding model ($A + B \leftrightarrow AB$) using least square minimization to calculate affinity constants (K_D).

9. Dynamic light scattering (DLS)

For the surface plasmon resonance experiments with BIACORE instrument, the buffer of *Pho*EF-2 sample was substituted by Superdex 200 pg 26/60 gel-filteration column (GE Healthcare) equilibrated with the buffer F and concentrated by ultrafiltration using Amicon 30K (Merck), however, the *Pho*EF-2 sample was disappeared. Then, in order to confirm the stabilities of *Pho*EF-2 samples in some buffers. the particle size measurement was performed using dynamic light scattering (DLS). DLS results were collected on a ZETASIZER NANO ZS (Malvern, United Kingdom) at 25 °C in a plastic disposable cuvette. The *Pho*EF-2 samples were dialyzed in buffers E, F, and a buffer G [10 mM HEPES, 150 mM NaCl, 100 μM $MgCl_2$], respectively. The concentration of *Pho*EF-2 was 1 mg/mL by using absorption.

10. Pocket-Cavity Search Application (POCASA)

For confirming the P1-binding pocket of *Pho*EF-2, *Pho*EF-1α, *Rco*RTA and predicting that of *Ape*IF5B and *Sce*EF-2, we used the freely available web server Pocket-Cavity Search Application (POCASA). The prediction program of POCASA was described

previously (49). We set default parameters (probe radius: 2 Å, single point flag: 16, protein depth flag: 18, grid size: 1 Å, and the number of results to show: 0 which show all candidates). The results were shown pockets and cavities around a molecule as the probe spheres.

11. Building a GTPase recruitment model

In order to understand the relationship between *Pho*EF-2 and P1 stalk at the GTPase-associated center of ribosome, we built a GTPase recruiting model. Because no structure of archaeal 70S ribosome complexed with EF-2, we built the model in four steps (Figure 2-7). Firstly, the stalk structure of P0-$[P1]_2[P1]_2[P1]_2$ (PDBID: 3A1Y) (14) was fitted to cryo-EM structure of 70S ribosome complexed with two tRNAs in P-site and E-site from *Pyrococcus furiosus* (PDBID: 4V6U) (8). Then crystal structure of 70S ribosome with two tRNAs in A/P-site and P/E-site and mRNA stalled EF-G from *Thermus thermophiles* (PDBID: 4V5F) (19) was superposed on the cryo-EM structure of 70S ribosome. Finally, current structure of *Pho*EF-2-GMPPCP-P1C11 was superposed on the structure of EF-G of the model. Finally, the linker between P1C11 and the stalk structure of P0-$[P1]_2[P1]_2[P1]_2$ was built as previous description (Figure 2-7) (24).

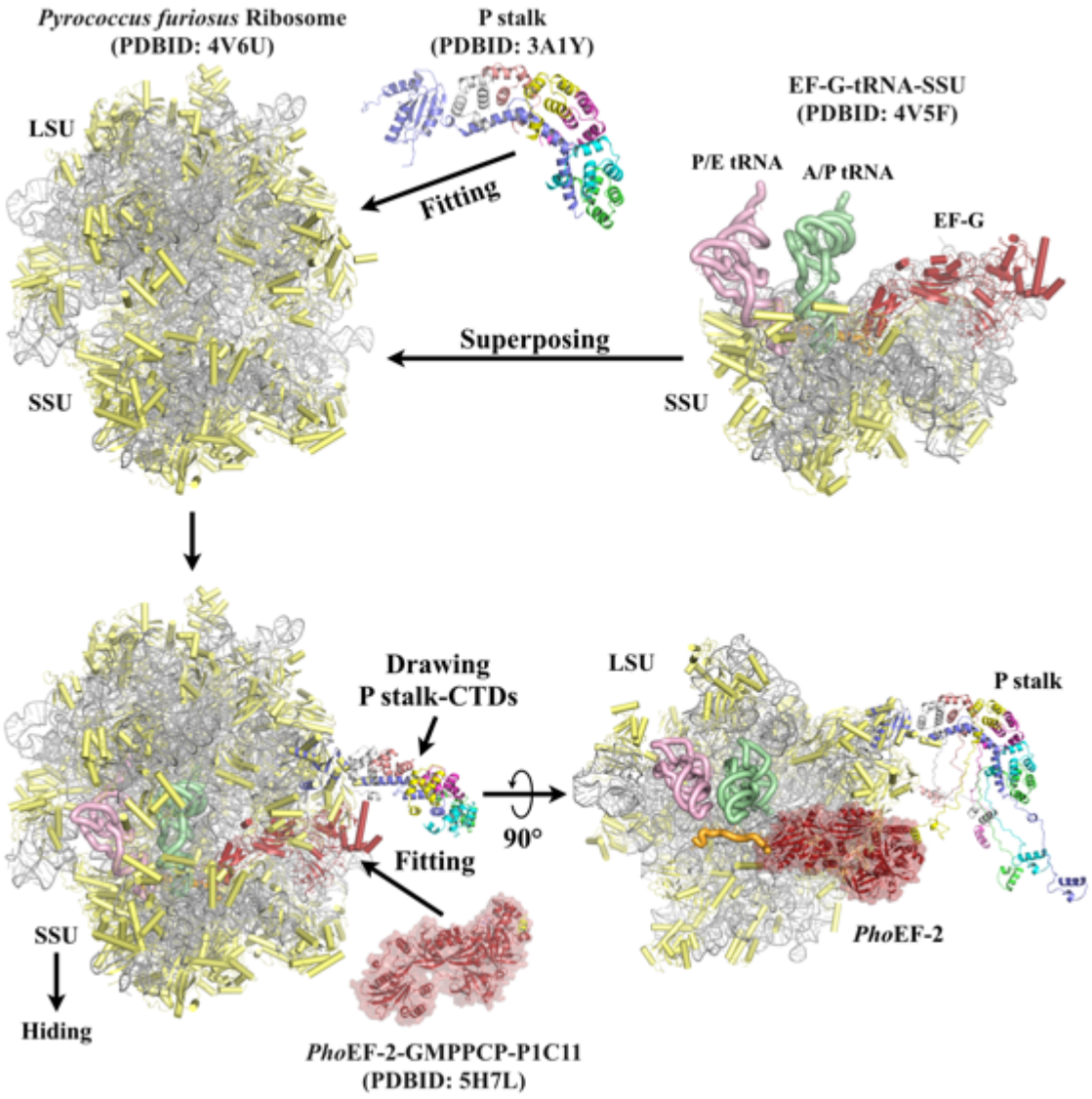

Figure 2-7. How to build a GTPase recruiting model which contains archaeal ribosome from the cryo-EM structure of *Pyrococcus furiosus* (PDBID: 4V6U), the crystal structures of archaeal ribosomal stalk from *Pyrococcus horikoshii* (PDBID: 3A1Y), archaeal elongation factor 2 (EF-2) from *Pyrococcus horikoshii* (PDBID: 5H7L), and EF-G-tRNA-mRNA-SSU from *Thermus thermophiles*. The details of the model building were shown in section 10 of MATERIAL & METHODS.

RESULTS

1. Crystal structures of *Pho*EF-2

The crystal structure of *Pho*EF-2-GMPPCP was determined at a resolution of 2.3 Å, which showed that there were two molecules in the asymmetric unit. One of these molecules was bound to GMPPCP (Figure 3-1A), whereas another was nucleotide free (hereafter referred to as *Pho*EF-2-Apo) (Figure 3-1B), despite that GMPPCP was added at a high concentration for crystallization (see Material & Methods). The final model of *Pho*EF-2-GMPPCP was built 693 of 735 residues: we were unable to build N-terminal ten residues, C-terminal two residues, and residues 51–75 and 305–310 due to the poor-quality electron density map. The structure of *Pho*EF-2-Apo also had disorders, but in different regions: N-terminal 11 residues, and residues 49–75, 304–308, and 427–432. The crystal structure of *Pho*EF-2-D2-GDP was determined at a resolution of 1.6 Å, and there is one molecule in the asymmetric unit. The molecule was bound to GDP, which was derived from the expression host *E. coli*. The final model contained a GDP molecule and residues 1–386, except for missing residues 56–69 (Figure 3-2).

Similar to eEF-2 and EF-G, the overall structure of *Pho*EF-2 consists of five structural domains and a functional subdomain (Figure 3-1): domain G (residues 1–213 and 245–259), subdomain G′ (residues 214–245), domain II (residues 260–386), domain III (residues 387–466), domain IV (residues 467–624 and 701–735), and domain V (residues 625–700). However, subdomain G′ differs between eEF-2 and *Pho*EF-2 in both sizes, sequences, and structures (Figures 3-3A and 3-3B), consisting of 109 residues with six α-helices and one β-sheet (composed of four β-strands) in eEF-2, and only 31 residues with

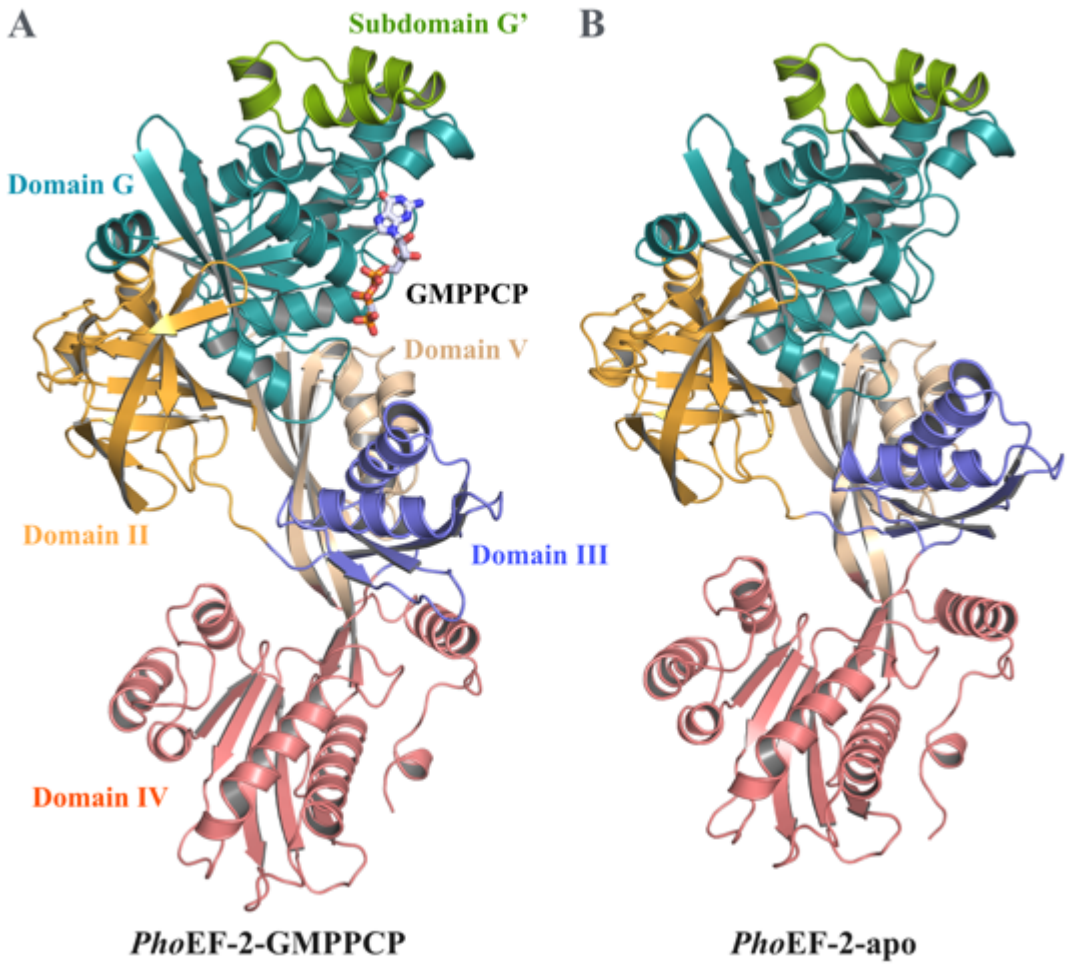

Figure 3-1. The structures of EF-2. (**A**) The structure of *Pho*EF-2-GMPPCP. *Pho*EF-2 and GMPPCP are represented by ribbon and stick models, respectively. Domains G, II, III, IV, and V, and subdomain G′ of *Pho*EF-2 are colored deep teal, orange, slate, pale pink, wheat, and green, respectively. The C, N, O, and P atoms of GMPPCP are colored pale blue, blue, red, and orange. (**B**) The structure of *Pho*EF-2-Apo. *Pho*EF-2 is shown in the same way as in (A).

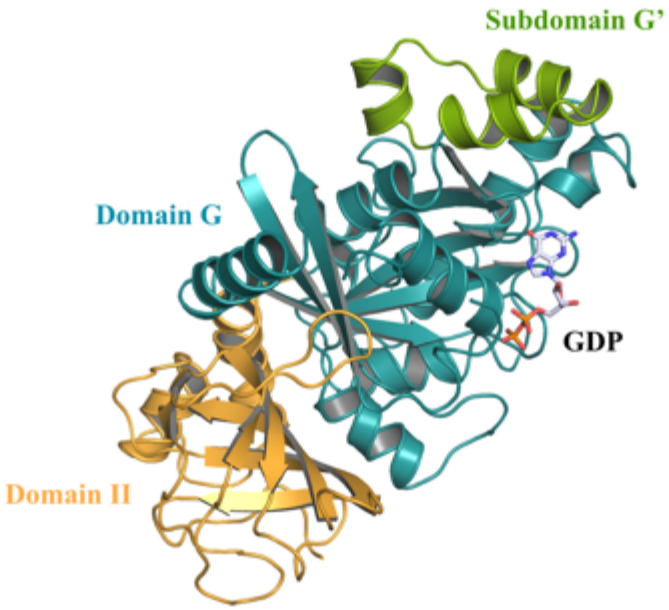

Figure 3-2. The structures of *Pho*EF-2-D2-GDP. The domains G and II, and subdomain G' of *Pho*EF-2 are shown in the same way as in Figure 3-1A. The GDP is represented by stick model. The C, N, O, and P atoms of GMPPCP are colored pale blue, blue, red, and orange.

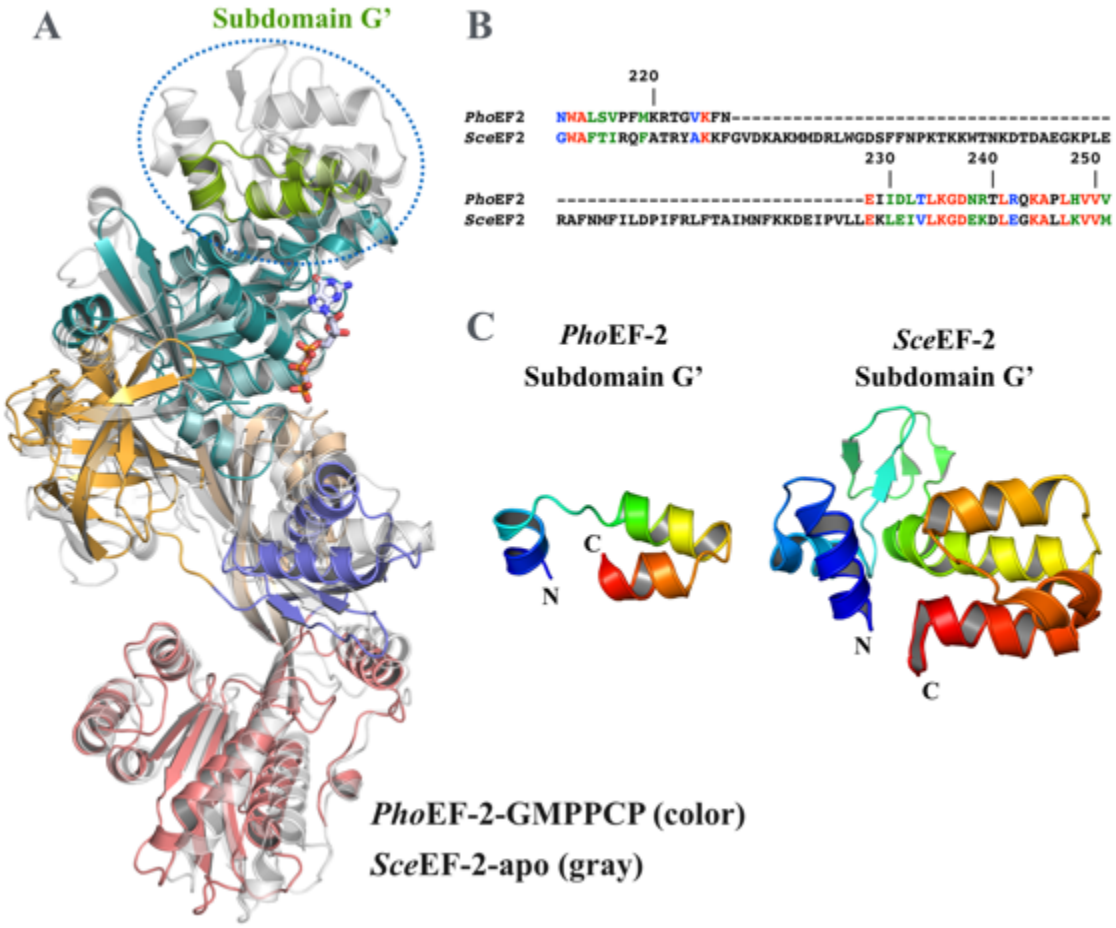

Figure 3-3. The subdomain G' of *Pho*EF-2 and *Sce*EF-2. (**A**) The comparison of the subdomain G' between *Pho*EF-2 and *Sce*EF-2 by superposing domain G. *Pho*EF-2 is shown in the same way as in Figure 3-1A. *Sce*EF-2 is represented by ribbon model and colored gray. (**B**) The sequences of subdomain G′ of *Pho*EF-2 and *Sce*EF-2 were compared. The amino acid residues between *Pho*EF-2 and eEF-2 are colored as follows: completely identical, red; strongly similar, green; weakly similar, blue. (**C**) The structures of subdomain G′ of *Pho*EF-2 and eukaryotic EF-2 from *Saccharomyces cerevisiae* (*Sce*EF-2; PDBID: 1N0V). Both structures are shown in rainbow colors.

a helical structure (three α-helices) in *Pho*EF-2 (Figures 3-3B and 3-3C).

A structural comparison between *Pho*EF-2, *Sce*EF-2 (PDBID: 1N0V) (33), and *Sau*EF-G (PDBID: 2XEX) (50) showed that although the folding of the individual domains except for subdomain G′ is similar between these three proteins (Figures 3-4A), the orientation of each domain is different, indicating highly flexible between the domains (Figures 3-4B). A large rotation of domains III–V of EF-G has previously been demonstrated by comparing ribosome bound and unbound forms (51). Likewise, the domains III–V in *Pho*EF-2-Apo and *Pho*EF-2-GMPPCP exhibited different orientations even in the ribosome unbound state, with the orientations of the decoding tips in domain IV showing particularly large differences. When domain G was superposed, the shift and rotation angle between the two tips of *Pho*EF-2-Apo and *Pho*EF-2-GMPPCP were 11.8 Å and 14.9°, respectively (Figure 3-5A), and domain III also exhibited orientation differences of 4.5 Å and 5.7°, respectively (Figure 3-5A). By contrast, the relative positions of domains III–V hardly changed, and the contact surface between domains G and V was retained (Figure 3-5B).

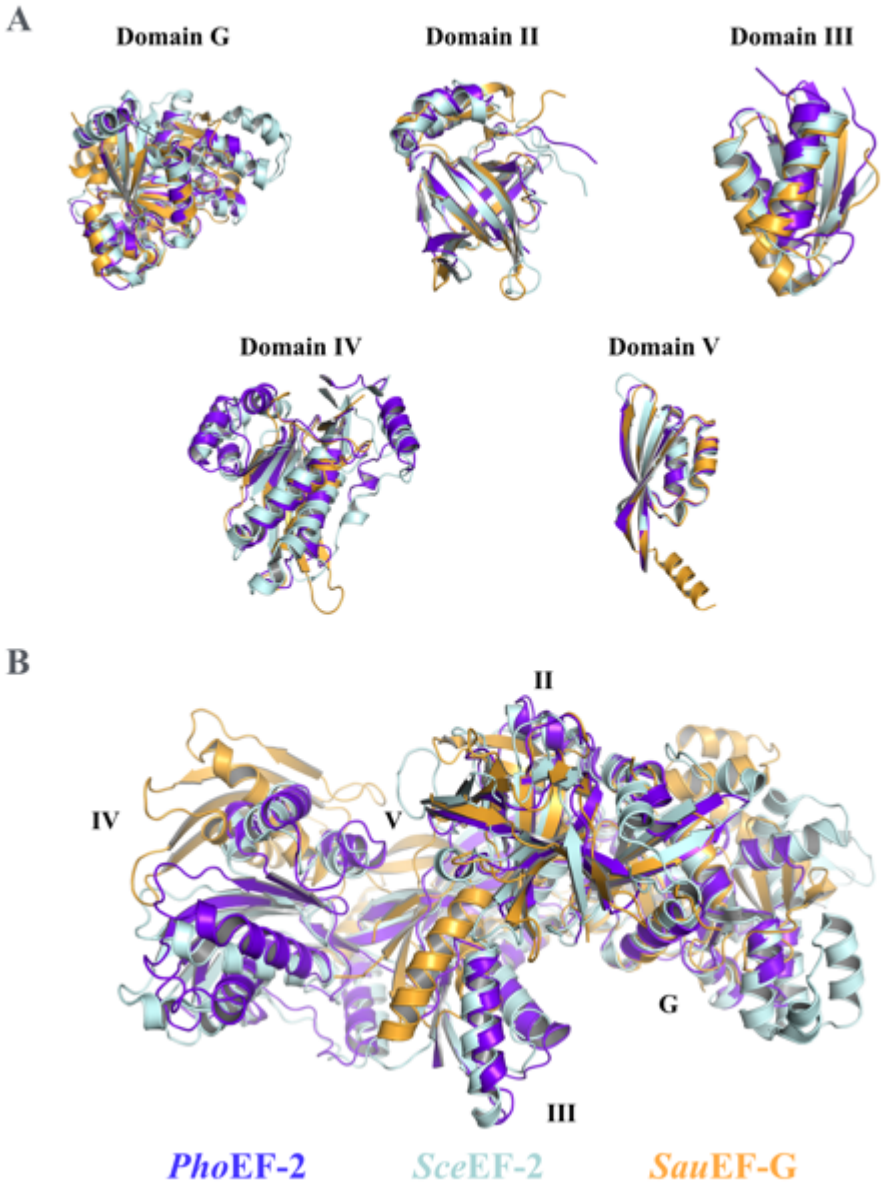

Figure 3-4. Comparison among aEF-2, eEF-2, and EF-G. (**A**) Structural superposition of domains G–V among *Pho*EF-2, *Sce*EF-2, and *Sau*EF-G. Each of domains G, II, III, IV, and V of *Pho*EF-2 (blue), *Sce*EF-2 (PDBID: 1N0V; pale cyan), and EF-G (PDBID: 1ELO; yellow) from *Staphylococcus aureus* were superposed separately. (**B**) Structural comparison of *Pho*EF-2 (blue), *Sce*EF-2 (pale cyan), and EF-G (yellow) as determined by superposing domain G.

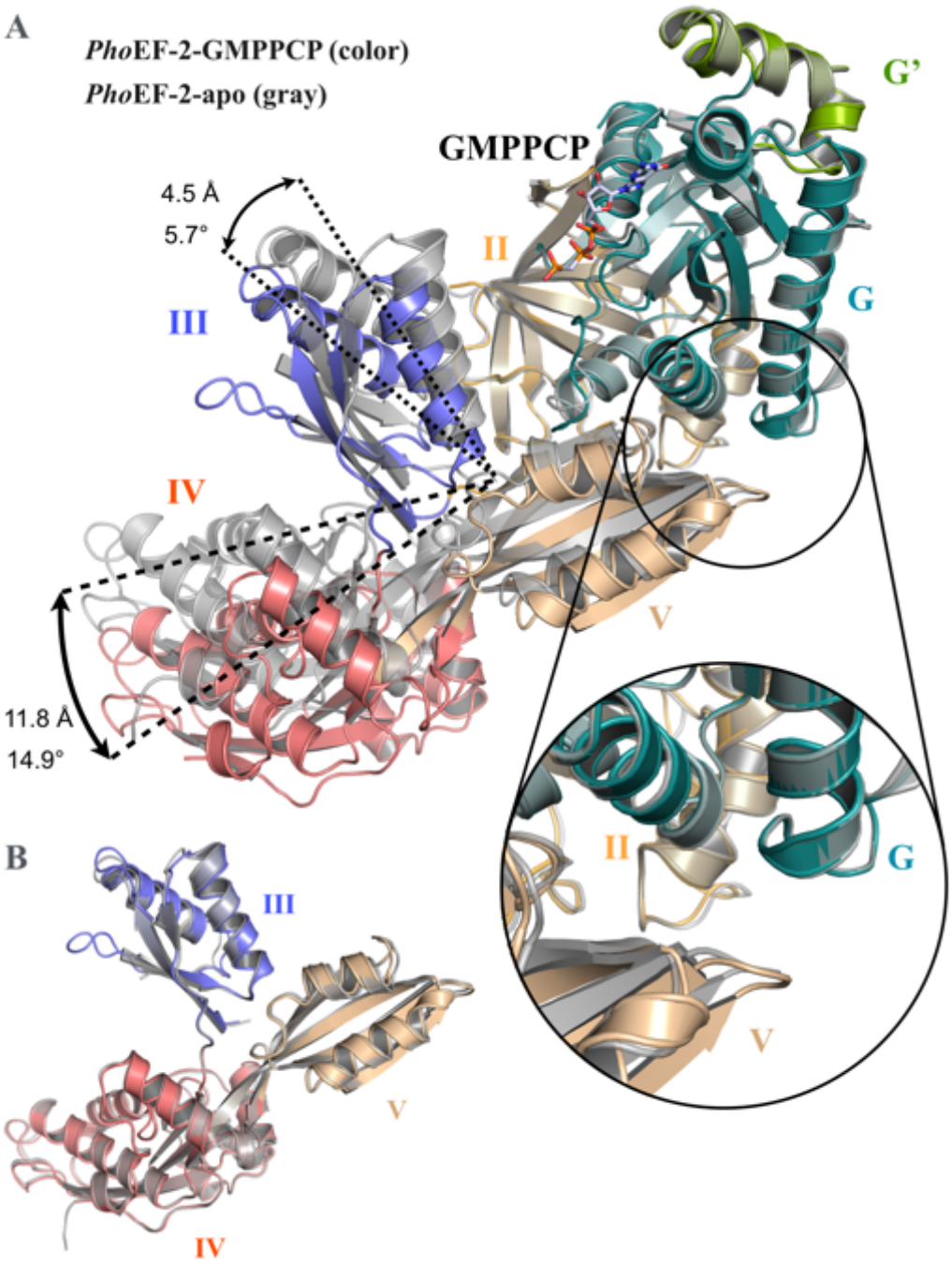

Figure 3-5. Structural comparison between *Pho*EF-2-Apo and *Pho*EF-2-GMPPCP. *Pho*EF-2-Apo is colored gray and *Pho*EF-2-GMPPCP is shown in the same colors as in Figure 3-1. (**A**) The two structures superposed using domain G. (**B**) Structural superposition of domains III–V.

2. The GTP binding site of *Pho*EF-2

In spite of the presence of GMPPCP with high mol-ratio in the crystallization condition (*Pho*EF-2:GMPPCP=1:25), only one of the two *Pho*EF-2 molecules in the asymmetric unit bound GMPPCP (Figure 3-1). By contrast, GDP in the *Pho*EF-2-D2 structure was captured from the expression host *E. coli* (Figure 3-2). Domain G of *Pho*EF-2 contains five GTP binding motifs, P-loop (A30–N43), Switch I (A48–N76), Switch II (D97–G117), G4 (N151–D154), and G5 (S207–Y209) (Figure 3-6), all of which except G5 are well-conserved in other translational GTPases (Figure 3-7) (52, 53).

The P-loop motif consists of a loop (A30–G36), and part of the following helix (K37–N43) mainly recognizes α- and β-phosphate of GMPPCP (Figure 3-6). Three residues in the P-loop (G36, K37, and T38) wraps α- and β-phosphates via a hydrophobic interaction and a hydrogen bond. Among these three residues, G36 and K37 are conserved in all GTPases (Figures 3-6 and 3-7) (54). The conformational change of the P-loop between *Pho*EF-2-GMPPCP and *Pho*EF-2-Apo is similar to that of EF-G (55). The loop including the side chain of I33 in the P-loop of *Pho*EF-2-Apo is closer to the GTP binding site than those of other GDP-form and GMPPCP-form (Figure 3-8A).

The Switch I region is very flexible and could not be visualized in previous studies. However, in the present study, we were able to build 12 residues of the Switch I region in the *Pho*EF-2-D2-GDP structure (Figure 3-8A). As shown in Figure 3-8A, the α-phosphate of GDP is recognized not only by the P-loop, but also by the side chain of R71 (R65 in *S. cerevisiae* eEF-2 and R59 in *E. coli* EF-G) in the Switch I. R71 is highly conserved in all GTPases (Figure 3-7) and it is known that the *E. coli* mutant of R59A

(which corresponds to R71 of *Pho*EF-2) reduces GTPase activity on the ribosome and causes a defect in promoting translocation (54, 56).

The Switch II is composed of a highly conserved loop that changed its conformation to interact with the γ-phosphate of GMPPCP by H101 and the following helix in the *Pho*EF-2-GMPPCP structure (Figures 3-6 and 3-8A). The structural comparison of the GTP binding site between *Pho*EF-2-GMPPCP and *Pho*EF-2-Apo showed that the Switch II had a large conformational change (Figure 3-8B). The H101 of *Pho*EF-2-Apo which was away from that of *Pho*EF-2-GMPPCP bound γ-phosphate of GMPPCP contacted to Cβ atom of F104 (Figure 3-8B). Moreover, the residue F104 of the *Pho*EF-2-GMPPCP interacted with both residues of L442 (domain III) and W693 (domain V), that of *Pho*EF-2-Apo contacted to only the L442 (Figure 3-8B), implying that this difference of the binding manners was affected by the rotations of the domains III-V of *Pho*EF-2 (Figure 3-5A).

The guanine base of GMPPCP or GDP is sandwiched between the side chains of K152 and D154 of the G4 motif, and S207 of the G5 motif (Figure 3-6).

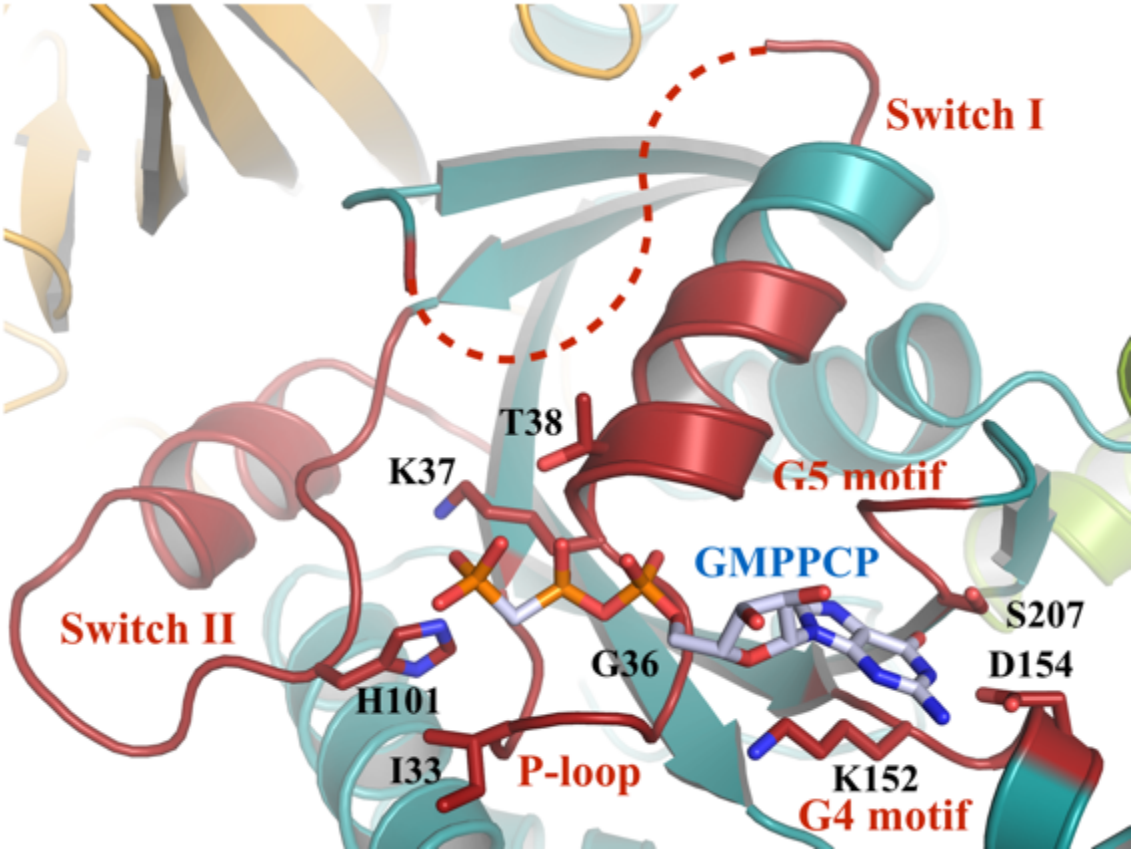

Figure 3-6. Structure of the GTP binding site of *Pho*EF-2-GMPPCP. EF-2 and the GMPPCP and the side chains of residues that are involved in GMPPCP binding are represented by ribbon and stick models, respectively. The O and N atoms are colored red and blue, respectively. The P-loop, Switch I region, Switch II region, G4 motif, and G5 motif (including C atoms of the side chains) are colored red. The C atoms of GMPPCP are colored pale blue. The disorder region of the Switch I is shown in a broken line.

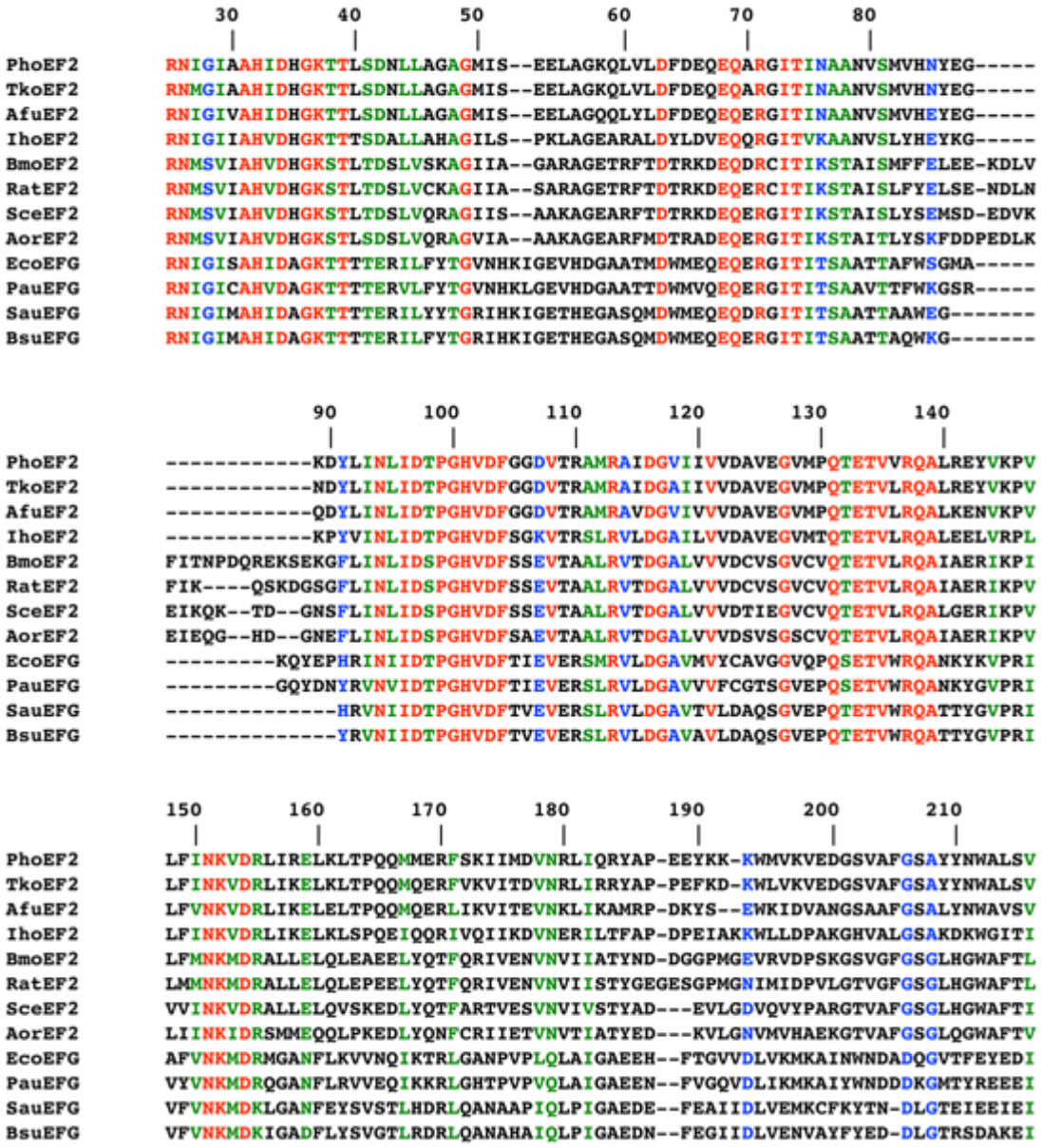

Figure 3-7. Sequence alignments of the GTP binding site among aEF-2, eEF-2, and EF-G. The sequences of the following GTP binding sites were compared: aEF-2 from *Pyrococcus horikoshii* (Pho), *Thermococcus kodakarensis* (Tko), *Archaeoglobus fulgidus* (Afu), and *Ignicoccus hospitalis* (Iho); eEF-2 from *Bombyx mori* (Bmo), *Rattus norvegicus* (Rat), *Saccharomyces cerevisiae* (Sce),

and *Aspergillus oryzae (Aor); and EF-G from Escherichia coli (Eco), Pseudomonas aeruginosa (Pau), Staphylococcus aureus (Sau), and Bacillus subtilis (Bsu).* The amino acid residues between aEF-2, eEF-2, EF-G are colored as follows: completely identical, red; strongly similar, green; weakly similar, blue.

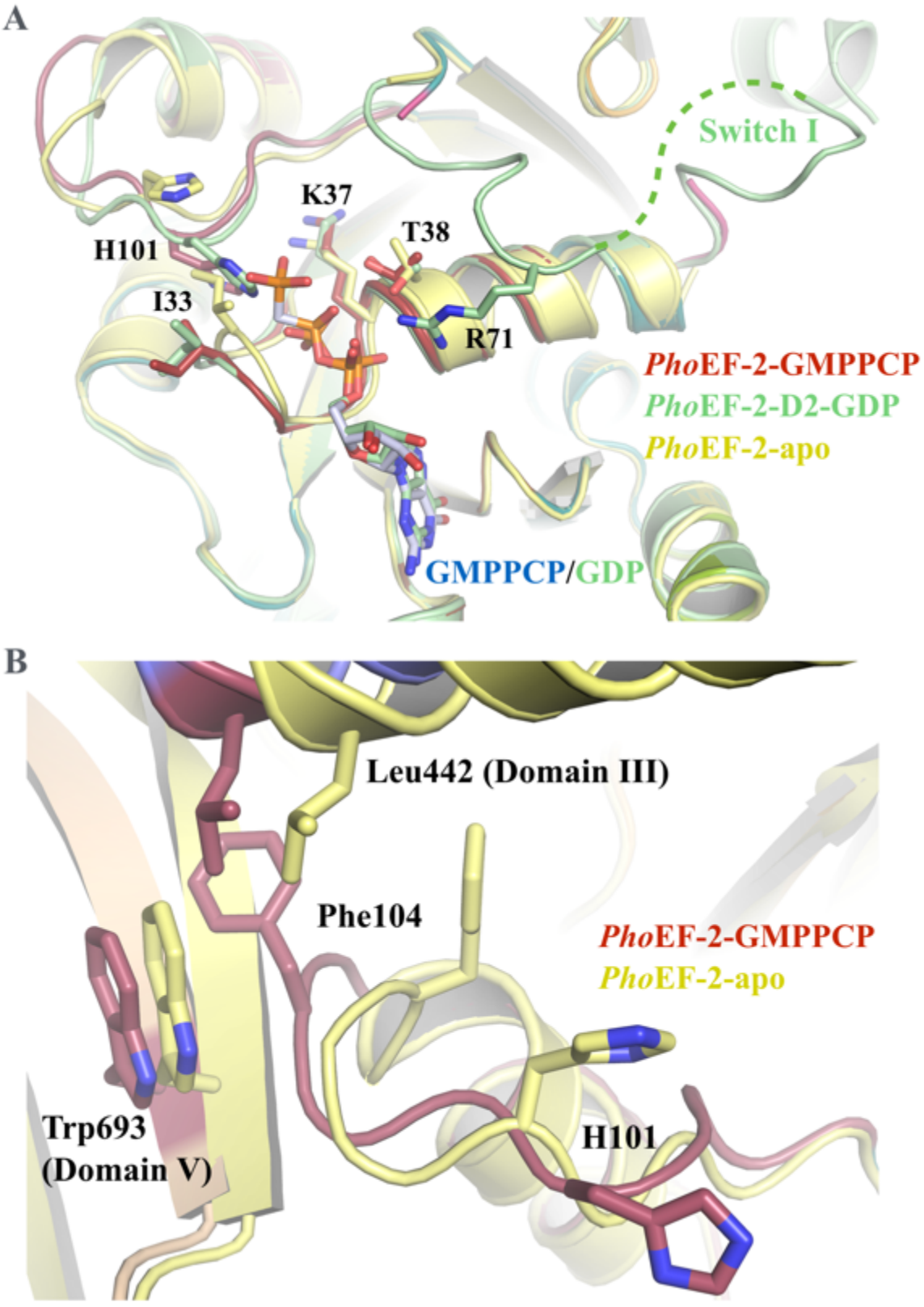
A
Switch I
K37
T38
H101
I33
R71
PhoEF-2-GMPPCP
PhoEF-2-D2-GDP
PhoEF-2-apo
GMPPCP/GDP
B
Leu442 (Domain III)
Phe104
PhoEF-2-GMPPCP
PhoEF-2-apo
Trp693
(Domain V)
H101

Figure 3-8. Detailed views of the GTP binding site in its different forms. EF-2 and GMPPCP, GDP, and the side chains of residues that are involved in GMPPCP or GDP binding are represented by ribbon and stick models, respectively. The O and N atoms are colored red and blue, respectively. (**A**) Structural comparison of the GTP binding sites of *Pho*EF-2-Apo (pale yellow), *Pho*EF-2-D2-GDP (pale green), and *Pho*EF-2-GMPPCP (red) by superposing domain G. The C atom of GMPPCP and GDP is colored pale blue and pale green, respectively. The residues that changed conformation are labeled. (**B**) Detailed view of the structural comparison of the Switch II between *Pho*EF-2-Apo (pale yellow) and *Pho*EF-2-GMPPCP (red). The residues that changed conformation are labeled.

3. Crystal structure of *Pho*EF-2 complexed with P1CTD

To reveal the recognition mechanism of *Pho*EF-2 by P1CTD, we determined the crystal structure of *Pho*EF-2-GMPPCP in a complex with the C-terminal fragment of P1 (*Pho*EF-2-GMPPCP-P1C11) at a resolution of 3.1 Å (Figure 3-9A). Both two molecules in the asymmetric unit (molecules A and B) bound to GMPPCP and P1C11 (Figure 3-9A). The final model of the *Pho*EF-2-GMPPCP-P1C11 complex contained residues 1–735 of *Pho*EF-2 and 98–108 of P1C11. The disorder region in molecule A is N-terminal 11 residues, and residues 51–75 and 304–308 of *Pho*EF-2, and N-terminal two residues of P1C11; while that of molecule B is N-terminal ten residues, and C-terminal two residues, and residues 51–76 and 305–310 of *Pho*EF-2, and N-terminal one residue of P1C11.

The complex structure of *Pho*EF-2-GMPPCP-P1C11 revealed that P1C11 formed an α-helix (Figure 3-9A), and bound hydrophobically to a groove formed by the domain G and the subdomain G′ of *Pho*EF-2 (Figures 3-9B and 3-9C), which is a different binding position from that of *Pho*EF-1α (57) and bacterial EF-G (17, 18). The sequence of P1CTD from *Pyrococcus horikoshii* is well conserved in other archaeal and eukaryotic organisms (aP1 from *Thermococcus kodakarensis* (*Tko*), and *Archaeoglobus fulgidus* (*Afu*); eukaryotic P1 from *Bombyx mori*, *Rattus norvegicus*, and *Saccharomyces cerevisiae*), especially, the sequences of archaeal P1C11 fragment are almost identified (Figure 3-11A). Domain G of *Pho*EF-2 is involved mainly in the formation of the P1C11 binding groove, while the subdomain G′ interacts directly with P1C11, as indicated by the gel mobility shift assay described below (Figures 3-10A and 3-12). In *Pho*EF-2-GMPPCP-P1C11, three C-terminal residues that are crucial for binding GTPases (L103,

L106, and F107 of P1C11) (Table 2) (15) were located on the same surface of the α-helix and were bound to the hydrophobic groove between domain G and subdomain G′ of *Pho*EF-2 (Figures 3-10A, 3-11A). Furthermore, G102 of P1C11 was first shown to contribute to the interaction with *Pho*EF-2 (Figure 3-10A). These four key residues of P1 were recognized by residues of domain G (P164, M167, M168, F171, V198, and F205) and subdomain G′ (L214, V216, M219, K225, F226, and N227 of *Pho*EF-2) (Figures 3-10A and B). The sequence of the P1-binding region of *Pho*EF-2 is well conserved in archaeal as well as that of the binding partner, P1CTD (Figure 3-11B). In twelve P1-binding residues, six residues P164, M167, V198, F205, L216, and F226 are completely identical, and five residues M168, F171, L214, M219, and N227 are strongly similar in archaea. Only 225th residue is different from three organisms such as lysine in *Pho*EF-2, serine in *Tko*EF-2, and glycine in *Afu*EF-2 (Figure 3-11B). On the other hand, the P1-binding sequence of *Pho*EF-2 is not conserved in other eEF-2 and EF-G at all (Figure 3-11C). As mentioned above, it is known that bacterial stalk L12CTD which contains of three β strands and two α helices, recognizes specific region of the subdomain G' of EF-G (17, 18), and subdomains between EF-G and aEF-2 are not identified entirely as well as the sequences and structures of stalk in both kingdoms (Figure 1-6). Although the sequence similarity between *Pho*EF-2 and *Sce*EF-2 is high (approximately 63 %) and P1 recognizes both molecules, the size of subdomain G' of *Pho*EF-2 is much smaller than that of *Sce*EF-2 from crystal structures (Figure 3-3). From the sequence alignment as shown in Figure 3-3B, most of the subdomain G' of *Sce*EF-2 was inserted into original archaeal EF-2 during evolution. Therefore, the corresponding position of the P1-binding region of *Pho*EF-2 was covered with the subdomain G' of *Sce*EF-2.

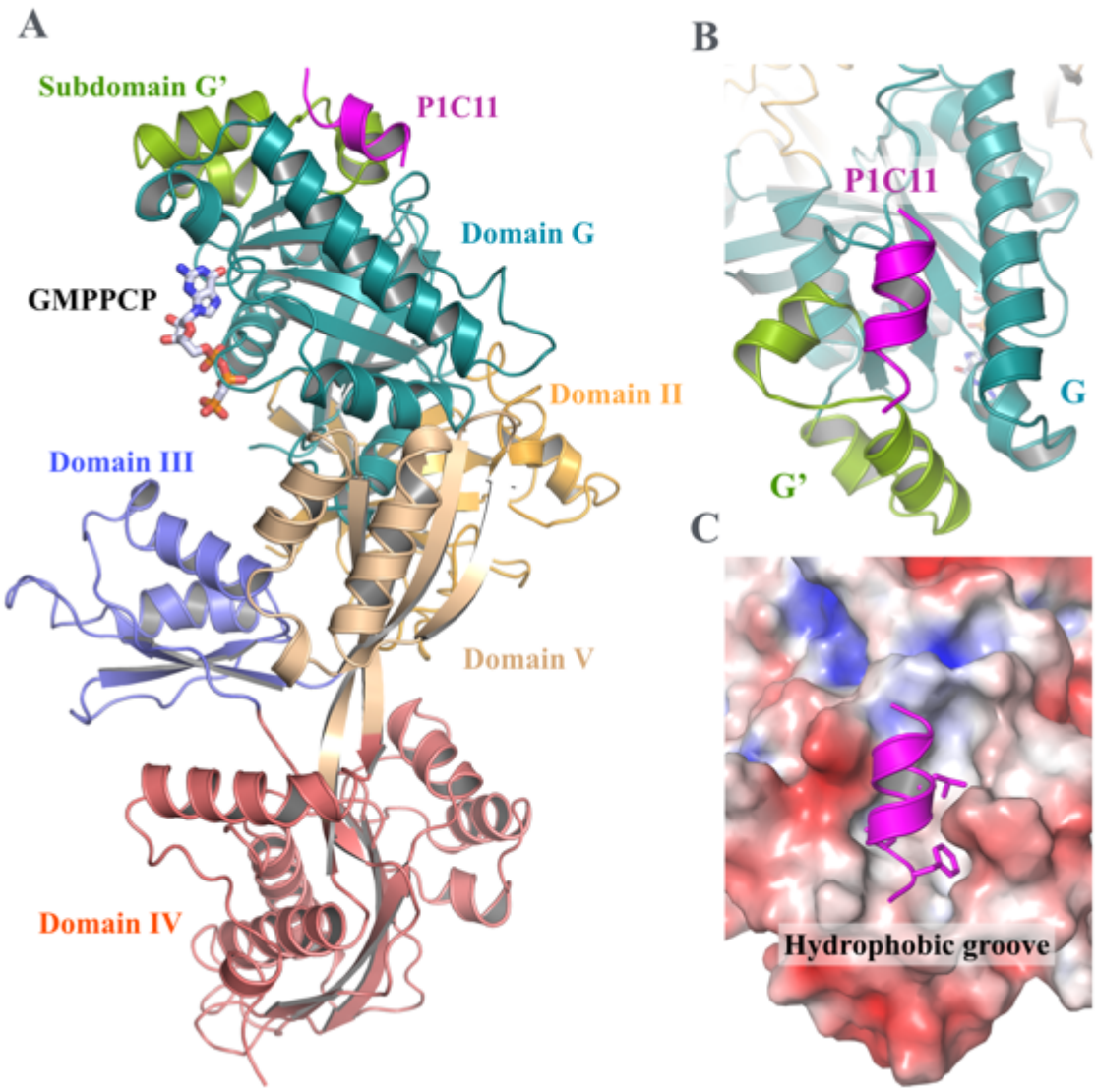

Figure 3-9. Structure of *Pho*EF-2-GMPPCP in a complex with the 11 C-terminal residues of P1 (*Pho*EF-2-GMPPCP-P1C11). (**A**) Overall structure of *Pho*EF-2-GMPPCP- P1C11. *Pho*EF-2 and GMPPCP are shown in the same way as in Figure 3-1. P1C11 is represented by a ribbon model (magenta). (**B**) Diagram illustrating how P1C11 was bound to a groove between subdomain G′ and domain G. (**C**) The electrostatic molecular surface of the P1 binding groove of *Pho*EF-2. Positive, negative, and neutral electrostatic surface potentials are

shown in blue, red, and white, respectively. The residues L103, L106, and F107 of P1C11, which are critical for binding *Pho*EF-2 (15), are represented by stick models.

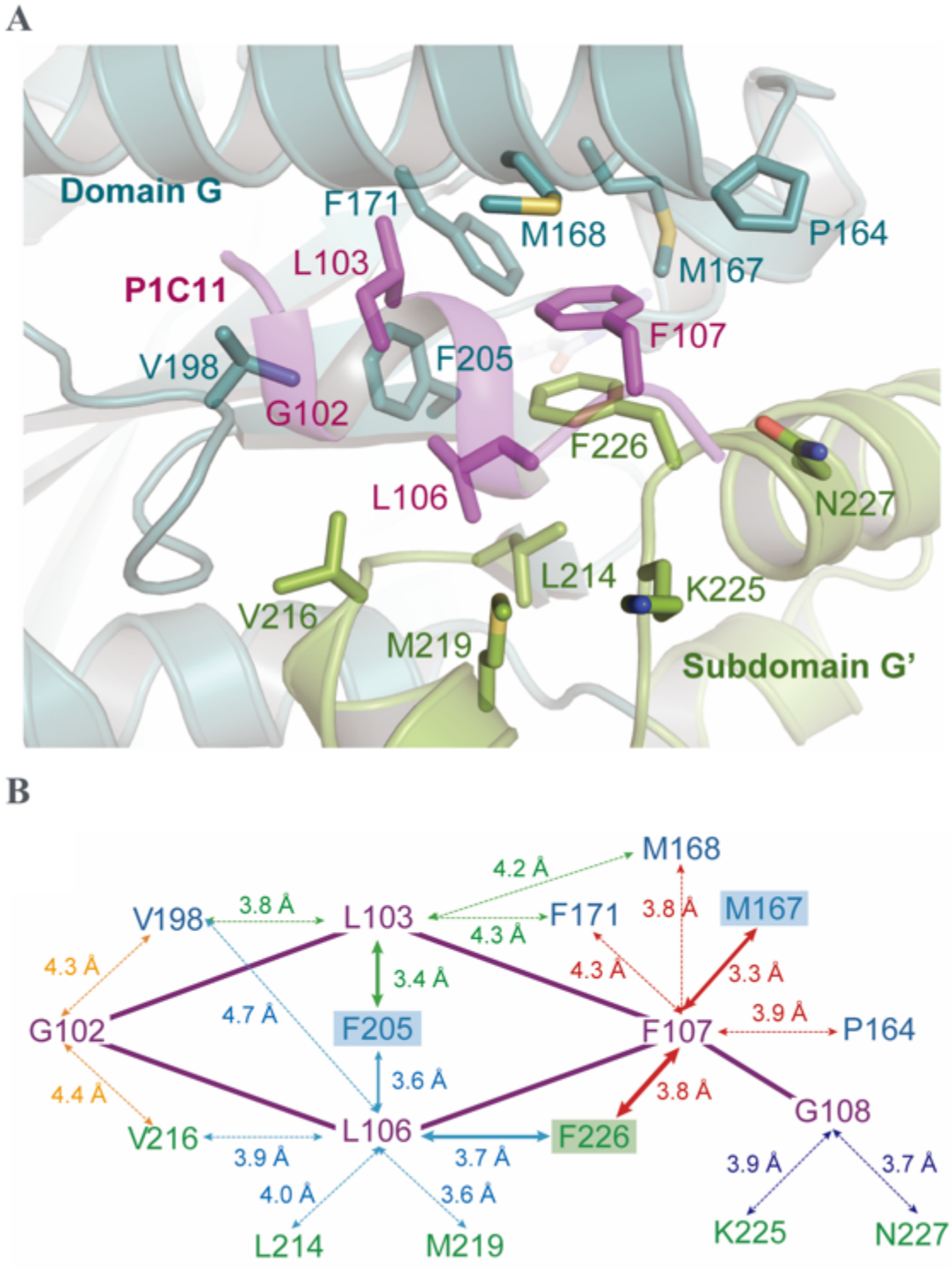

Figure 3-10. Structural details of the interaction between *Pho*EF-2 and P1. (**A**) Close-up view of the structure of the P1C11 binding groove. The side chains of

residues of P1C11 and *Pho*EF-2 that are involved in the interaction are represented by stick models. The S atoms are colored yellow. *Pho*EF-2 and P1C11 are colored in the same way as in Figure 3-9. Residue G102 of P1C11 contacted residues V198 (domain G) and V216 (subdomain G′) of *Pho*EF-2. Residue L103 of P1C11 interacted with residues M168, F171, V198, and F205 (domain G). Residue L106 of P1C11 interacted with residues V198 and F205 (domain G), and residues L214, V216, M219, and F226 (subdomain G′). Finally, residue F107 bound to residues P164, M167, M168, and F171 (domain G), and residue F226 (subdomain G′). (**B**) Schematic overview of the interaction between P1C11 and *Pho*EF-2. The color-coding of labels is the same as in (A). The dashed-arrows indicate the stacking interactions.

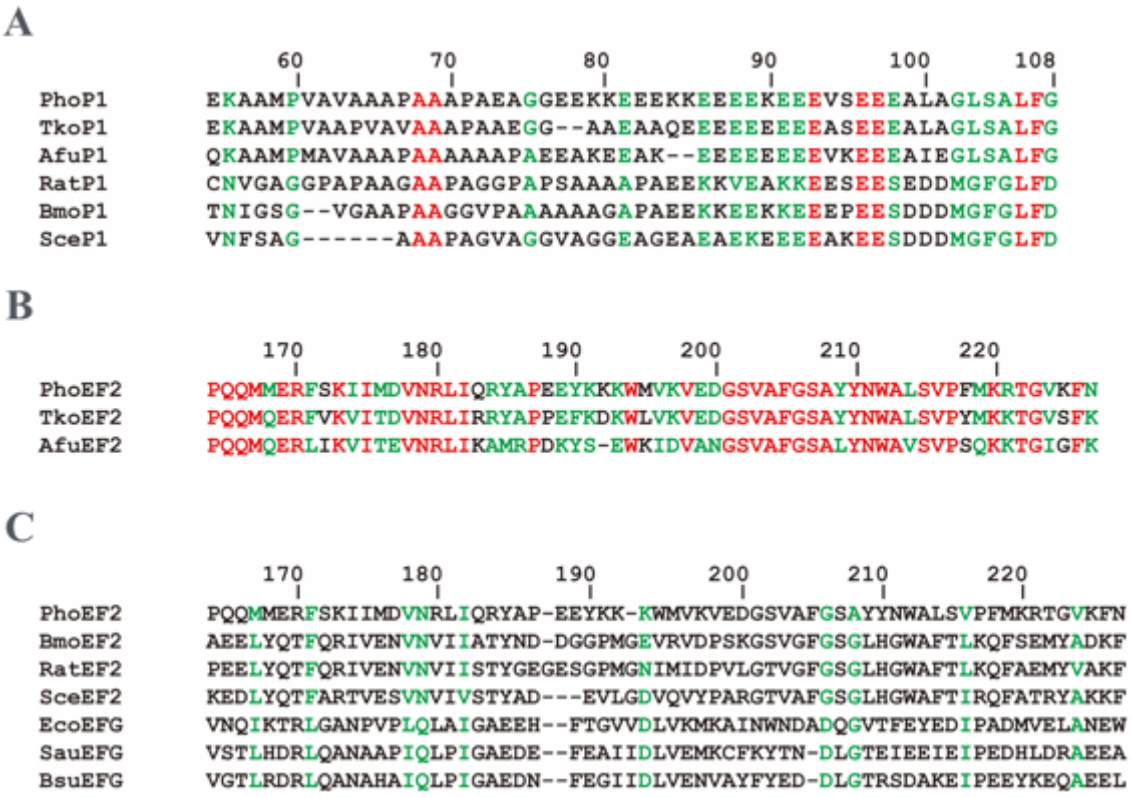

Figure 3-11. Sequence alignments of the C-terminal region of P1 and the P1-binding region among aEF-2 in several archaeal organisms, or aEF-2, eEF-2, and EF-G. (**A**) The sequences of the following the C-terminal domain of P1 (P1CTD) in archaea and eukaryote were compared: aP1 from *Pyrococcus horikoshii* (Pho), *Thermococcus kodakarensis* (Tko), and *Archaeoglobus fulgidus* (Afu); P1 of P1-P2 heterodimer from *Bombyx mori* (Bmo), *Rattus norvegicus* (Rat), and *Saccharomyces cerevisiae* (Sce). (**B**) The sequences of the following P1-binding region of aEF-2 were compared: Pho, Tko, and Afu (**C**) The sequences of the following P1-binding region were compared: aEF-2 from Pho; eEF-2 from Bmo, Rat, and Sce; and EF-G from Eco, Pau, and Sau. The amino acid residues between aEF-2, eEF-2, EF-G are colored as follows: completely identical, red; strongly similar, green.

Among the P1-binding residues, the side chain of F226 in subdomain G' exhibited π-stacking and hydrophobic interactions with L106 and F107 of P1C11 at distances of approximately 3.7 and 3.8 Å, respectively (Figures 3-10B and 3-12M). The structure also revealed that M167 of domain G, contacted to F107 of P1C11 with a distance of 3.3 Å (Figures 3-10B and 3-12M). Similarly, F205 in domain G interacted hydrophobically with P1C11 L103 and L106 at distances of approximately 3.4 and 3.6 Å, respectively (Figures 3-10B and 3-12M).

4. Interaction between *Pho*EF-2 and P1CTD

In order to validate the structural information of these interactions, we performed mutation analysis using a gel-mobility shift assay for 12 residues of *Pho*EF-2 (P164, M167, M168, F171, V198, and F205 in domain G; L214, V216, M219, K225, F226, and N227 in subdomain G') (Table 1 and Figures 3-10A and 3-10B). Circular dichroism spectroscopy was used to confirm that there were no significant conformational changes between the wild-type (Figures 3-12I) and the following three mutants F226S (Figures 3-12J), L214S/V216S (Figures 3-12K), and V198S/L214S/V216S (Figures 3-12L). One of the P1-binding residues, F226S completely disrupted P1-binding (Figures 3-12C, 3-12N, and 3-12G), highlighting that it plays the crucial role of F226 in P1-binding. Furthermore, the *Pho*EF-2 mutants M167S or F205S also partially affected the binding affinity of P1 (Figures 3-12A, 3-12B, and 3-12N), suggesting that M167 and F205 not only play a role in hydrophobic groove formation but also exhibit an important interaction with P1 (Figures 3-9C, 3-10A, 3-10B, and 3-12M).

Although the residues P164, M168, F171, and V198 in domain G, and L214, V216, and M219 in subdomain G' are involved in P1C11-binding hydrophobic groove formation, no effects were detected for the point mutations P164S, M168S, F171S, V198S, and M219S, and even the double mutation L214S/V216S (Figures 3-12D, 3-12E, 3-12N, and Table 1). However, *Pho*EF-2 mutants with multiple amino acid substitutions (P164S/M167S, M168S/V198S, or V198S/L214S/V216S) completely disrupted P1-binding (Figure 3-12F), as they worked together to form the hydrophobic binding groove of *Pho*EF-2 (Figures 3-10A and 3-10B). Furthermore, The binding assay between *Pho*EF-2 and P1 mutant G102S was also performed by Native-PAGE, showing that G102S completely disrupted binding to *Pho*EF-2 as well as other three residues of P1, L103, L106, and F107 (Figures 3-10A, 3-10B, 3-13A, 3-13B, and Table 2) (15). On the other hand, the structure of *Pho*EF-2-GMMPPCP-P1C11 showed that only two charged and hydrophilic residues K225 and N227 in subdomain G' are located around the hydrophobic groove close to G108 of the C-terminal residue of P1, but no interaction because the lengths between G108 and K225 or N227 are 3.9 Å and 3.7 Å, respectively (Figures 3-10A and 3-10B) and these lengths cannot form hydrogen bonds. Following the suggestion, we mutated K225S and N227S of *Pho*EF-2 and ΔC1 that is deleted the C-terminus of P1 (ΔG108) for the gel-mobility shift assay. The results showed that K225S and N227S did not detect the effect of P1-binding (Figures 3-12D, 3-12N, and Table 1), and ΔC1 of P1 did not affect the P1-binding affinity (Figures 3-13C, 3-13D, and Table 2). Previously the mutants of the side chain of G108, G108D and G108A did also not detect the effect of the interaction with *Pho*EF-2 (Figure 3-13E and Table 2) (15). Thus, no hydrophilic residue around the P1-binding groove of *Pho*EF-2 involves in the interaction of P1 (Figures 3-10A, 3-10B, 3-12E, and Table 1).

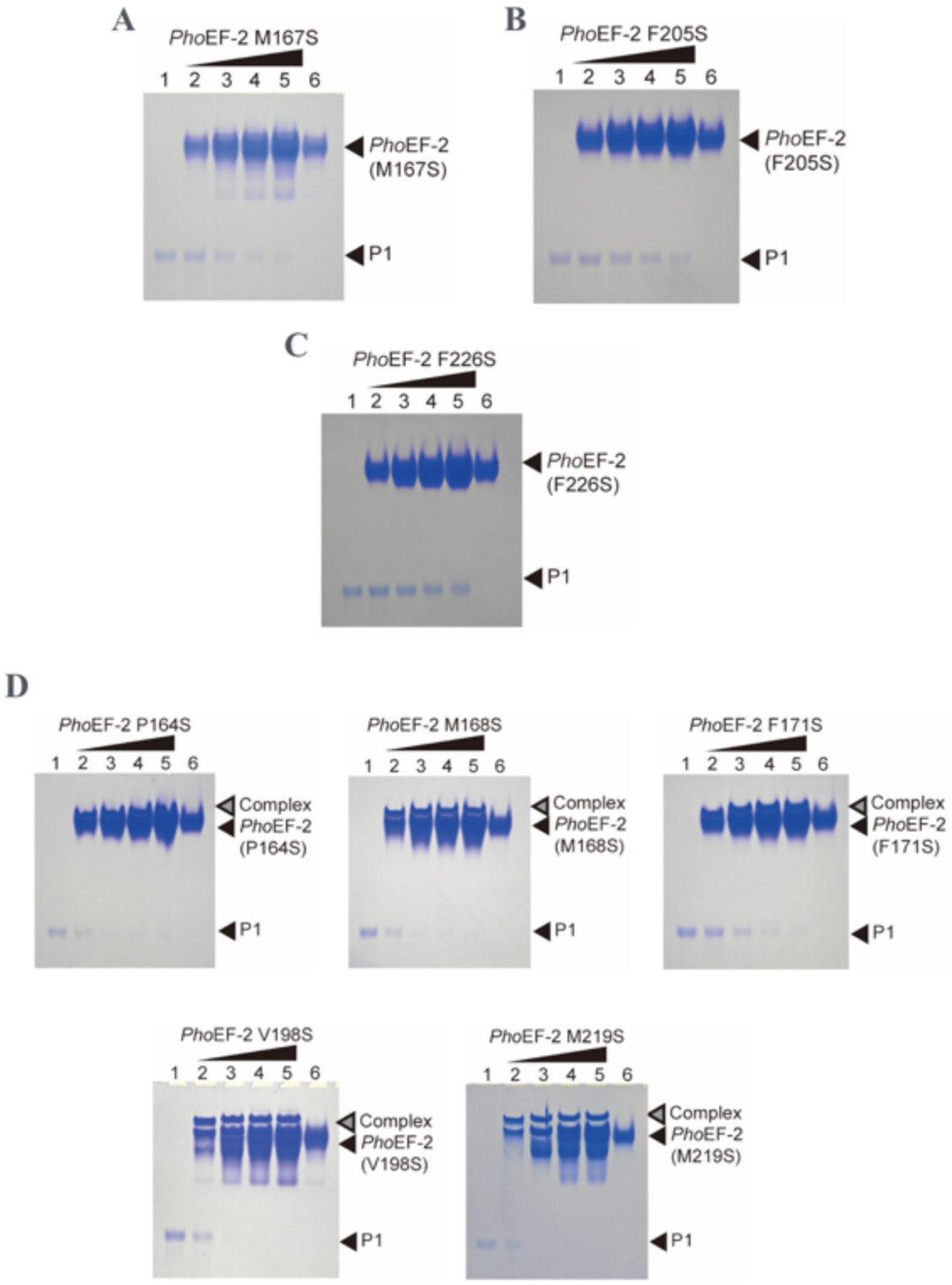
A
PhoEF-2 M167S
1 2 3 4 5 6
PhoEF-2 (M167S)
P1
B
PhoEF-2 F205S
1 2 3 4 5 6
PhoEF-2 (F205S)
P1
C
PhoEF-2 F226S
1 2 3 4 5 6
PhoEF-2 (F226S)
P1
D
PhoEF-2 P164S
1 2 3 4 5 6
Complex
PhoEF-2 (P164S)
P1
PhoEF-2 M168S
1 2 3 4 5 6
Complex
PhoEF-2 (M168S)
P1
PhoEF-2 F171S
1 2 3 4 5 6
Complex
PhoEF-2 (F171S)
P1
PhoEF-2 V198S
1 2 3 4 5 6
Complex
PhoEF-2 (V198S)
P1
PhoEF-2 M219S
1 2 3 4 5 6
Complex
PhoEF-2 (M219S)
P1

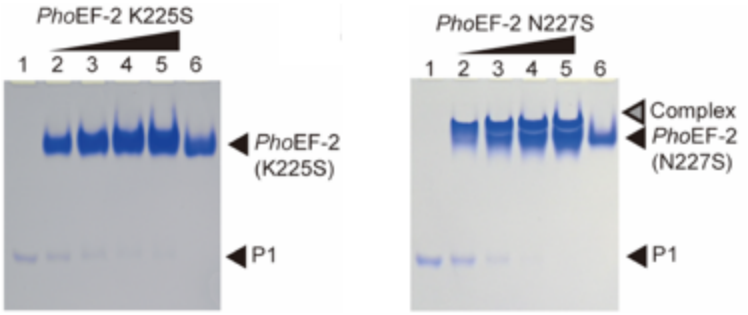
PhoEF-2 K225S
1 2 3 4 5 6
PhoEF-2 (K225S)
P1
PhoEF-2 N227S
1 2 3 4 5 6
Complex
PhoEF-2 (N227S)
P1

E

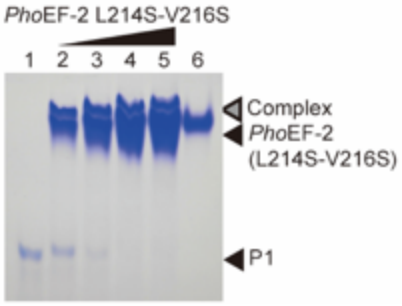
PhoEF-2 L214S-V216S
1 2 3 4 5 6
Complex
PhoEF-2 (L214S-V216S)
P1

F

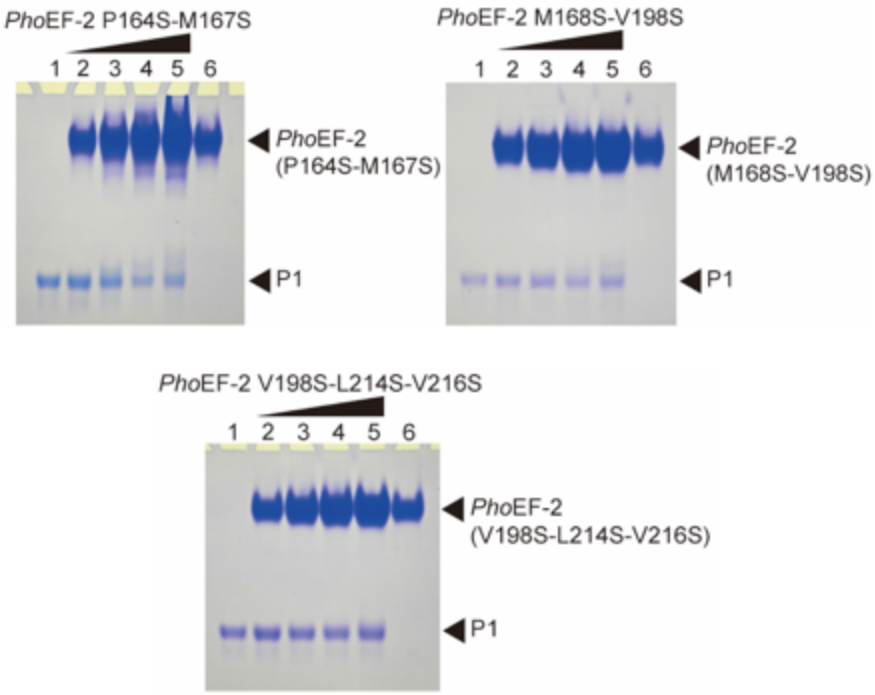
PhoEF-2 P164S-M167S
1 2 3 4 5 6
PhoEF-2 (P164S-M167S)
P1
PhoEF-2 M168S-V198S
1 2 3 4 5 6
PhoEF-2 (M168S-V198S)
P1
PhoEF-2 V198S-L214S-V216S
1 2 3 4 5 6
PhoEF-2 (V198S-L214S-V216S)
P1

G

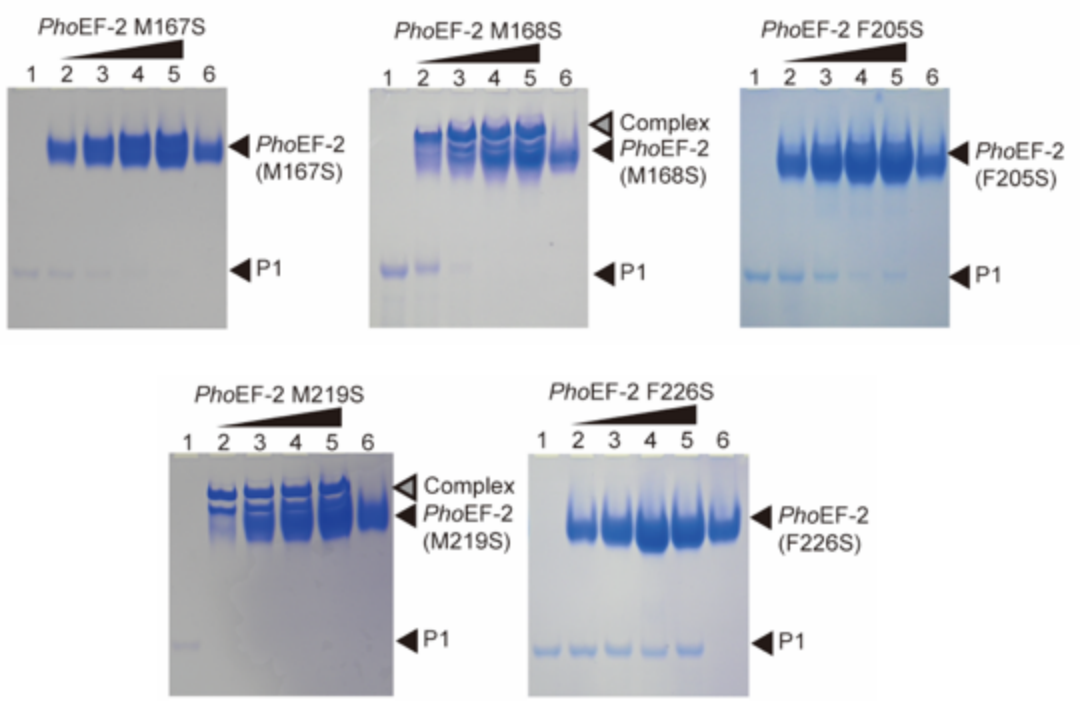
PhoEF-2 M167S
1 2 3 4 5 6
PhoEF-2 (M167S)
P1
PhoEF-2 M168S
1 2 3 4 5 6
Complex
PhoEF-2 (M168S)
P1
PhoEF-2 F205S
1 2 3 4 5 6
PhoEF-2 (F205S)
P1
PhoEF-2 M219S
1 2 3 4 5 6
Complex
PhoEF-2 (M219S)
P1
PhoEF-2 F226S
1 2 3 4 5 6
PhoEF-2 (F226S)
P1

H

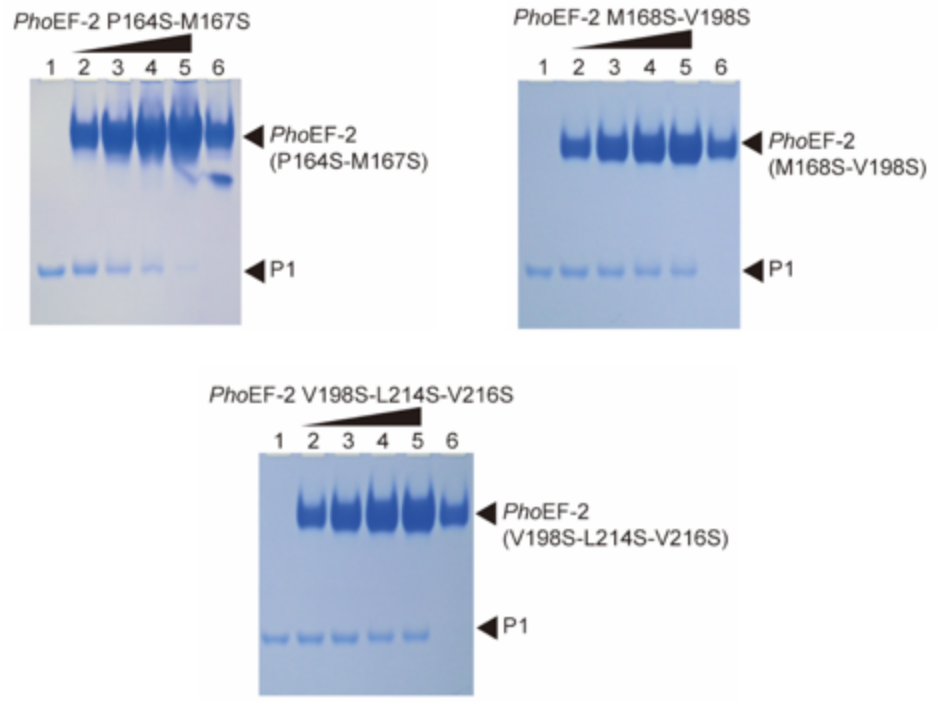
PhoEF-2 P164S-M167S
1 2 3 4 5 6
PhoEF-2 (P164S-M167S)
P1
PhoEF-2 M168S-V198S
1 2 3 4 5 6
PhoEF-2 (M168S-V198S)
P1
PhoEF-2 V198S-L214S-V216S
1 2 3 4 5 6
PhoEF-2 (V198S-L214S-V216S)
P1

I

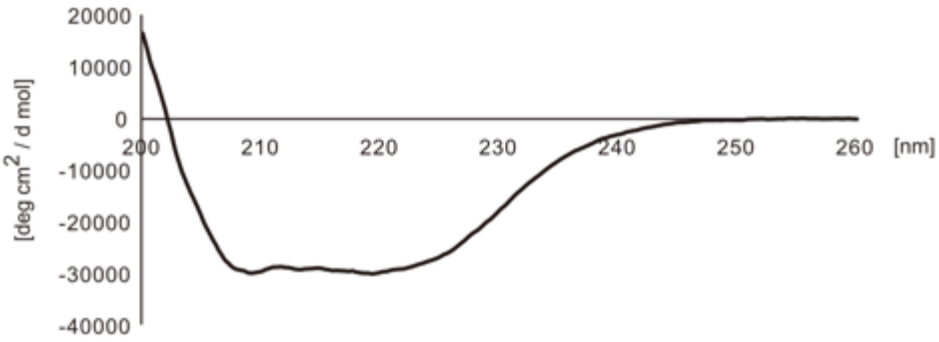
*Pho*EF-2 wild type
20000
10000
0
-10000
-20000
-30000
-40000
200
210
220
230
240
250
260
[nm]
[deg cm^2 / d mol]

J

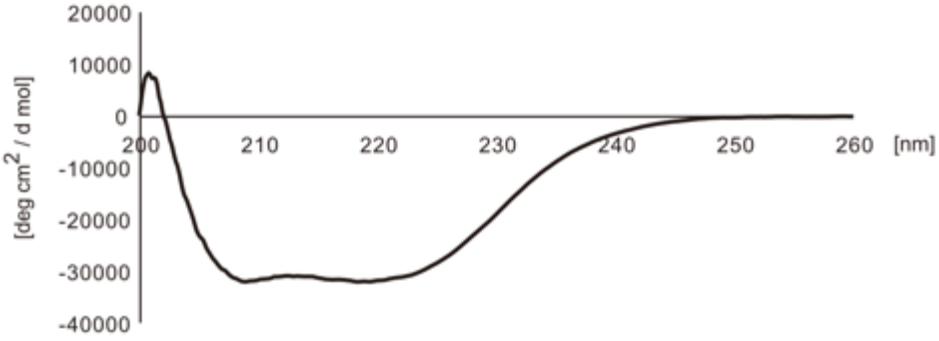
*Pho*EF-2 F226S
20000
10000
0
-10000
-20000
-30000
-40000
200
210
220
230
240
250
260
[nm]
[deg cm^2 / d mol]

K

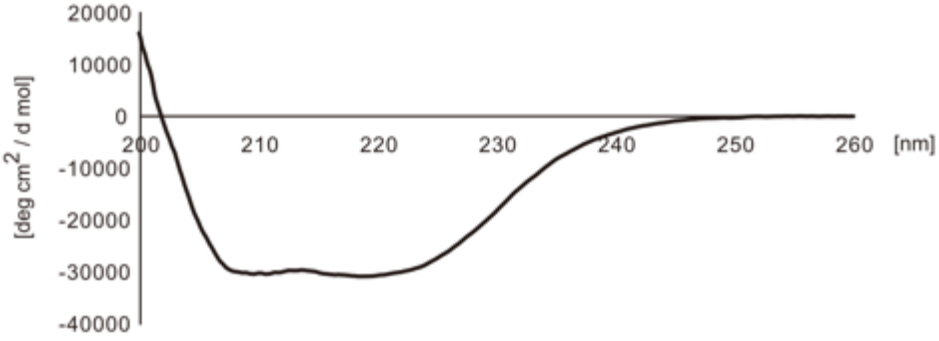
*Pho*EF-2 L214S/V216S
20000
10000
0
-10000
-20000
-30000
-40000
200
210
220
230
240
250
260
[nm]
[deg cm^2 / d mol]

L

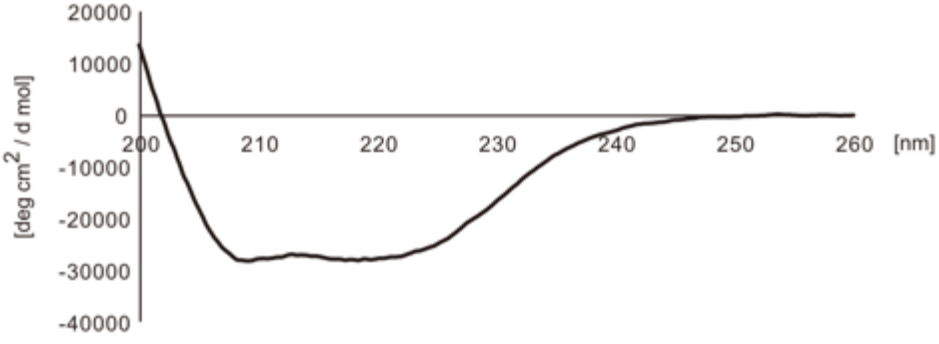
*Pho*EF-2 V198S/L214S/V216S
20000
10000
0
-10000
-20000
-30000
-40000
200
210
220
230
240
250
260
[nm]
[deg cm^2 / d mol]

M

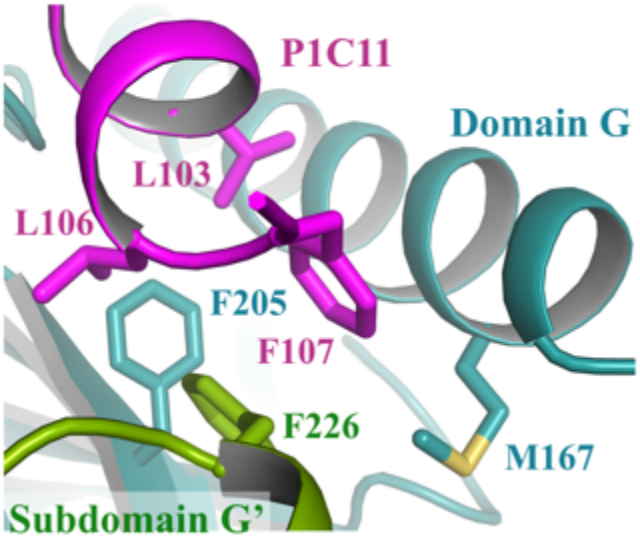

N

Binding assay	
*Pho*EF-2 mutant	P1 binding (GMPPCP/GDP)
Wild type	++
P164S	++
M167S	+/+
M168S	++/++
F171S	++
V198S	++
F205S	+/+
L214S/V216S	++
M219S	++/++
K225S	++
F226S	-/-
N227S	++
P164S/M167S	-/-
M168S/V198S	-/-
V198S/L214S/ V216S	-/-

Figure 3-12. P1-binding analysis of GMPPCP-bound or GDP-bound *Pho*EF-2 using point mutants, and the secondary structures of *Pho*EF-2 and its mutants. (**A**)–(**C**) P1-Binding analyses of the GMPPCP-bound form of *Pho*EF-2 single point mutations M167S (**A**), F205S (**B**), and F226S (**C**). (**D**) Binding assays between P1 and the other single point variants of *Pho*EF-2-GMPPCP P164S, M168S, F171S, V198S, M219S, K225S, and N227S. (**E**) Binding assay between P1 and the *Pho*EF-2-GMPPCP double mutant L214S-V216S. (**F**) Binding assays between P1 and the *Pho*EF-2-GMPPCP mutants (double or ternary mutant) P164S-M167S, M168S-V198S, and V198S-L214S-V216S. (**G**) Binding assays between P1 and GDP-bound form of *Pho*EF-2 mutants M167S, M168S, F205S, M219S, and F226S which involved in the interaction and recognition of P1C11 by the gel-mobility shift assays between P1 and GMPPCP-form of *Pho*EF-2 (A)–

(C) and changing conformations between the crystal structures of *Pho*EF-2-GMPPCP and *Pho*EF-2-GMPPCP-P1C11. (**H**) Binding assays between P1 and the *Pho*EF-2-GDP mutants (double or ternary mutant) P164S-M167S, M168S-V198S, and V198S-L214S-V216S as well as (F). In these gel-mobility shift assays, the homodimer of P1 (100 pmol) was incubated without the *Pho*EF-2 mutants (lane 1), or with 100 pmol (lane 2), 200 pmol (lane 3), 300 pmol (lane 4), or 400 pmol (lane 5) of the *Pho*EF-2 mutants in 5 μL solution at 70 °C. Each *Pho*EF-2 mutant (100 pmol) was also incubated without P1 (lane 6). (**I**)-(**L**) The secondary structures of wild type and some mutants of *Pho*EF-2. Four of *Pho*EF-2 wild type (I) and its mutants, F226S (J), L214S-V216S (K), V198S-L214S-V216S (L), which curves were colored black, were investigated their secondary structures by Circular dichroism (CD) spectrometry. The vertical axis of the graph is [deg cm^2 / d mol] and the horizontal axis is wavelength from 200 Å to 260 Å. All CD spectrometry of them are almost similar, indicated no significant conformational changes between *Pho*EF-2 and its mutants. (**M**) Detailed view of the interaction between M167, F205, and F226 of *Pho*EF-2 and G102, L103, L106, and F107 of P1C11 in the *Pho*EF-2-GMPPCP-P1C11 crystal structure. The side chains of these residues are represented by stick models. S atom of M167 is colored yellow. (**N**) Comparison of the P1 binding ability of the GMPPCP-form or GDP-form of all of *Pho*EF-2 mutants in this study. The binding ability of each mutant is displayed as ++ (comparable to the wild type), + (less similar to the wild type), or – (undetectable).

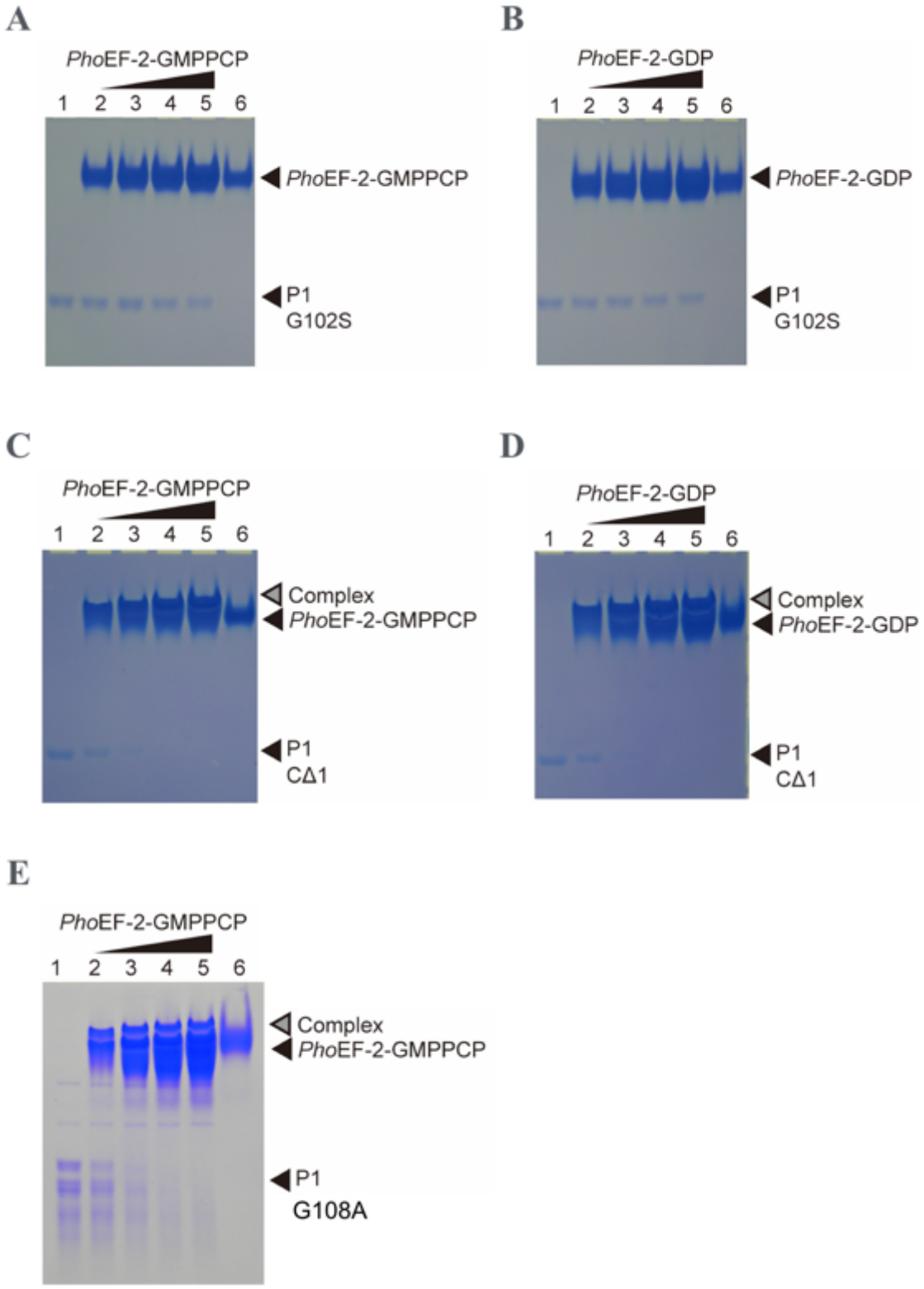
A
PhoEF-2-GMPPCP
1 2 3 4 5 6
PhoEF-2-GMPPCP
P1
G102S
B
PhoEF-2-GDP
1 2 3 4 5 6
PhoEF-2-GDP
P1
G102S
C
PhoEF-2-GMPPCP
1 2 3 4 5 6
Complex
PhoEF-2-GMPPCP
P1
CΔ1
D
PhoEF-2-GDP
1 2 3 4 5 6
Complex
PhoEF-2-GDP
P1
CΔ1
E
PhoEF-2-GMPPCP
1 2 3 4 5 6
Complex
PhoEF-2-GMPPCP
P1
G108A

Figure 3-13. *Pho*EF-2 binding analyses of P1 single point mutants by gel-mobility shift assays using Native-PAGE. (**A**)-(**B**) Binding assay between P1 single point mutant G102S and GMPPCP-bound (**A**) or GDP-bound (**B**) form of *Pho*EF-2. (**C**)-(**D**) Binding assay between the truncated variant of the P1 C-terminus CΔ1 and *Pho*EF-2-GMPPCP (**C**) or *Pho*EF-2-GDP (**D**). (**E**) Binding assay between P1 single point mutant G108A and *Pho*EF-2-GMPPCP. Homodimer of P1 mutant (100 pmol) was incubated without *Pho*EF-2 (lane 1), or with 100 pmol (lane 2), 200 pmol (lane 3), 300 pmol (lane 4), or 400 pmol (lane 5) of *Pho*EF-2 in 5 μL solution at 70 °C. *Pho*EF-2 (100 pmol) was also incubated without P1 mutant (lane 6).

Up to now, quantitative determination of the binding between ribosomal P stalk (P0-$[P1]_2[P1]_2[P1]_2$ complex or P1 dimer) and translational GTPases including *Pho*EF-2 has not been obtained, but only qualitative binding assays each other have detected. We performed the gel-mobility shift assays using Native-PAGE between P0-$[P1]_2[P1]_2[P1]_2$ complex and several forms of *Pho*EF-2: *Pho*EF-2-GMPPCP, *Pho*EF-2-GDP, and *Pho*EF-2-Apo and it was revealed that the P stalk-binding affinities of *Pho*EF-2-GMPPCP and *Pho*EF-2-GDP did not change (Figures 3-16A and 3-16B), however, that of *Pho*EF-2-Apo seemed to be slightly weaker than them (Figure 3-16C). We further precisely confirm the difference of P1-binding and dissociation rate analyses of *Pho*EF-2-GMPPCP, *Pho*EF-2-GDP, or *Pho*EF-2-Apo using BIACORE 3000 instrument as surface plasmon resonance (SPR) signal. Firstly, we confirmed the stabilities of *Pho*EF-2 with buffer F for SPR measurement (10 mM HEPES, 150 mM NaCl, 100 μM $MgCl_2$, 0.005 % polyoxyethylene sorbitan monolaurate, pH 7.4) by dynamic light scattering (DLS) as compared to original *Pho*EF-2 sample buffer E (20 mM Tris-HCl pH8.0, 100 mM KCl, 1 mM DTT) and buffer G (10 mM HEPES, 150 mM NaCl, 100 μM $MgCl_2$, pH 7.4) which was SPR buffer without the detergent 0.005 % polyoxyethylene sorbitan monolaurate (Figure 3-14). As the results of the SPR measurements, the difference in the dissociation of several forms of *Pho*EF-2 from P1 was not shown since the interactions with P1 have not only swift dissociation rate (Figures 3-15A, 3-15B, and 3-15C) but also weak and affinity and unstable interactions (Figures 3-15D, 3-15E, and 3-15F). Therefore, the estimated K_D value of the GDP-form was comparable with that of the GTP-form, although the k_{off} values could not be measured (Figures 3-15A, 3-15B, and 3-15C). The results showed that nucleotide-independent P1-binding affinity is extremely weak (only detected μM level), and dissociation of P1 from EF-2 is exceedingly fast. The K_D value

of *Pho*EF-2-GMPPCP or *Pho*EF-2-GDP on P1 was 5.06 μM or 4.05 μM, respectively, on the other hand, that of *Pho*EF-2-Apo was 12.7 μM (Figures 3-15D, 3-15E, and 3-15F). The affinity of *Pho*EF-2-Apo on P1 was comparably weaker than that of nucleotide-bound *Pho*EF-2 (Figure 3-15D), being in accord with the result of the gel-mobility shift assay between P0-$[P1]_2[P1]_2[P1]_2$ stalk and *Pho*EF-2-Apo (Figure 3-16C).

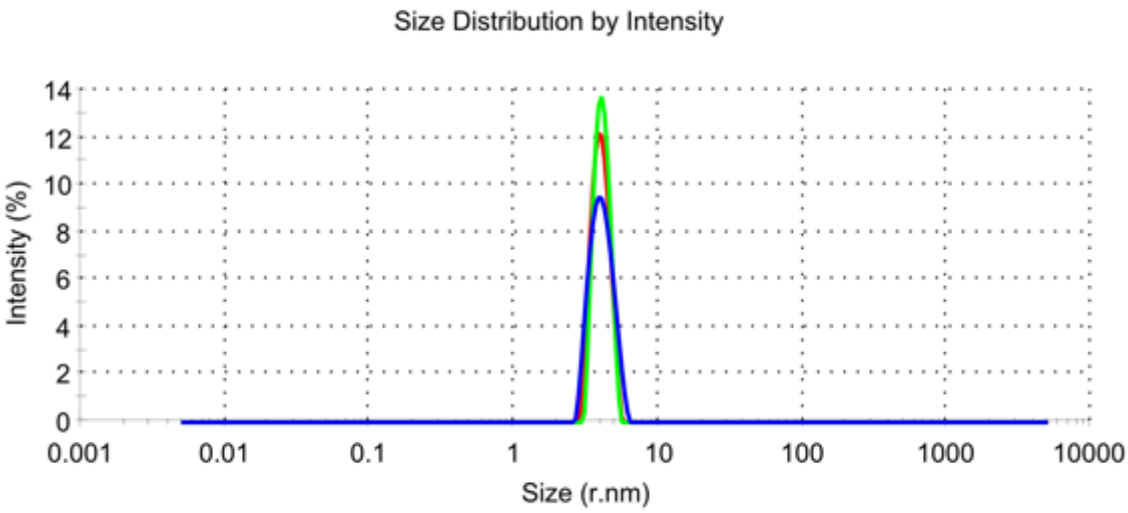

Figure 3-14. Confirming the stabilities of three *Pho*EF-2 buffers using dynamic light scattering (DLS). In the graph of size distribution by intensity, the lines of buffer E (20 mM Tris-HCl pH 8.0, 100 mM KCl, 1 mM DTT), buffer F (10 mM HEPES, 150 mM NaCl, 100 μM $MgCl_2$, 0.005 % polyoxyethylene sorbitan monolaurate, pH 7.4), and buffer G (10 mM HEPES, 150 mM NaCl, 100 μM $MgCl_2$) are colored green, blue, and red, respectively. The vertical axis is the intensity (%) of *Pho*EF-2 in each buffer, and the horizontal axis in the size (nm of radius) of the *Pho*EF-2 in the corresponding buffer condition.

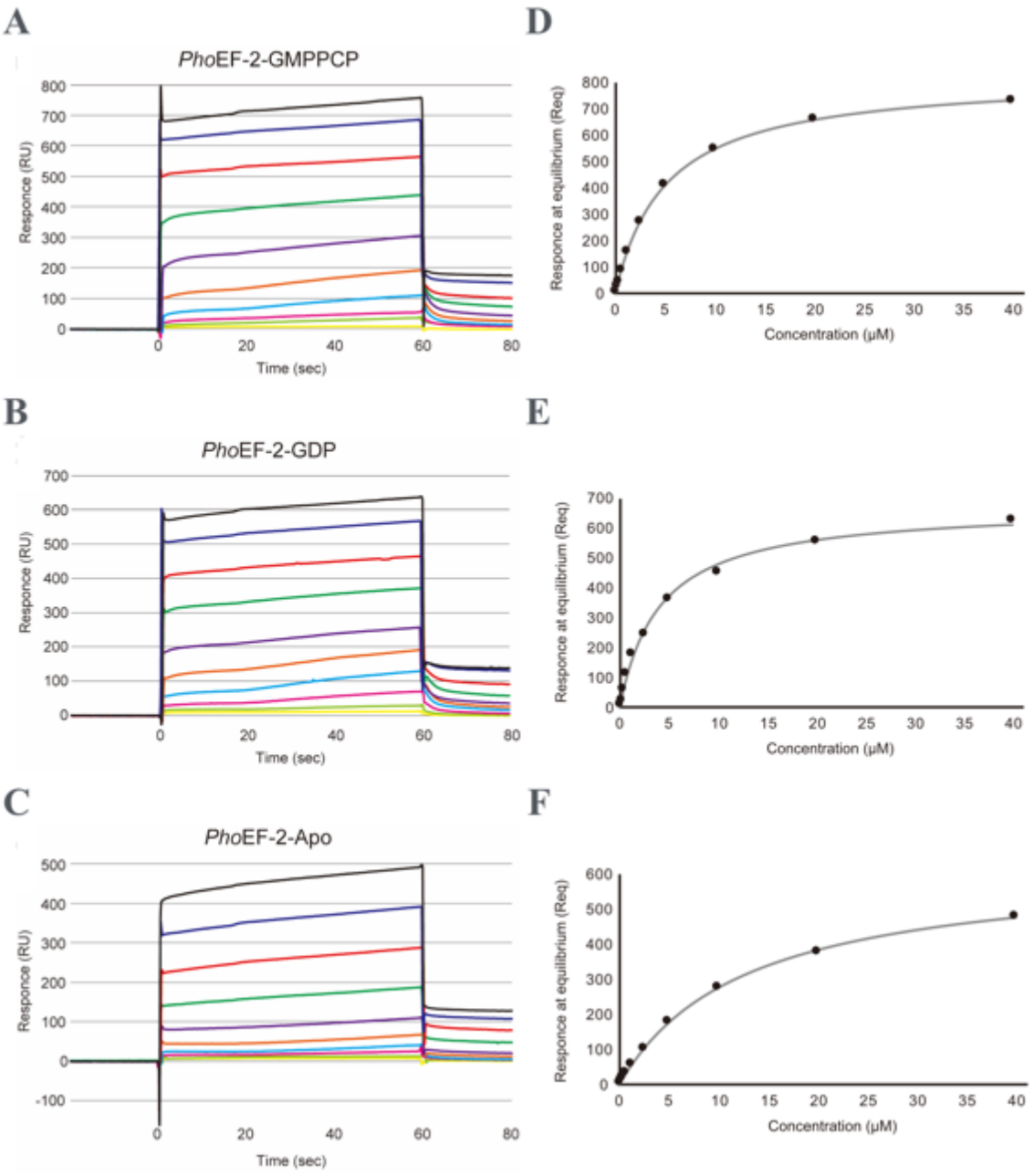

Figure 3-15. Quantitative binding assays between P1 and several forms of PhoEF-2 by surface plasmon resonance (SPR) technique using BIACORE 3000 instrument (GE Healthcare). (**A**)-(**C**) Sensorgrams of the kinetics to determine the P1 association and dissociation rates of *Pho*EF-2-GMPPCP (**A**), *Pho*EF-2-GDP

(**B**), and *Pho*EF-2-Apo (**C**). The vertical axis of the sensorgram is the binding response (RU) and the horizontal axis is the time (second) to flow the individual *Pho*EF-2 samples into the sensor chip CAP (GE healthcare) which was used for the immobilization of biotinylated P1. In each sensorgram, the lines of the signal which are colored black, blue, red, green, purple, orange, light blue, magenta, light green, yellow are represented by the individual concentrations (μM) which are 40, 20, 10, 5, 2.5, 1.25, 0.625, 0.312, 0.156, 0.078, respectively. (**D**)-(**F**) Affinity graphs between P1 and *Pho*EF-2-GMPPCP (**D**), *Pho*EF-2-GDP (**E**), and *Pho*EF-2-Apo (**F**). The vertical axis of the graph is the response at equilibrium (Req) and the horizontal axis is the concentration (μM) of each *Pho*EF-2 sample. The dots of each graph were plotted by the P1-binding response unit (RU) of the individual ten kinds of concentrations of PhoEF-2 in equilibrium of a sensorgram. The line of affinity graphs was shown that each resonance unit was fitted to simple 1:1 Langmuir binding model ($A + B \leftrightarrow AB$) using least square minimization to calculate affinity constants (K_D).

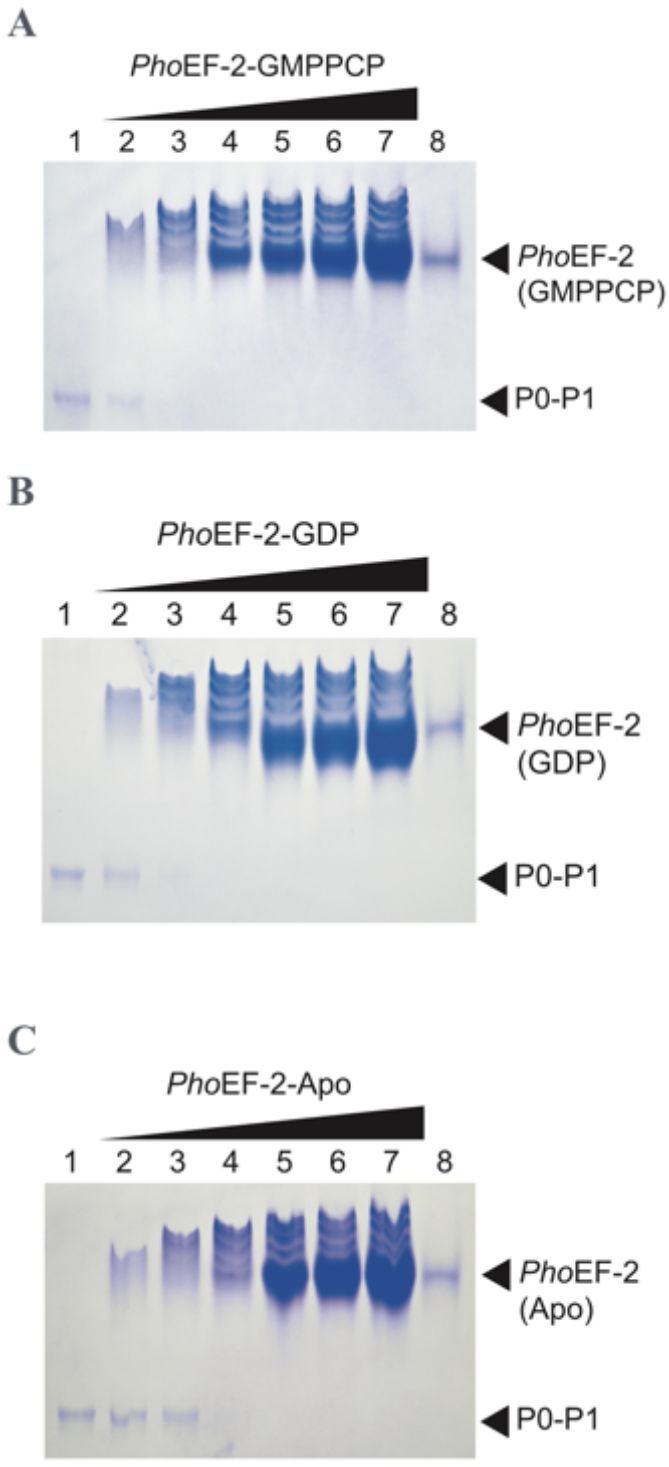
A
PhoEF-2-GMPPCP
1 2 3 4 5 6 7 8
PhoEF-2 (GMPPCP)
P0-P1
B
PhoEF-2-GDP
1 2 3 4 5 6 7 8
PhoEF-2 (GDP)
P0-P1
C
PhoEF-2-Apo
1 2 3 4 5 6 7 8
PhoEF-2 (Apo)
P0-P1

Figure 3-16. Ribosomal P stalk **(**P0-P1)-binding analysis of several forms of *Pho*EF-2 by gel-mobility shift assays using Native-PAGE. (**A**)-(**C**) Binding assays between P0-$[P1]_2[P1]_2[P1]_2$ stalk and GMPPCP-bound (**A**), GDP-bound (**B**), or Apo (**C**) form of *Pho*EF-2. In these gel-mobility shift assays, the heptamer of P0-$[P1]_2[P1]_2[P1]_2$ (2.5 pmol) was incubated without the *Pho*EF-2 (lane 1), or with 2.5 pmol (lane 2), 5 pmol (lane 3), 10 pmol (lane 4), 20 pmol (lane 5), 25 pmol (lane 6) or 37.5 pmol (lane 7) of the *Pho*EF-2 mutants in 5 μL solution at 70 °C. Each *Pho*EF-2 mutant (2.5 pmol) was also incubated without P1 (lane 8).

5. Conformational changes of *Pho*EF-2 when bound to P1C11

As described above, the folds of each domain of *Pho*EF-2 between its different forms were almost same, although the orientation of each domain was different (Figures 3-1, 3-2, 3-4, 3-5, and 3-9). However, the P1 binding residues M167, F205, and F226 clearly exhibited considerable conformational changes when P1C11 was bound to *Pho*EF-2 (Figure 3-17). Compared with the structure of *Pho*EF-2-GMPPCP, the side chains of F205 and F226 in *Pho*EF-2-GMPPCP-P1C11 maintained a similar hydrophobic interaction each other to that of *Pho*EF-2-GMPPCP, but rotated by approximately 62° and 38°, respectively, when interacting with L106 and F107 of P1C11 (Figures 3-10A, 3-10B, 3-12M, 3-17, Tables 1, and 2). Furthermore, although M168 in domain G and M219 in subdomain G′ of *Pho*EF-2 did not interact with P1C11 (Figures 3-10A, 3-10B, 3-11D, 3-12N, and Table 1), their side chains, interestingly, rotated by approximately 70° and 47°, respectively, when bound to P1C11, which appeared to work as a gate for P1C11 (Figure 3-17). In addition, some of the main chains surrounding the P1C11 binding groove of *Pho*EF-2 also exhibited small conformational changes with P1C11 binding. Helix P164-Y185 in domain G and region T222–K235 in subdomain G′ shifted by a maximum distance of 1.7 Å and 1.4 Å, respectively (Figure 3-17). The conformational change in M167 appeared to correspond with that of F205 and F226 of subdomain G′ (Figure 3-17).

In *Pho*EF-2-GMPPCP-P1C11, the P1C11 binding groove looks to be a long distance from the GTP binding site (approximately 20 Å). However, the P1 binding groove connects to parts of the GTP binding motifs G4 and G5 (Figure 3-18). The side chain of V153 in the G4 motif forms a hydrophobic core with P1C11-bound residues M167, F205, and F226,

and F205 is also involved in the G5 motif (Figure 3-18). These structural relationships imply that P1CTD binding may be affected by nucleotide binding. Therefore, considering the previous finding that P1 also binds to the GDP-form of *Pho*EF-2, we attempted to build a docking model of GDP-bound *Pho*EF-2 in the presence of P1C11 (hereafter referred to as *Pho*EF-2-GDP-P1C11) by MD simulation based on the crystal structures solved in this study (Figures 3-19A, 3-19D). This *Pho*EF-2-GDP-P1C11 model can be hypothesized to be the state in which *Pho*EF-2 probably dissociates with P1CTD from the ribosome following GTP hydrolysis.

In the MD simulated model of *Pho*EF-2-GDP-P1C11, the C-terminal part of P1C11 had a similar structure to that of *Pho*EF-2-GMPPCP-P1C11, forming a helix (Figure 3-19A). While the three residues M167, F205, and M219 retained almost the same position in *Pho*EF-2-GDP, the side chains of M168 and F226 exhibited slight conformational changes according to the position of F107 of P1C11 (Figures 3-20A–3-20B). Compared with *Pho*EF-2-GMPPCP-P1C11, it seems that such conformation of the P1C11 binding groove favors the dissociation of P1C11 from *Pho*EF-2-GDP.

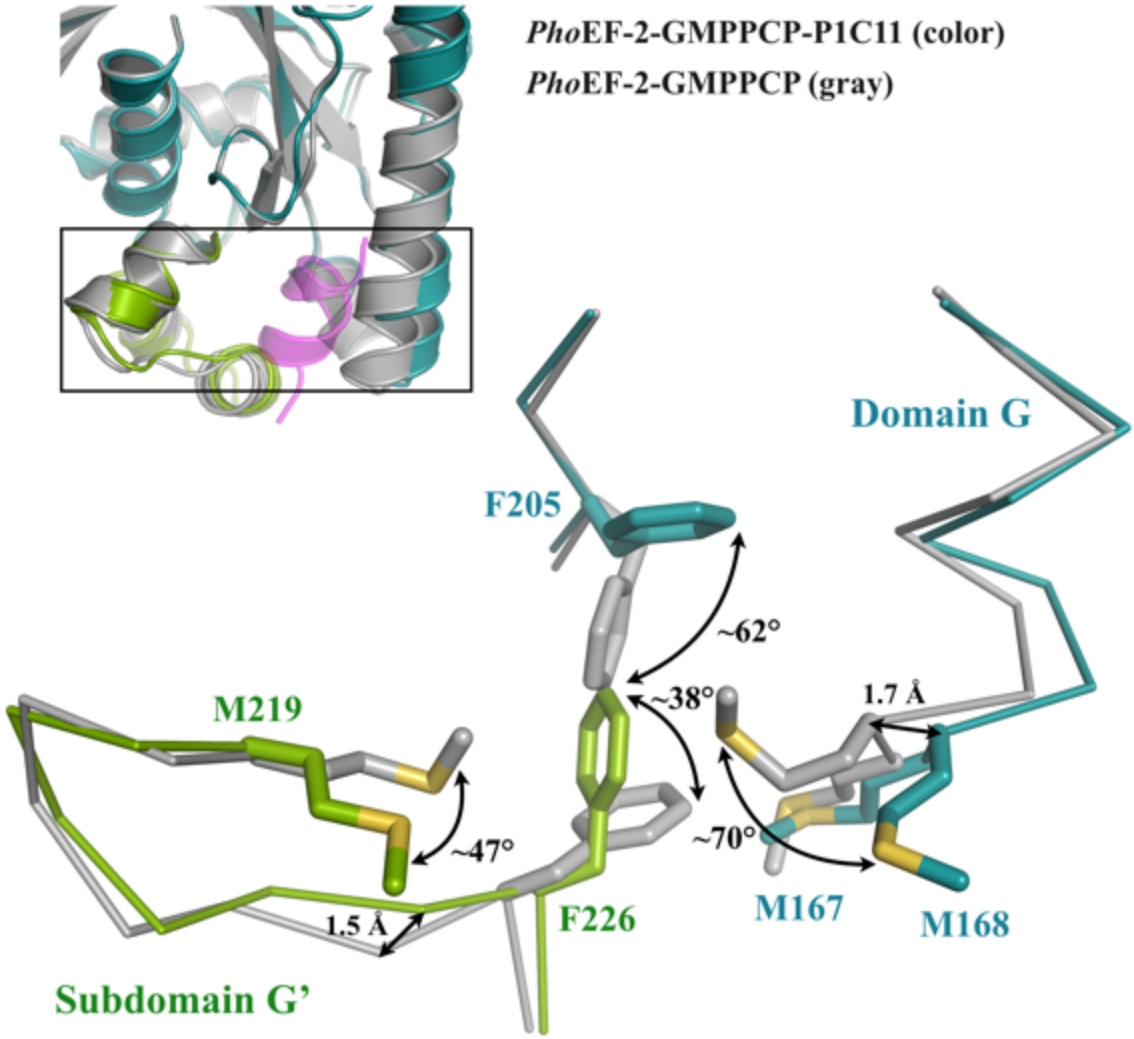

Figure 3-17. Structural comparison of the P1 binding groove by superposing domain G between *Pho*EF-2-GMPPCP and *Pho*EF-2-GMPPCP-P1C11. *Pho*EF-2-GMPPCP is colored gray and *Pho*EF-2-GMPPCP-P1C11 is shown in the same way as in Figure 3-9. In the close-up view, the *Pho*EF-2 structures and side chains of residues that exhibit conformational changes when they bind to P1 are represented by line and stick models, respectively.

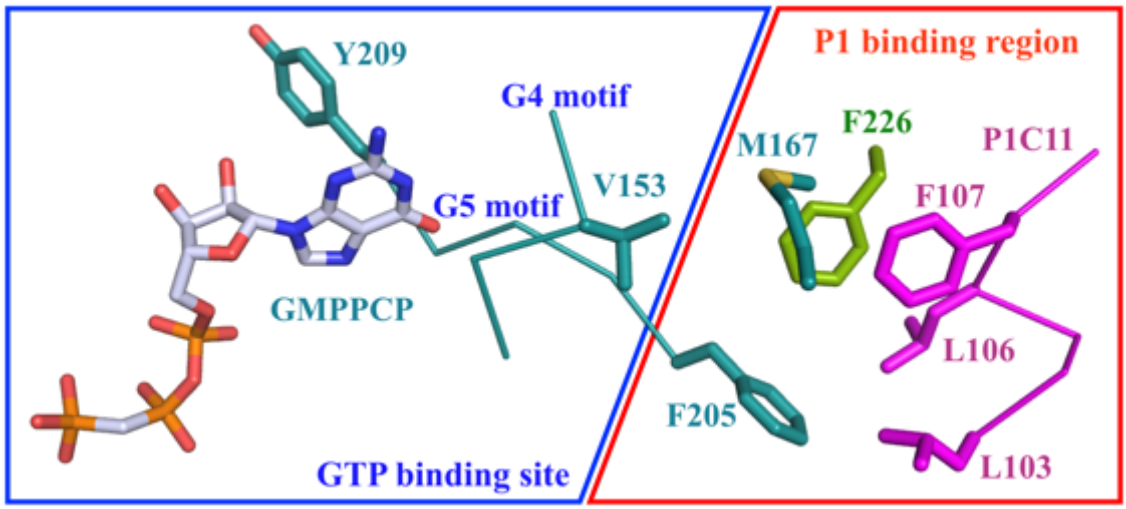

Figure 3-18. Structural relationship between the P1 binding region and GTP binding site of *Pho*EF-2-GMPPCP-P1C11. The color-coding is the same as used in Figure 3-9. The main chain and side chains are represented by line and stick models, respectively. The GTP binding site and P1 binding region are shown as dark-blue and red boxes, respectively.

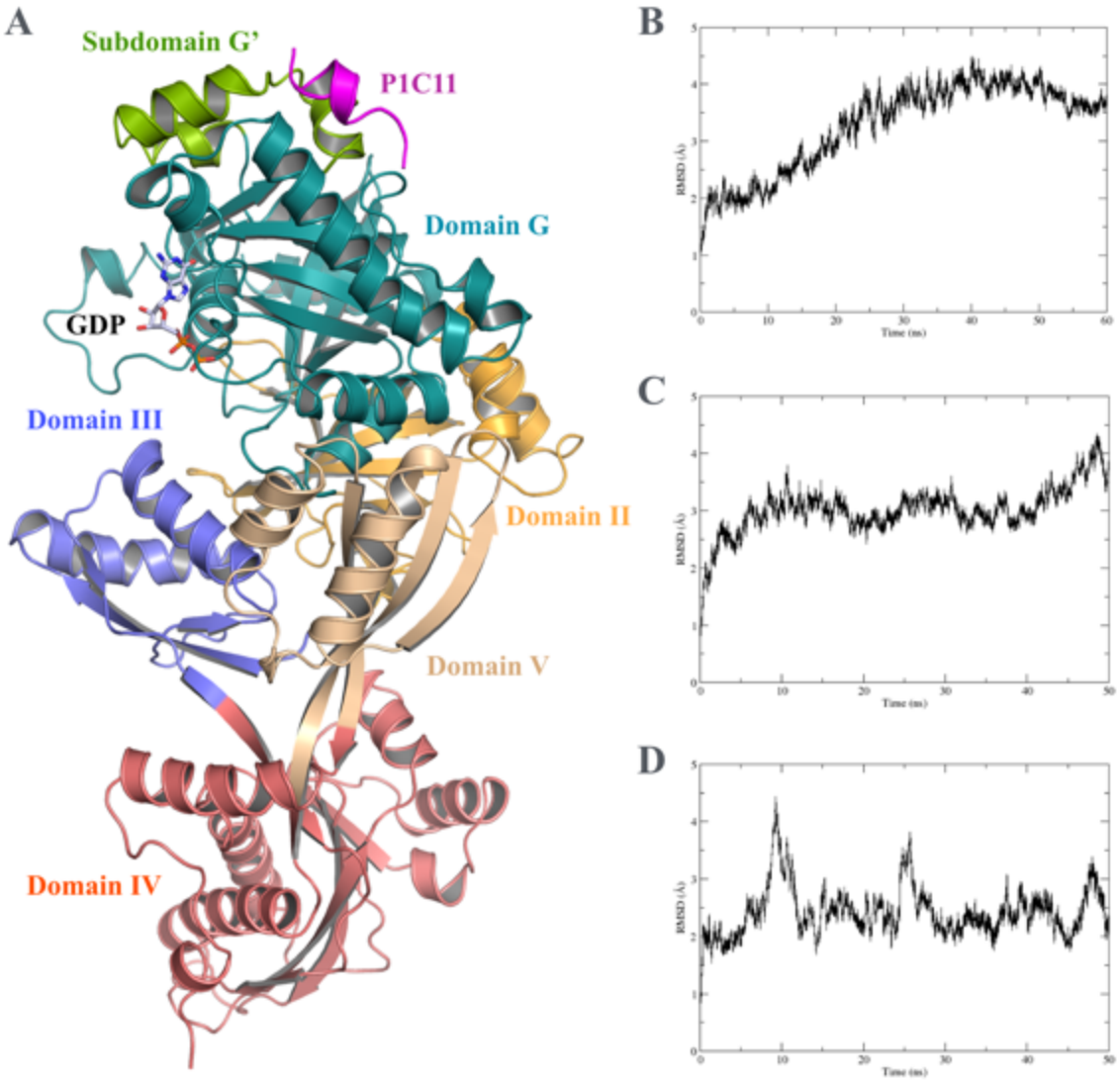

Figure 3-19. The molecular dynamics (MD) simulation model of GDP-bound *Pho*EF-2 in the presence of P1C11 (*Pho*EF-2-GDP-P1C11). (**A**) Overview of the MD simulation model. *Pho*EF-2-GDP-P1C11 is colored in the same way as in Figure 3A. (**B**–**D**) MD simulation trajectory of *Pho*EF-2-GTP, *Pho*EF-2-GDP, and *Pho*EF-2-GDP-P1C11, in which the vertical axis is the root mean square deviation (RMSD) (Å) and the horizontal axis is the simulation time (ns). The RMSD of *Pho*EF-2-GTP, *Pho*EF-2-GDP, and *Pho*EF-2-GDP-P1C11 was

calculated as described previously (44). (**B**–**C**) The energy of *Pho*EF-2-GTP and *Pho*EF-2-GDP were minimized and simulated for 60 and 50 ns, respectively. (**D**) The energy of *Pho*EF-2-GDP-P1C11 was minimized and simulated for 50 ns to analyze how the structure of *Pho*EF-2-GDP responds to the presence of P1C11. The RMSD of the simulation was measured to determine the time at which the simulation was stable. Following an initial increase of approximately 3–4 Å in the RMSD, *Pho*EF-2-GDP-P1C11 stabilized at 15 ns.

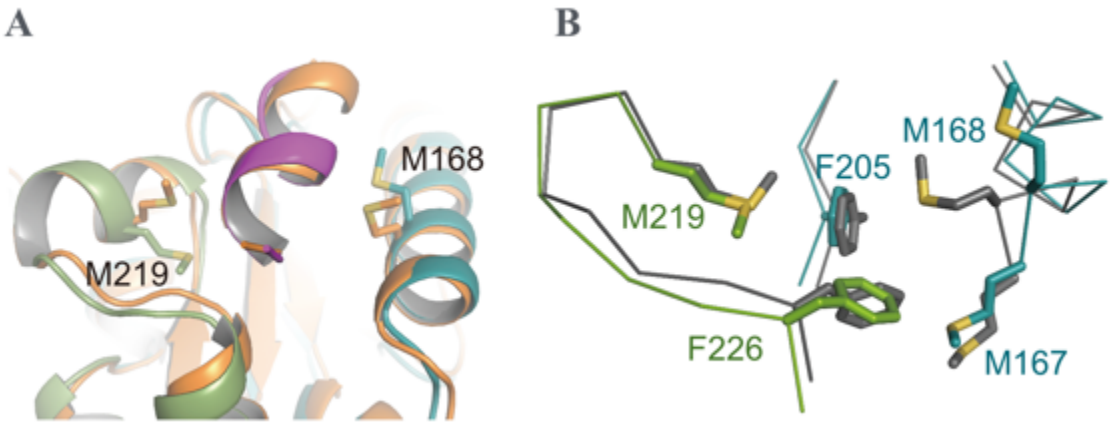

Figure 3-20. Conformational changes between *Pho*EF-2-GDP-P1C11 model and four *Pho*EF-2 crystal structures. (**A**)–(**B**) Structural comparison of the P1C11-binding groove between the MD simulation model and crystal structures of *Pho*EF-2-GMPPCP-P1C11 (orange) (**A**), *Pho*EF-2-D2-GDP (gray) (**B**) by superposing P1-binding region. The side chains of important residues are represented by stick models, and the main chains are represented by ribbon and line models, respectively. S atoms are colored yellow.

6. Structure of *Pho*EF-1α-GDP-P1C11

The crystal structure of *Pho*EF-1α-GDP-P1CTD (PDBID: 3WY9) was determined previously and there were two molecules in the asymmetric unit (57). However, both helical-formed P1CTD did not only interact with the hydrophobic groove between domains G and III of *Pho*EF-1α, but also they were crossing each other and the N-terminal part of the peptide in one *Pho*EF-1α-GDP-P1CTD also contacted to the domain III of *Pho*EF-1α in another complex molecule (57). Moreover, the peptide seemed to work as a crystallization tag. Because these results did not support previous data of several biochemical experiments (14, 15), we determined the 2.4 Å resolution crystal structure of *Pho*EF-1α-GDP in a complex with P1C11 (*Pho*EF-1α-GDP-P1C11) in spite of the addition of GMPPCP with high mol-ratio in the crystallization condition (Figure 3-21). There were one molecules in the asymmetric unit. The final model of the *Pho*EF-1α-GDP-P1C11 complex contained residues 1–428 of *Pho*EF-1α and 98–108 of P1C11. The disorder region in the molecule is N-terminal two residues, and residues 40–52, 76–77, and the C-terminal one residue of *Pho*EF-1α, and N-terminal three residues of P1C11.

The P1C11 of the *Pho*EF-1α-GDP-P1C11 complex structure formed an α-helix (Figures 3-21) and interacted with the hydrophobic groove formed by domains G and III as well as previous structure of *Pho*EF-1α-GDP-P1CTD (Figures 3-21 and 3-22A). In case of *Pho*EF-1α, the domain III involved mainly in the formation of the P1C11 binding groove, whereas both domains G and III interacted directly with P1C11 as indicated by the gel mobility shift assay described previous and below (Figures 3-22B, 3-22C, 3-23) (57). In *Pho*EF-1α-GDP-P1C11, the C-terminal three residues of P1C11 as well as that of the *Pho*EF-2-GMPPCP-P1C11 interacted with *Pho*EF-1α. Moreover, the C-terminus of

P1C11, G108 was shown to contact to the domain III of *Pho*EF-1α (Figures 3-22B and 3-22C) (57). These four key residues of P1 were recognized by residues of domain G (K125 and F129) and domain III (K324, A360, L361, I369, I384 and S432) (Figures 3-22B and 3-22C). The structural comparison of the P1C11 binding region between *Pho*EF-1α-GDP-P1C11 and *Pho*EF-1α-GDP-P1CTD by superposing the domain G showed that although the P1C11 bound to the same position of *Pho*EF-1α-GDP-P1CTD, those binding manners were slightly different (Figures 3-22A and 3-22C), implying that the C-terminal P1CTD may not be retained to stay in the P1 binding groove of *Pho*EF-1α by the crossing of P1CTD one another and the binding between N-terminal P1CTD and domain III of *Pho*EF-1α (Figure 3-22C). As the result, the conformations of some residues between both molecules had different forms (Figures 3-22D and 3-22E). Firstly, previous study showed that F129 (domain G) π-stacking interacted with F107 (P1CTD) (57). However, F107 (P1C11) in this study interacted with F129 (domain G) hydrophobically because F107 (P1C11) was close to the P1 binding groove of *Pho*EF-1α as compared to previous structure (Figure 3-22D). Secondly, although R132 (domain G) of previous structure had a large conformational change for binding to P1CTD when it was includes in *Pho*EF-1α (57), that of the *Pho*EF-1α-GDP-P1C11 had the same conformation of *Pho*EF-1α-GDP (PDBID: 3WYA) (Figure 3-22D), suggesting that R132 (previous) worked to retain P1CTD in the binding region. Finally, I369 (domain III) in the present structure was first shown to interact with F107 and L106 at the distance of ~4.0 Å (Figure 3-22D). To confirm the structural evidence for this interaction, we performed the gel mobility shift assay for mutant I369S of *Pho*EF-1α. The results showed that I369S disrupted the interaction with P1 (Figure 3-23), indicating that it is one of the key residues of the P1 binding.

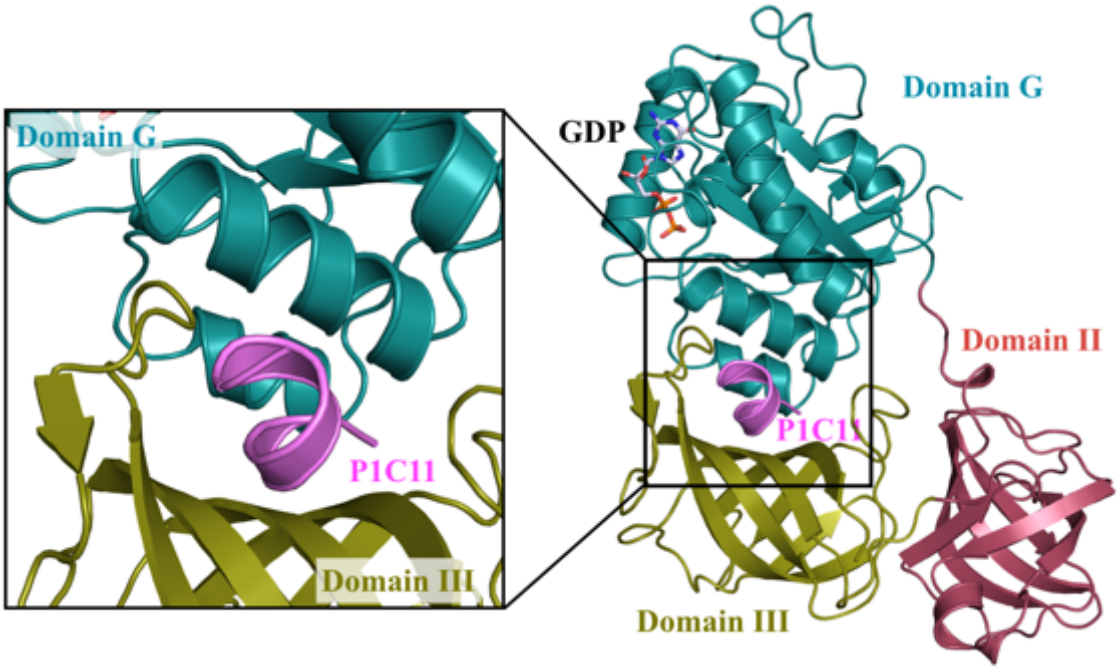

Figure 3-21. Overall structure of *Pho*EF-1α-GDP in a complex with the C-terminal 11 residues of P1 (*Pho*EF-1α-GDP-P1C11). Crystal structure of *Pho*EF-1α-GDP-P1C11 (right) and expanded view of the P1C11 binding groove (left). *Pho*EF-1α, P1C11 and GDP are represented by ribbon and stick models, respectively. Domains G, II, and III of *Pho*EF-1α, and P1C11 are colored deep teal, raspberry, olive, and pink, respectively. The color-coding of the C, N, O, and P atoms of GDP are the same as used in Figure 3-2.

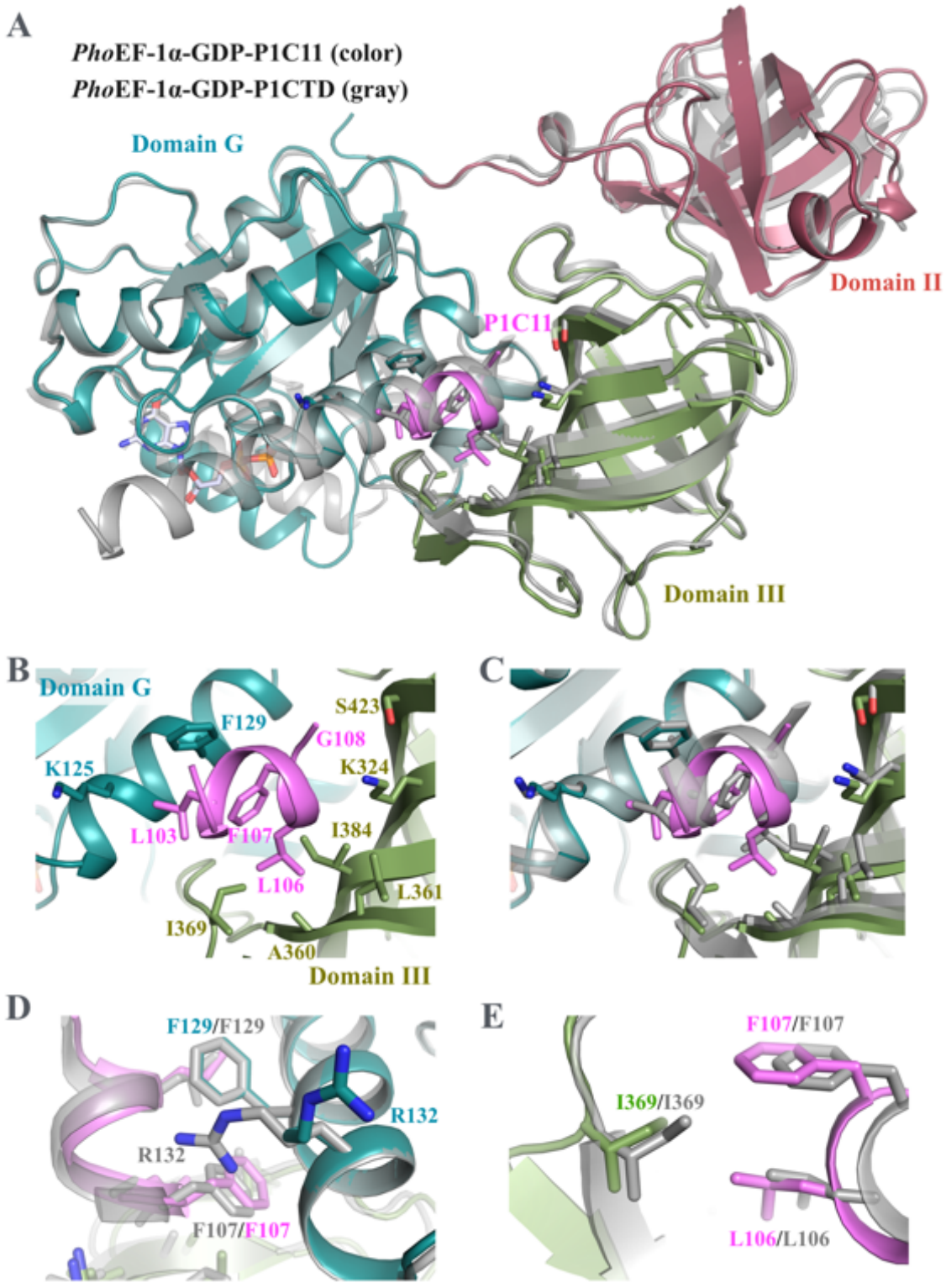
A
PhoEF-1α-GDP-P1C11 (color)
PhoEF-1α-GDP-P1CTD (gray)
Domain G
Domain II
P1C11
Domain III
B
Domain G
S423
F129
G108
K125
K324
L103
F107
I384
L106
L361
I369
A360
Domain III
C
D
F129/F129
R132
R132
F107/F107
E
I369/I369
F107/F107
L106/L106

Figure 3-22. Structural comparison between previous *Pho*EF-1α-GDP-P1CTD (PDBID: 3WY9) and *Pho*EF-1α-GDP-P1C11. *Pho*EF-1α-GDP-P1CTD is colored gray and *Pho*EF-1α-GDP-P1C11 is shown in the same colors as in Figure 3-15. (**A**) The two structures superposed using domain G. (**B**) Close-up view of the structure of the P1C11 binding groove. The side chains of residues of P1C11 and *Pho*EF-1α that are involved in the interaction are represented by stick models. Residue F103 of P1C11 contacted residues K125 and F129 (domain G) of *Pho*EF-1α. Residue L106 of P1C11 interacted with residues A360, L361, I369, and I384 (domain III) of *Pho*EF-1α. Residue F107 bound to residue F129 (domain G). Finally, G108 contacted to residues K324 and S423 (domain III). (**C**) Detailed view of the structural comparison of P1C11 binding groove between *Pho*EF-1α-GDP-P1CTD (gray) and *Pho*EF-1α-GDP-P1C11 (color). The P1CTD of *Pho*EF-1α-GDP-P1CTD shows the only C-terminal 11 residues in ribbon model. The side chains of residues of P1C11 and *Pho*EF-1α that are involved in the interaction are the same as used in (B). (**D**) Two structures of residues F129, R132 (domain G), and F107 (P1C11) were compared by superposing domain G. (**E**) Structural comparison of the residues L106, F107 (P1C11) and I369 (domain III) of the two structures.

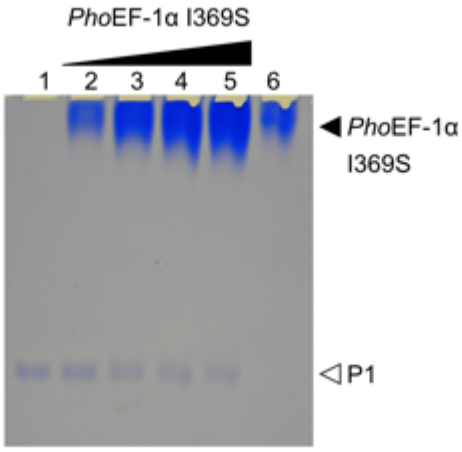

Figure 3-23. P1 binding analysis of GDP-bound *Pho*EF-1α using point mutant I369S. The homodimer of P1 (200 pmol) was incubated without the *Pho*EF-1α mutants (lane 1), or with 100 pmol (lane 2), 200 pmol (lane 3), 300 pmol (lane 4), or 400 pmol (lane 5) of the *Pho*EF-1α mutants in 5 μL solution at 70 °C. The *Pho*EF-1α mutant (200 pmol) was also incubated without P1 (lane 6).

7. Competitive interaction between *Pho*EF-2 and *Pho*EF-1α for P1CTD

Previously, the group determined the crystal structure of *Pho*EF-1α-GDP-P1CTD insisted that *Pho*EF-1α-GDP was highly stabilized by the interaction with P1 although it is an inactivated form (57). However, the stability of the binding between EF-1α-GDP and P1 may connect to decrease the efficiency of the GTP hydrolysis on the ribosome during the translation elongation, and conclusively, to inhibit the binding of the other GTPases, EF-2. Hence, for better elucidating which of two GTPases, *Pho*EF-2 and *Pho*EF-1α interact strongly with P1, we used the gel mobility shift assay and performed the competition experiments between GMPPCP or GDP form of the *Pho*EF-2 and the *Pho*EF-1α-GDP for P1 (Figure 3-24). From these results of the binding assays, the interactions between the P1 and both of the *Pho*EF-2-GMPPCP and the *Pho*EF-2-GDP were stronger than the interaction between the P1 and the *Pho*EF-1α-GDP (Figures 3-24A and 3-24B) despite that the P1 (100 pmol) was added to more the *Pho*EF-1α-GDP (400 pmol) than *Pho*EF-2-GMPPCP or *Pho*EF-2-GDP (each form of *Pho*EF-2 is 100 pmol) (Figure 3-24B). Moreover, the comparison of the bands in the Native-PAGE between lane 1 and 3 of Figure 3-24C was clearly showed that the pattern of the band among *Pho*EF-2-GMPPCP, *Pho*EF-1α-GDP, and P1 in before and after that the *Pho*EF-2-GMPPCP and the mixture of the P1 and the *Pho*EF-1α-GDP were incubated at 70°C. While the band of *Pho*EF-2-GMPPCP and the complex band of *Pho*EF-1α-GDP-P1 overlapped before the incubation, the P1 interacted with *Pho*EF-2-GMPPCP instead of *Pho*EF-1α-GDP after the incubation. Therefore, we provided that *Pho*EF-1α-GDP did not always interacted strongly and stably with P1.

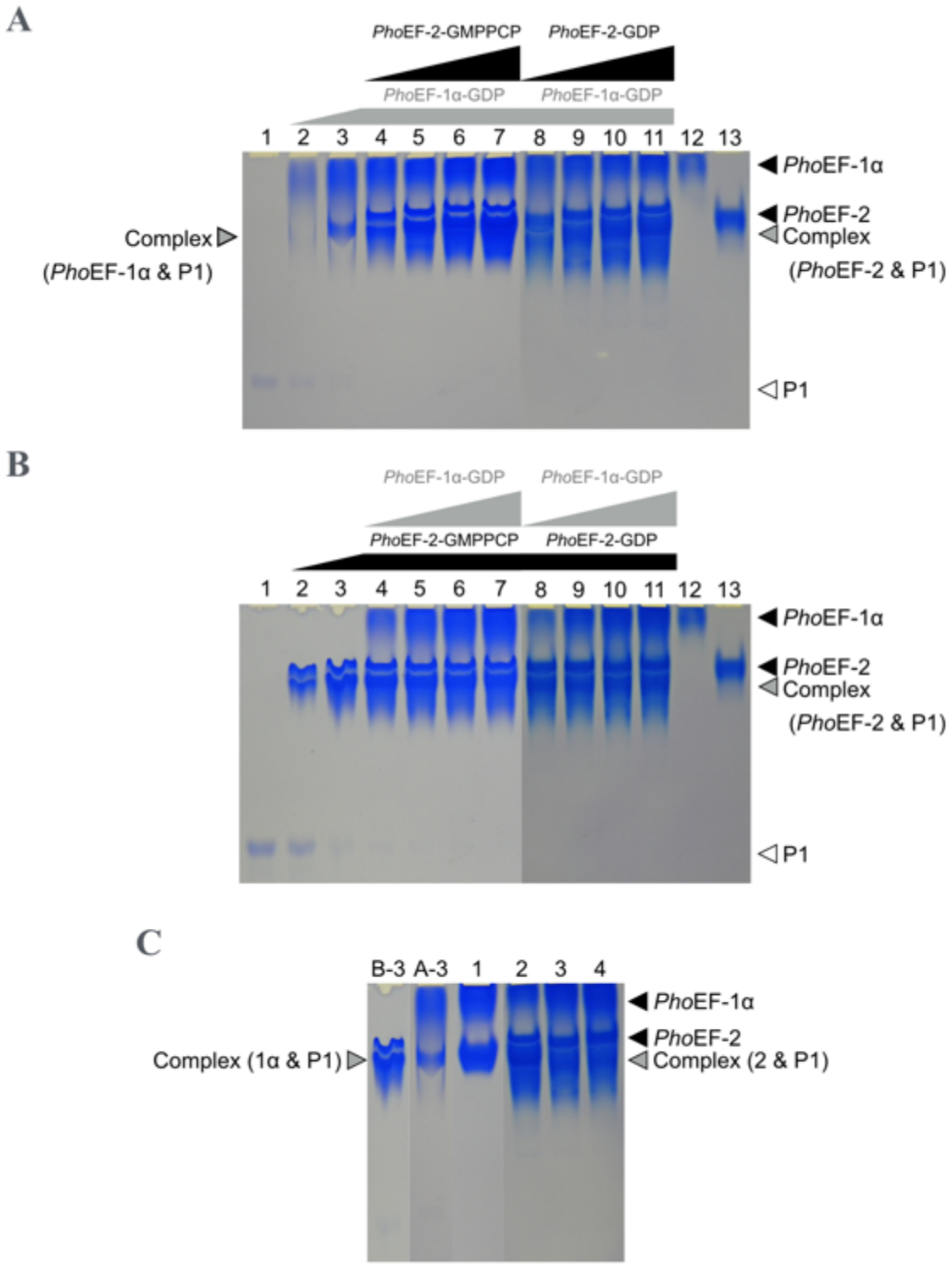
A
PhoEF-2-GMPPCP
PhoEF-2-GDP
PhoEF-1α-GDP
PhoEF-1α-GDP
1 2 3 4 5 6 7 8 9 10 11 12 13
PhoEF-1α
PhoEF-2
Complex
(PhoEF-2 & P1)
Complex
(PhoEF-1α & P1)
P1
B
PhoEF-1α-GDP
PhoEF-1α-GDP
PhoEF-2-GMPPCP
PhoEF-2-GDP
1 2 3 4 5 6 7 8 9 10 11 12 13
PhoEF-1α
PhoEF-2
Complex
(PhoEF-2 & P1)
P1
C
B-3 A-3 1 2 3 4
PhoEF-1α
PhoEF-2
Complex (1α & P1)
Complex (2 & P1)

Figure 3-24. Qualitative competition experiments between *Pho*EF-1α and *Pho*EF-2 for P1 by the gel mobility shift assay using Native-PAGE. (**A**) The homodimer of P1 (100 pmol) was incubated without the *Pho*EF-1α-GDP (lane 1), or with 100 pmol (lane 2), 200 pmol (lane 3) of the *Pho*EF-1α-GDP, or lane 3 with 100 pmol (lane 4), with 200 pmol (lane 5), with 300 pmol (lane 6), with 400 pmol (lane 7) of the *Pho*EF-2-GMPPCP, or lane 3 with 100 pmol (lane 8), with 200 pmol (lane 9), with 300 pmol (lane 10), with 400 pmol (lane 11) of the *Pho*EF-2-GDP in 10 μL solution at 70 °C. The *Pho*EF-1α or *Pho*EF-2 (100 pmol) was also incubated without P1 (lanes 12, and 13, respectively). (**B**) The homodimer of P1 (100 pmol) was incubated without the *Pho*EF-2 (lane 1), or with 100 pmol (lane 2), 200 pmol (lane 3) of the *Pho*EF-2-GMPPCP, or lane 3 with 300 pmol (lane 4), with 200 pmol (lane 5), with 300 pmol (lane 6), with 400 pmol (lane 7) of the *Pho*EF-1α-GDP, or 200 pmol of the *Pho*EF-2-GDP with 100 pmol (lane 8), with 200 pmol (lane 9), with 300 pmol (lane 10), with 400 pmol (lane 11) of the *Pho*EF-1α-GDP in 10 μL solution at 70 °C. The *Pho*EF-1α or *Pho*EF-2 (100 pmol) was also incubated without P1 (lanes 12, and 13, respectively). (**C**) The lane B-3 is the same as lane 3 of (B), and the lane A-3 is the lane 3 of (A). The homodimer of P1 (100 pmol) was incubated with 400 pmol the *Pho*EF-1α-GDP in 8 μL solution at 70 °C, and then gently added to 100 pmol (2 μL) of the *Pho*EF-2-GMPPCP without the incubation of 70°C (lane1). Conversely, the P1 (100 pmol) was incubated with 400 pmol the *Pho*EF-2-GMPPCP in 8 μL solution at 70 °C, then, added to 100 pmol (2 μL) of the *Pho*EF-1α-GDP (lane 2). In addition, the lanes 1 and 2 were finally incubated in 5 μL solution at 70 °C (lanes 3 and 4, respectively).

DISCUSSION

1. GTP binding sites among four *Pho*EF-2 structures

The crystal structures determined in the present study shed light on the conformational details of *Pho*EF-2 in its different forms (Apo, GTP, and GDP), as well as the interaction between *Pho*EF-2 and P1CTD. Among the five GTP binding motifs of our structures, the Switch I always retained its flexibility, and the P-loop and the Switch II changed their conformation depending on their binding states, whereas the G4 and G5 motives exhibited similar conformations across the different forms. It was explicitly demonstrated that the α-phosphate of GDP was recognized not only by the P-loop, but also by the side chain of residue R71 of the Switch I (Figure 3-8A), which is known to involve in increasing the GTPase activity on the ribosome and promoting translocation (54, 56). Previous research displayed that when a larger part of Switch I in *Sce*EF-2 was replaced by the homologue sequence from *E. coli* EF-G, the mutant reduced ability to bind to the GTPase binding region (SRL) of ribosome. Although the Switch I of EF-2/EF-G and EF-1α/EF-Tu differs length (53) and they are not interchangeability (54), the arginine of Switch I such as R71 of *Pho*EF-2, interestingly, is conserved in aEF-1α, eEF-1α, and EF-Tu as well as eEF-2 and EF-G (54, 58-60), and all the Switch I containing the arginine are known to have tryptic cleavage sites (61-65). While the side chain of I33 in the P-loop changed the conformation to stack the base part of GTP or GDP, H101 of the Switch II changed conformations in different forms to recognize the γ-phosphate of GTP in GTP form, and then bind to the β-phosphate of GDP after the GTP hydrolysis (Figure 3-8A). The Switch II of EF-2/EF-G in all organisms, especially, the loop including H101 and F104 is high flexible (Figure 3-8). From the structures of *Pho*EF-2-GMPPCP and *Pho*EF-

2-Apo in this study, F104 also contributes to promote the rotation of domains III-V and the recognition of the γ-phosphate of GTP by H101 (Figure 3-8B).

2. Recognition of recruitment partners by P1CTD

2-1. Comparison of P1-recognition mechanism between aEF-1α and aEF-2

Comparing to the structure of *Pho*EF-1α-GDP-P1CTD (PDBID: 3WY9) (57), the P1 binding region of *Pho*EF-2 and *Pho*EF-1α are completely difference in both of position and sequence, however the hydrophobic groove with the shape for the helix of P1CTD is uniform (Figure 4-1A). The P1-binding features of PhoEF-2 are 1) only hydrophobic residues interact each other; 2) the most hydrophobic residues in groove work together except F226; 3) GTP-binding site is close to P1-binding groove (Figures 3-18 and 4-1B). Previous report indicated that F129, K324, and I384 interacted with P1CTD (57), and our structures *Pho*EF-1α-GDP-P1C11 showed that I368 also contacted to P1 (Figures 3-22E and 3-23). From the results, those four residues interacted independently and directly with the binding partner of P1. Then, we grasped and compared the positions of P1-binding residues between *Pho*EF-2 and *Pho*EF-1α. Firstly, although F129 of *Pho*EF-1α as well as F226 of *Pho*EF-2 exhibited π-stacking with F107, it existed in the opposite side of F226. From the structural comparison, the configuration of F129 corresponded to M168 of *Pho*EF-2 which did not involve in the interaction with P1 (Figures 3-12D, 3-12G, and 4-1C). Secondly, the side chain of K324 of *Pho*EF-1α existed near that of the same amino acid K225 of *Pho*EF-2 spatially. While K324 bound to A105 and L106 (57), K225 did not involve in the interaction with P1 (Figures 3-12D and 4-1C). Thirdly, in this study,

we further clarified the P1-binding ability of I368 of *Pho*EF-1α. The configuration of I368 was in accord with that of F205 of *Pho*EF-2 (Figure 4-1C). F205 partially interacted with L103 of P1 (Figure 3-10), however, I368 bound to L106 and F107 of P1 (Figures 3-22E, 3-23). Fourthly, the spatial position of I384 of *Pho*EF-1α was comparably near that of F226 of *Pho*EF-2. F226 exhibited π-stacking and hydrophobic interaction with F107 and L106, respectively, whereas, I384 contacted to only L106 (Figures 3-10 and 4-1C). Finally, there is not any residues of *Pho*EF-1α corresponding to M167 which interacted partially with F107 (Figure 4-1C).

Combining with previous research that the conserved C-terminal portion of aP1 recognized directly individual translational GTPases aEF-2, aEF-1α and aIF5B (15), it can be considered indicated that responding to the diversity of binding partners, the P stalk does not recognize the specific sequences and positions, but may recognize a hydrophobic groove of its binding partners by hydrophobic interaction with G102, L103, L106 and F107 of aP1. Based on this proposal, we discuss the P1CTD-binding manner of other GTPases by superposing their G-domain upon that of *Pho*EF-2-GMPPCP-P1C11.

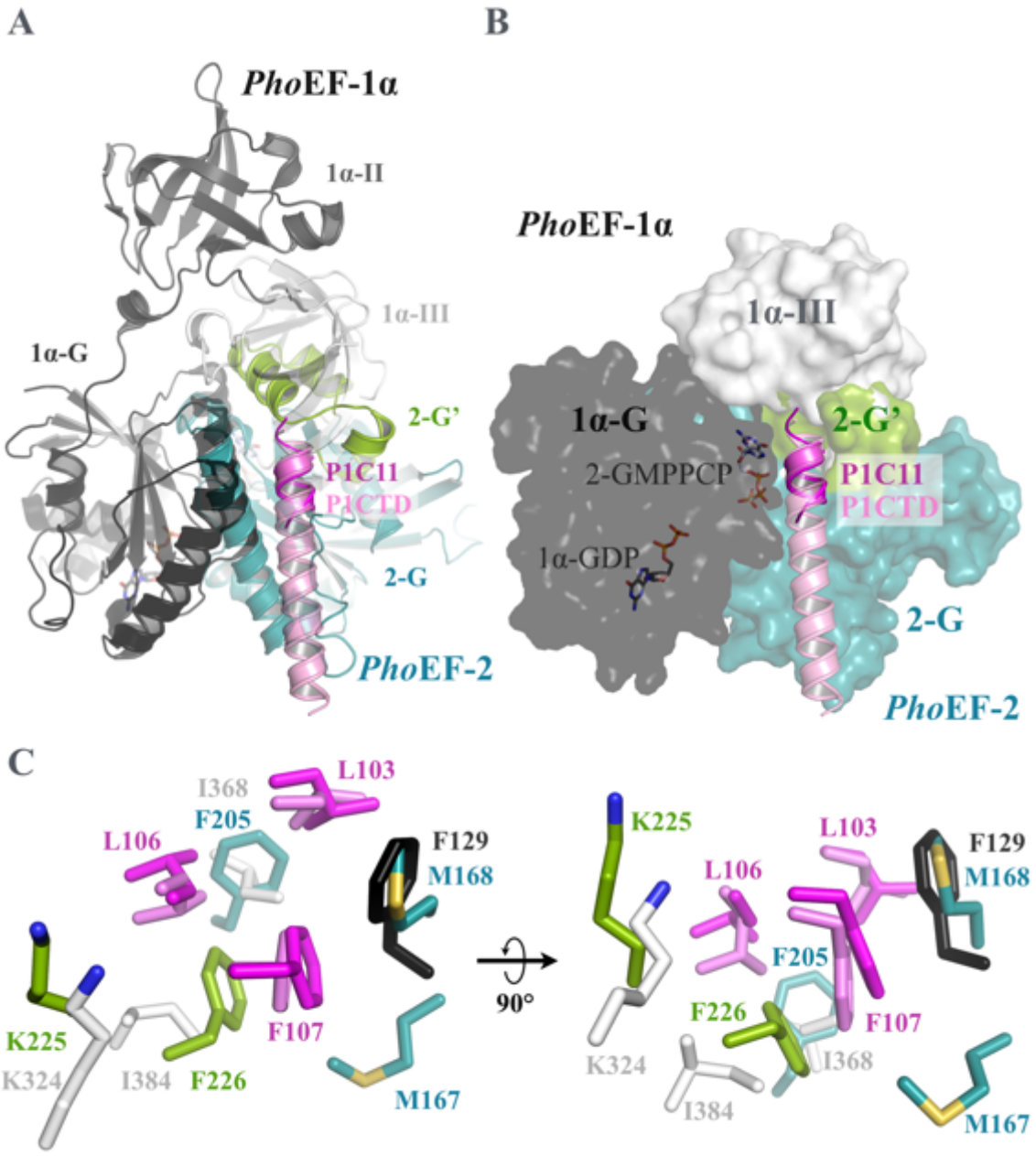

Figure 4-1. Structural comparison between GDP-bound *Pho*EF-1α in a complex with P1CTD (*Pho*EF-1α-GDP-P1CTD) (PDBID: 3WY9) and *Pho*EF-2-GMPPCP-P1C11. (**A**) *Pho*EF-1α-GDP-P1CTD superposed on *Pho*EF-2-GMPPCP-P1C11 by arranging P1C11. (**B**) Closed view of the P1-binding region between *Pho*EF-1α (domains G and III) and *Pho*EF-2 (domain G and subdomain G′). (**C**) Detailed

view of the side chain of the P1-binding region between *Pho*EF-1α and *Pho*EF-2. These domains and GDP/GMPPCP are represented by surface and stick models, respectively. Domain G and subdomain G' of *Pho*EF-2-GMPPCP-P1C11 are colored in the same way as in Figure 3-9A, while domains G, II, and III of *Pho*EF-1α are colored black, gray, and white, respectively. The side chains of (C) are represented by stick models and the S atoms of M167 and M168 are colored yellow.

2-2. Estimated P1-recognition mechanism of aIF5B

P stalk binding GTPase, aIF5B shares domain G with aEF-2 and aEF-1α, but no subdomain G' as aEF-1α (31, 66) (Figure 4-2A). The structure of aIF5B have already been determined by some groups. However, there is no information where of aIF5B recognizes P1CTD and which residues involve in the interaction with P1CTD. In order to estimate the P1-binding region and residues of aIF5B, we compared the domain G between *Pho*EF-2-GMPPCP-P1C11 and *Ape*IF5B (PDBID: 5FG3) (66). By the structural superposing, we found a hydrophobic groove in the opposite side of the GTP binding site of *Ape*IF5B (Figure 4-2B), which composed of F157, I161, R162, R169, L172, E173, V176, L192 and R195 (Figure 4-2C). The positions of M167, M168, and F226 of *Pho*EF-2 are corresponded to those of L172, E173, and I161, respectively to some extent and they may relate to interact with aP1CTD.

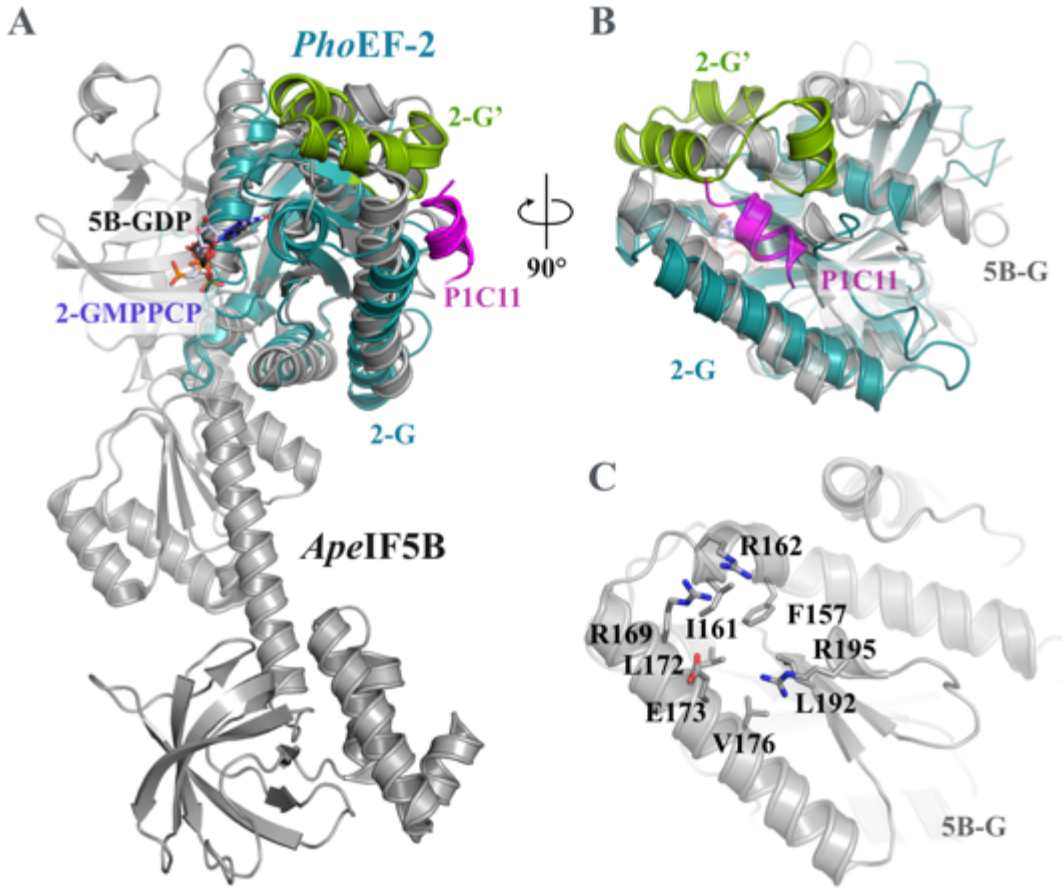

Figure 4-2. Structural comparison between aIF5B and *Pho*EF-2-GMPPCP-P1C11 without domains II–V. (**A**) Domain G of aIF5B from *Aeropyrum pernix* (*Ape*IF5B-GDP; PDBID: 5FG3) (gray) was superposed on that of *Pho*EF-2-GMPPCP-P1C11, which is colored in the same way as in Figure 3-9A. The GDP in *Ape*IF5B and GMPPCP in *Pho*EF-2-GMPPCP-P1C11 are shown in the stick model. (**B**) Close-up view of P1 binding region of *Pho*EF-2-GMPPCP-P1C11 in (A). (**C**) Predicted P1 binding region of *Ape*IF5B-GDP. The residues mentioned in the text are labeled and shown in the stick models.

2-3. Estimation of P1-recognition mechanism of eEF-2

Since previous studies have shown that aP1CTD binds to eEF-2 as well as aEF-2 (14, 15, 67), however, we have not known where and which residues of eEF-2 involve in the interaction with P1CTD as well as aIF5B. In order to estimate the P1•P2-binding region of eEF-2, we compared the structures of *Sce*EF-2 (PDBID: 1N0V) (33) and *Pho*EF-2-GMPCP-P1C11 (Figure 4-3A). Although the P1-binding region of *Pho*EF-2 was arranged inside subdomain G′ of *Sce*EF-2 (Figure 4-3B), we found a hydrophobic groove (α10–α12) on *Sce*EF-2 subdomain G′ that may be involved in the interaction with P1•P2 (Figure 4-3C), thus the large subdomain G′ of eEF-2 may have evolved from its ancestor by substituting a part of domain G to form a P1•P2 binding groove. As mentioned above, while aP1CTD also binds to eEF-2, eukaryotic P1•P2CTD do not recognize aEF-2 (67), suggesting that the different and nonconserved residues between aP1CTD and P1•P2CTD seem to play key parts in the interactions with respective aEF-2 and eEF-2.

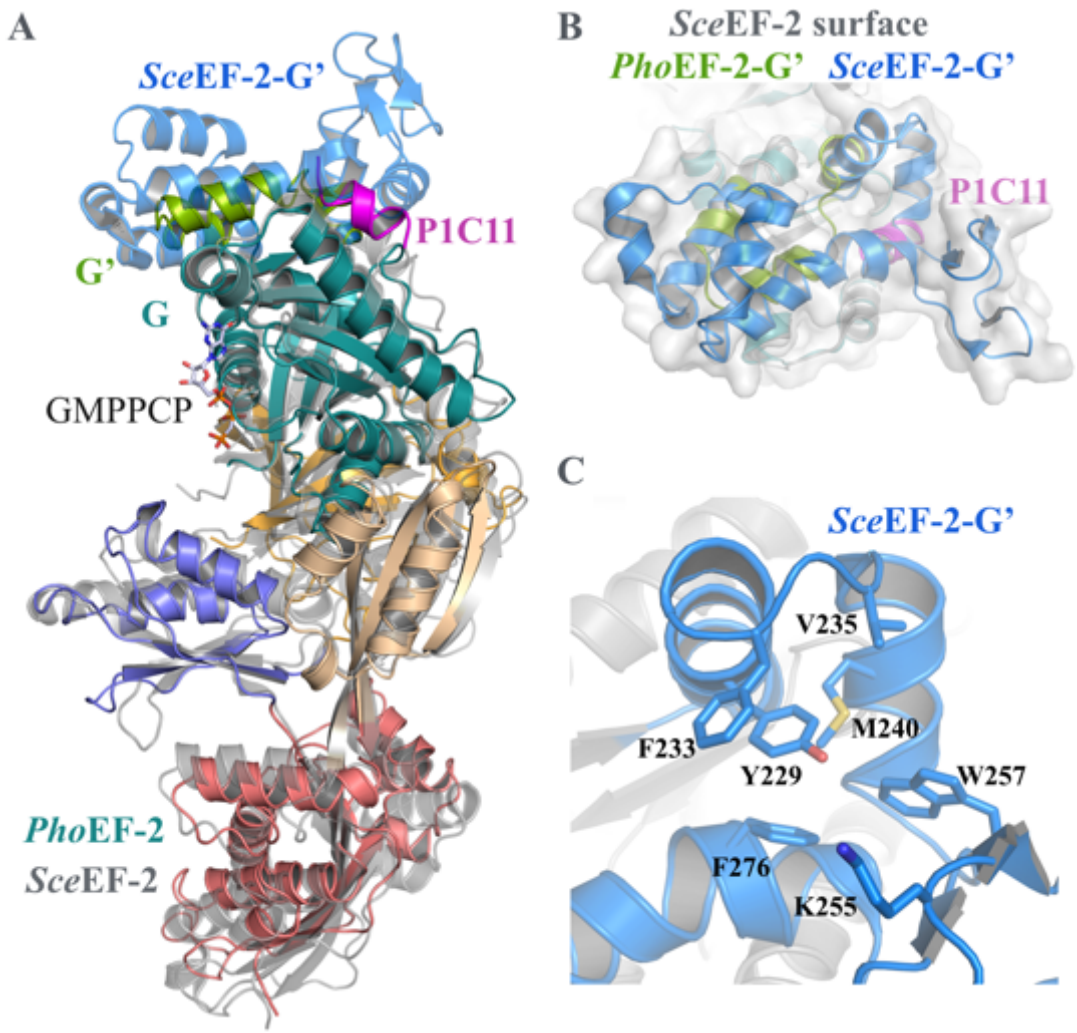

Figure 4-3. Structural comparison between eEF-2 and *Pho*EF-2-GMPPCP-P1C11. The subdomain G′ of *Sce*EF-2-Apo (PDBID: 1N0V) (33) is colored blue and the other domains are colored gray. *Pho*EF-2-GMPPCP-P1C11 is shown in the same way as in Figure 3-9A. *Sce*EF-2 is represented by cartoon models. (**A**) Structural superposition of domain G between *Sce*EF-2-Apo and *Pho*EF-2-GMPPCP-P1C11. (**B**) Top view of (A) of domain G and subdomain G′ with the molecular surface of *Sce*EF-2 colored in white. (**C**) Detailed view of the predicted stalk binding region of *Sce*EF-2. The residues mentioned in the text are labeled and shown in the stick models.

2-4. Difference of P stalk-binding mechanism between RTA and aEF-2

Ricin toxic subunit known as A-chain (RTA) that is a biological weapon, is a type II ribosome-inactivating protein (RIP), and is isolated from the seeds of *Ricinus communis.* This protein is a rRNA N-glycosyrase, which depurinates A4324 at the sarcin-ricin loop (SRL) of eukaryotic 28S rRNA, thus irreversible inactivating the ribosome by preventing GTPases (eEF-1α and eEF-2) and release factor (eRF3) from binding to the GTPase-associated center. Recent studies showed that RTA was recruited by the CTD of eukaryotic ribosomal P1•P2 stalk (68). Then, we compared the P stalk-binding region between *Rco*RTA in complex with the C-terminal 10 residues of P2 (*Rco*RTA-P2C10) (PDBID: 5DDZ) (68) and our *Pho*EF-2-GMPPCP-P1C11. As well as other translational GTPases, both regions are not conserved in each sequence, structure, and spatial configuration (Figure 4-4A). The P2-binding region of RTA seems to be able to interact specifically with the side chains of eukaryotic P1•P2CTD by the evolution from archaea to eukaryote. Firstly, the surface of binding groove of RTA has broader than that of *Pho*EF-2, and the large number of residues between *Rco*RTA and P2C10 involves in the interaction as compared to *Pho*EF-2 and P1C11 (Figure 4-4B). Although the position of M168 in *Pho*EF-2 is similar to that of Y183 in *Rco*RTA, the others have different configurations (Figure 4-4B). Because D115 of P2 is conserved in all eukaryotic P1•P2, not aP1, the hydrogen bond between the D115 and R235 in *Rco*RTA is characteristic of eukaryote. Moreover, L103 in aP1 overlaps with I251 in *Rco*RTA and the part of N-terminal fragment of P2C10 has a disorder, thus suggesting that aP1CTD forms an α-helix easier than eukaryotic P1•P2CTD.

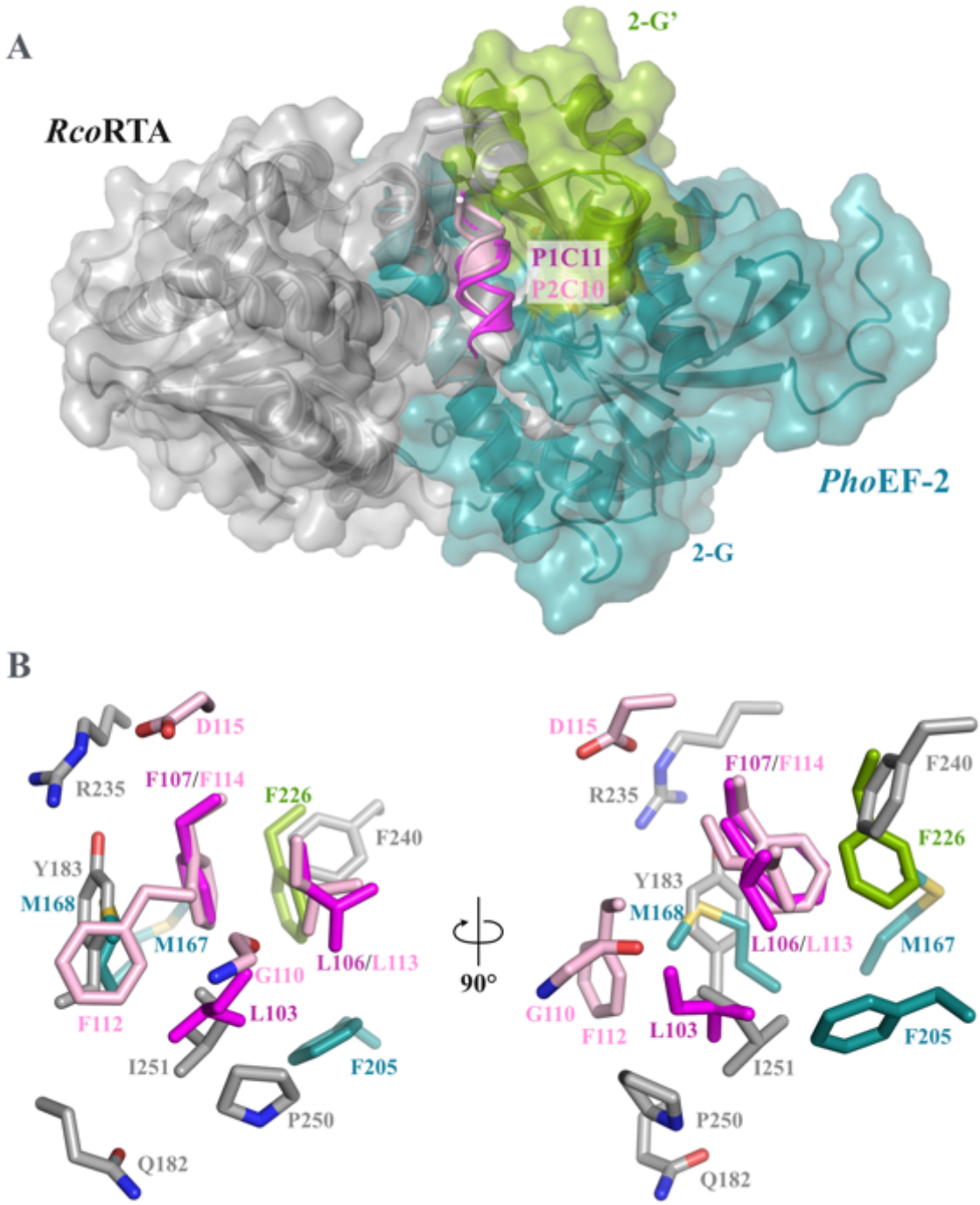

Figure 4-4. Structural comparison between *Rco*RTA-P2C10 and *Pho*EF-2-GMPPCP-P1C11. In *Rco*RTA-P2C10 complex structure, *Rco*RTA (PDBID: 5DDZ) is colored gray, and P2C10 is colored pale pink. *Pho*EF-2-GMPPCP-

P1C11 is shown in the same way as in Figure 3-9A. *Rco*RTA is represented by cartoon and surface models, and P2C10 is represented by cartoon model. (**A**) *Rco*RTA-P2C10 superposed on *Pho*EF-2-GMPPCP-P1C11 by arranging P1C11 and P2C10. (**B**) Detailed view of the side chain of the P1 or P2-binding residues between *Rco*RTA and *Pho*EF-2. The side chains and the main chain of G110 in (B) are represented by stick models. The S atoms of M167 and M168, the O atoms of G110 D115, Q182, and Y183, and the N atoms of G110, Q182, R235, and P250 are colored yellow, red, and blue, respectively.

2-5. The pocket size comparisons among several P-stalk binding partners

As these results of the complex structures *Pho*EF-2-GMPPCP-P1C11, *Pho*EF-1α-GDP-P1CTD, and *Rco*RTA-P2C10, the shape of P stalk-binding regions are similar, but are not accord in their sequences and structures. Then, we compared these binding pocket sizes by using the freely available web server Pocket-Cavity Search Application (POCASA) that was produced by Dr. Jian Yu in our laboratory (Figure 4-5) (49). As compared the P1-binding pocket of *Pho*EF-2 to other binding pockets of *Pho*EF-1α and *Rco*RTA, each pocket has different size which is the number of probe spheres in spite of the interaction with P1CTD (Figures 4-5A, 4-5B, and 4-5E). On the other hand, we found the spheres from the same position as our estimated P1-binding pocket of *Ape*IF5B (Figures 4-2 and 4-5C). Although the shape of pocket seems to be similar with that of *Pho*EF-2, the P1CTD-binding orientation may be at approximately right angle from these probe spheres (Figures 4-5A and 4-5C). In the case of *Sce*EF-2, the P1-binding pocket that we estimated includes the larger number of spheres than other P1-binding partners (Figure 4-5D). Since the subdomain G' of eEF-2 is enlarged from that of aEF-2 in the process of evolution, we just speculate that the right protrusion of the spheres in Figure 4-5D might be some side chains of P1•P2CTD which involve in the interaction with *Sce*EF-2. Taken all together, the sizes and shapes of several P1-binding grooves are not identified. This is because it might be key to not only macro-level such as the similar shape of pocket, but also micro-level such as the relationship of the side chains of binding residues each other.

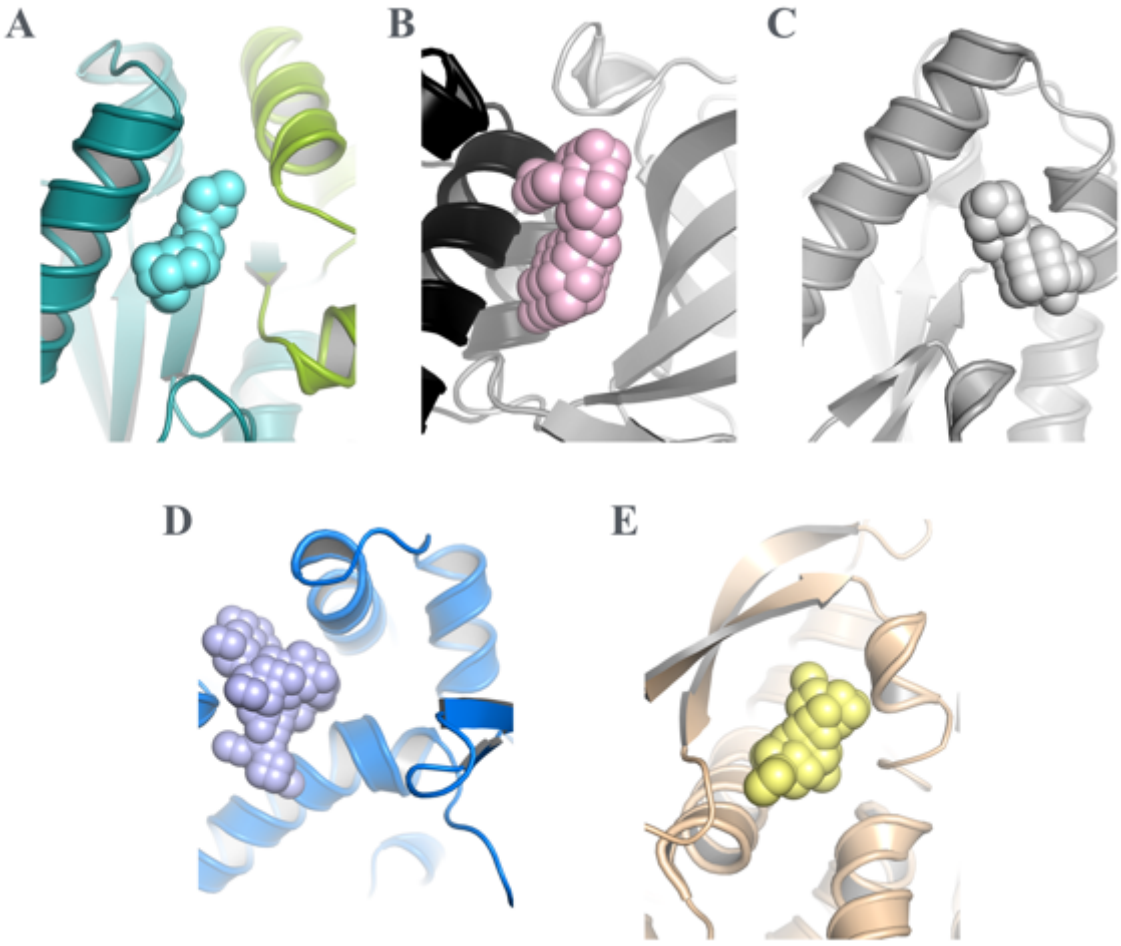

Figure 4-5. The pocket comparisons of P stalk-binding and the estimated groove among *Pho*EF-2 (**A**), *Pho*EF-1α (**B**), *Ape*IF5B (**C**), *Sce*EF-2 (**D**), and *Rco*RTA (**E**) using Pocket-Cavity Search Application (POCASA) web server (49), which is freely available at http://altair.sci.hokudai.ac.jp/g6/Research/POCASA_e.html and was produced for structure-based drug design. Structures of *Pho*EF-2, *Pho*EF-1α, *Ape*IF5B, *Sce*EF-2 are shown in the same way as in Figure 3-9A, Figure 4-1, Figure 4-2, Figure 4-3, respectively. *Rco*RTA is represented by cartoon model and is colored wheat. The probe spheres of *Pho*EF-2, *Pho*EF-1α, *Ape*IF5B, *Sce*EF-2, *Rco*RTA are colored pale cyan, pale pink, gray, pale blue, and pale yellow, respectively.

2-6. P1-recognition of elongation factors with or without ribosome

As mentioned above, the P stalk has the recognition-specificity, and intriguingly, the P1CTD needs to adapt for the diversity of the residues or the structures of binding partners (EF-2, EF-1α, and IF5B) in order to recognize various GTPases. However, generally, interactions between a protein and its binding partners are conserved to same extent. Consequently, we discuss and provide the relationship between the binding positions of the GTPases and their functions. Firstly, EF-1α changes the conformation between GTP-bound form and GDP-bound form since EF-1α-GTP binds to an aa-tRNA to deliver to the ribosome. The EF-1α-aa-tRNA (EF-Tu-aa-tRNA) is known to be a mimicked molecule of EF-2 (EF-G) (Figures 4-6E) and they similarly bound to the GTPase-associated center of the ribosome (Figures 4-6A, 4-6B). Comparing *Pho*EF-1α-GDP-P1CTD to ribosome-EF-Tu-tRNA (PDBID: 4V5D, Figure 4-6A) by superposing domain G, although the domains II and III of *Pho*EF-1α (EF-Tu) rotated from GTP-form to GDP-form, the P1CTD binding region of *Pho*EF-1α-GTP is predicted to be formed by the domains G and III as well as *Pho*EF-1α-GDP (Figure 4-6C). From the structures, the P1CTD binding region seems to be buried in the ribosome relatively (Figure 4-6C). On the other hand, in the case of EF-G, the subdomain G' is known to interact with the L12 stalk (17-20) and both subdomain G' exist in almost the same position spatially (Figures 4-6B, 4-6D, 4-6F). The GTP binding site is further away from the P1CTD binding groove in *Pho*EF-1α than in *Pho*EF-2 (Figure 4-1B), implying that rather than GTP or GDP binding, aa-tRNA binding may affect P1CTD binding in *Pho*EF-1α because aa-tRNA bunds to the domains II and III of *Pho*EF-1α-GTP (activated form) and it is known that both of the *Pho*EF-1α-GTP and *Pho*EF-1α-GDP (Figures 4-6G and 4-6H) (11, 69).

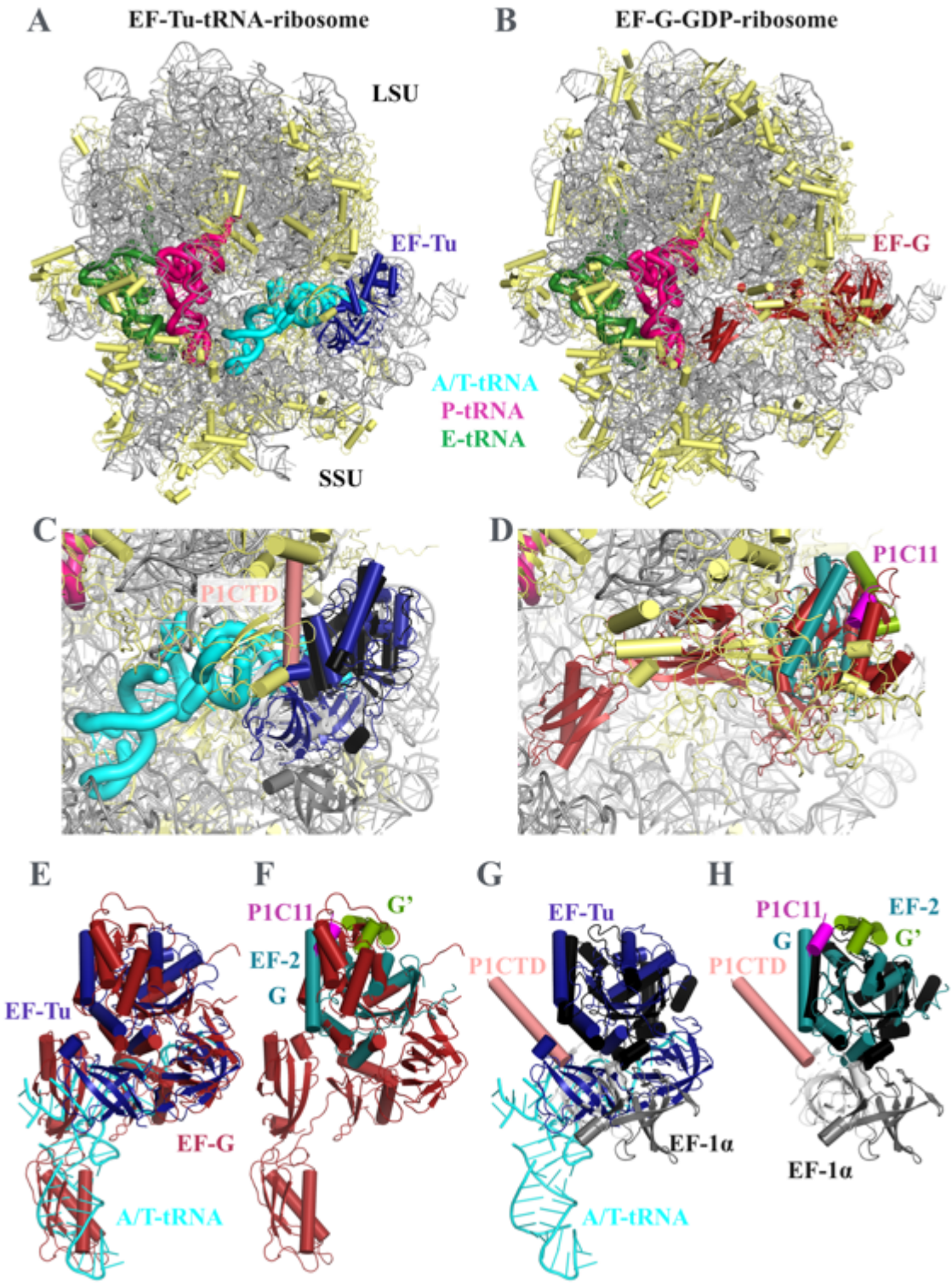
A
EF-Tu-tRNA-ribosome
LSU
EF-Tu
A/T-tRNA
P-tRNA
E-tRNA
SSU
B
EF-G-GDP-ribosome
EF-G
C
P1CTD
D
P1C11
E
EF-Tu
EF-G
A/T-tRNA
F
P1C11
G'
EF-2
G
G
EF-Tu
P1CTD
EF-1α
A/T-tRNA
H
P1C11
EF-2
G
G'
P1CTD
EF-1α

Figure 4-6. Structures of ribosome in complex with elongation factor GTPases. The ribosomal RNA (rRNA) and proteins are represented by ribbon models, and colored gray and pale yellow, respectively. (**A**) Crystal structure of ribosome complexed with aminoacyl tRNA (aa-tRNA) bound EF-Tu (ribosome-EF-Tu-tRNA, PDBID: 4V5G) (11). EF-Tu, A/T-tRNA, P-tRNA, and E-tRNA are represented by ribbon models and colored blue, cyan, magenta, and green, respectively. (**B**) Crystal structure of ribosome complexed with GMPPCP-bound EF-G (ribosome-EF-G-GDP, PDBID: 4V5F) (19). EF-G, P-tRNA, and E-tRNA are represented by ribbon models and colored red, magenta, and green, respectively. (**C**) Expanded view of the structural comparison between *Pho*EF-1α-GDP-P1CTD and ribosome-EF-Tu-tRNA by superposing domain G. *Pho*EF-1α-GDP-P1CTD is the same as Figure 4-1. (**D**) As well as (C), closed view of the structural superposition of domain G between domain G, subdomain G', and P1C11 of *Pho*EF-2-GMPPCP-P1C11 and ribosome-EF-G-GDP. *Pho*EF-2-GMPPCP-P1C11 is the same as Figure 3-9A. (**E**–**H**) Structural comparison among EF-Tu, EF-G, *Pho*EF-1α-GDP-P1CTD, and *Pho*EF-2-GMPPCP-P1C11 by domain G. Proteins and tRNA are represented by the same as (A–D). (**E**) Comparison between EF-Tu-tRNA and EF-G. (**F**) Comparison between EF-G and *Pho*EF-2-GMPPCP-P1C11. (**G**) Comparison between EF-Tu-tRNA and *Pho*EF-1α-GDP-P1CTD. (**H**) Comparison between *Pho*EF-1α-GDP-P1CTD and *Pho*EF-2-GMPPCP-P1C11.

2-7. P1-recognition of initiation factors with ribosome

Secondly, it is known that the IF5B with IF1A fixes the initiator Met-tRNA$_i^{Met}$ at the P-site of the ribosome (Figure 4-7A) (66, 70-72). In the translation initiation, IF5B is recruited to the small ribosomal subunit, therefore, the P stalk does not involve in the delivery of the IF5B. After the large ribosomal subunit is recruited to the small subunit, the IF5B retains the GTPase-associated center until the ribosome is ready for the preparation of the transition to the elongation stage (Figure 4-7A) and the IF5B dissociates from the ribosome by the P stalk followed by its GTP hydrolysis. The structural comparison between ribosome-eIF5B (PDBID: 4V8Y) and ribosome-EF-G (PDBID: 4V5F) by superposing domain G of both GTPases shows that, similar to the EF-Tu-GTP-aa-tRNA complex (PDBID: 4V5G), the eIF5B bound to the GTPase-associated center (Figure 4-7B). However, the C-terminal region of the eIF5B recognizes the peptidyl transferase center (Figures 4-7A and 4-7B) while the tip of the domain IV of EF-2 and the anticodon loop of aa-tRNA which bound to EF-1α recognize the codon of the mRNA in the decoding center (Figures 4-6A, 4-6B). In Figure 4-2, the P1CTD binding region of *Ape*IF5B could be explained on the assumption that the region of *Pho*EF-2 was formed by the domain G and the subdomain G'. Comparing to the EF-1α, the IF5B does not rotate the orientations of the individual domains, and the P1CTD involves in the only dissociation from the ribosome. Namely, it is suggested that the predicted P1CTD binding region of eIF5B is favorable for the recognition of the P stalk and similar position of that of *Pho*EF-2 accidentally.

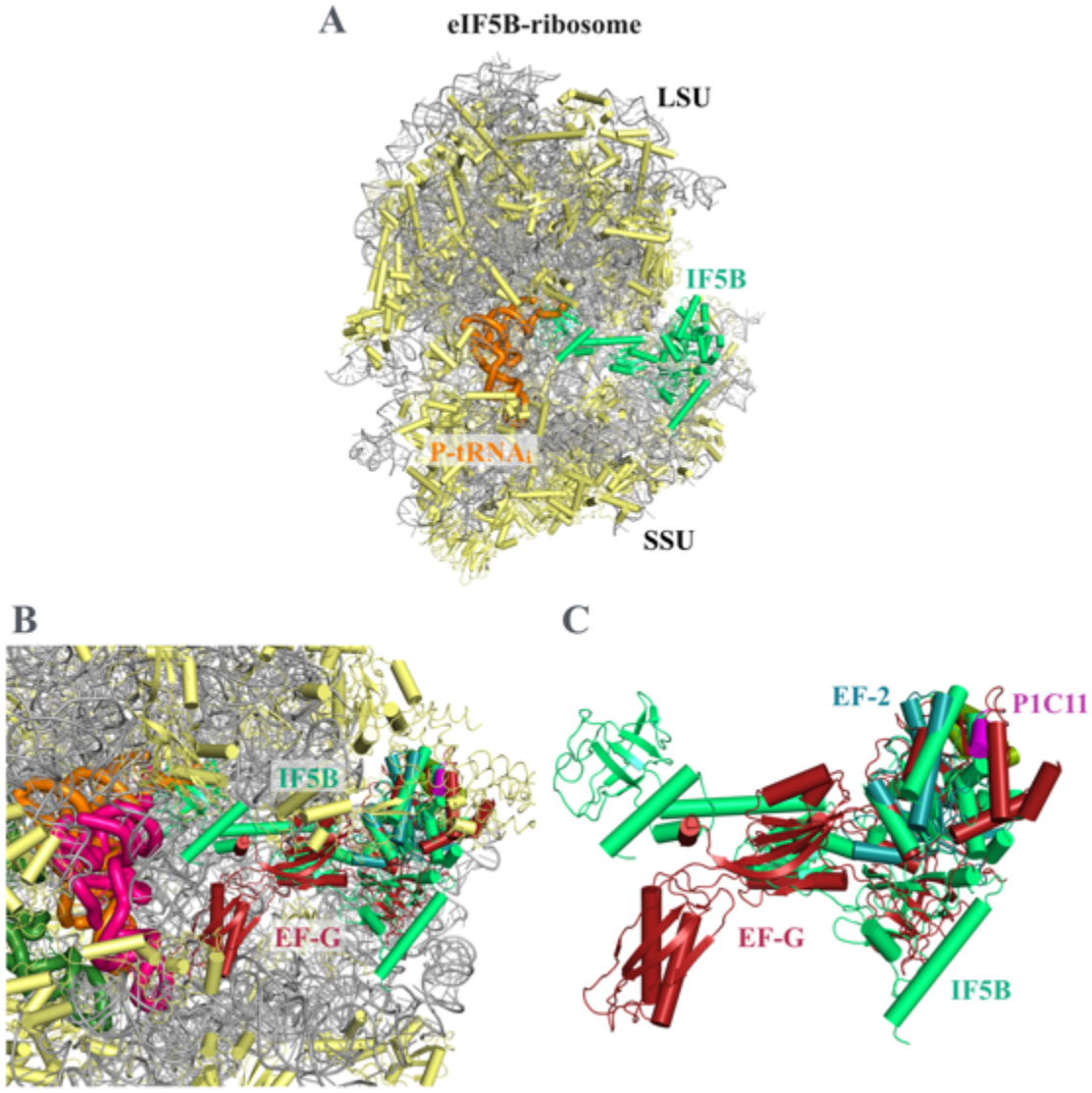

Figure 4-7. Structures of ribosome in complex with an initiation factor GTPase, IF5B. The ribosomal RNA (rRNA) and proteins are the same as using Figure 4-6. (**A**) Crystal structure of ribosome complexed with eIF5B (ribosome-eIF5B, PDBID: 4V8Y) (71). eIF5B and P-tRNA$_i$ are represented by ribbon models and colored lime green and orange, respectively. (**B**) Expanded view of the structural comparison among the domain G and subdomain G' of *Pho*EF-2-GMPPCP-P1C11, EF-G and ribosome-eIF5B by superposing domain G. *Pho*EF-2-

GMPPCP-P1C11 is the same as Figure 3-9A and EF-G is the same as Figure 4-6B. (**C**) Closed view of the GTPases: the domain G and subdomain G' of *Pho*EF-2-GMPPCP-P1C11, EF-G and eIF5B of (B).

2-8. GTPases not contact to P stalk

On the other hand, some GTPases are not recruited and/or released by the P-stalk to the GTPase-associated center of the ribosome. Firstly, a hydrophobic groove was also found in the opposite side of the GTP binding site of *Pho*IF2γ (PDBID: 2D74) domain G (Figure 4-9A), but this region interacts with the N-terminal two helices of *Pho*IF2β specifically (73) in concordance with that P1 cannot bind to *Pho*IF2γ (Figure 4-9B) (15). Secondly, while archaeal aEF-1α binds to RF1 and deliver to the GTPase-associated center (Figure 4-9A) (29, 74, 75), in eukaryotic eRF3 instead of eEF-1α recognizes RF1 or RF2 (Figure 4-9B) (25-28, 76). Recently, several studies showed that eRF3 interacted with the poly adenosyl (A) binding protein (PABP) which bound to the 3'-untranslated region (3'-UTR) of mRNA (77-79), therefore, suggesting that the P1CTD cannot contact to the eRF3. Similar to them, the elongation factor Selenocysteine (EF-Sec) which deliver Sec-tRNA^{Sec} to the recoding UGA codon of the mRNA at the A-site of the ribosome is known to interact with SBP2 complexed with the special 3'-UTR termed SECIS of the mRNA (Figure 4-9C) (80-82). The composition of the domains G, II, and III of IF2γ, RF3, and EF-Sec are highly similar to that of EF-1α (Figure 4-9). However, interestingly, they do not have the different conformations between their GTP-forms and GDP-forms (Figures 4-9B, 4-9C, and 4-9D) although EF-1α changes the conformation from its GTP-form to the GDP-form when the GTP hydrolysis occurs in the ribosome (Figure 4-9A). Thus, it is suggested that the reason why the P1CTD does not recognize GTPases which have high similarity with EF-1α does not only have the advantages and specializations of their functions, but also slightly differences of the shape of P1CTD binding groove.

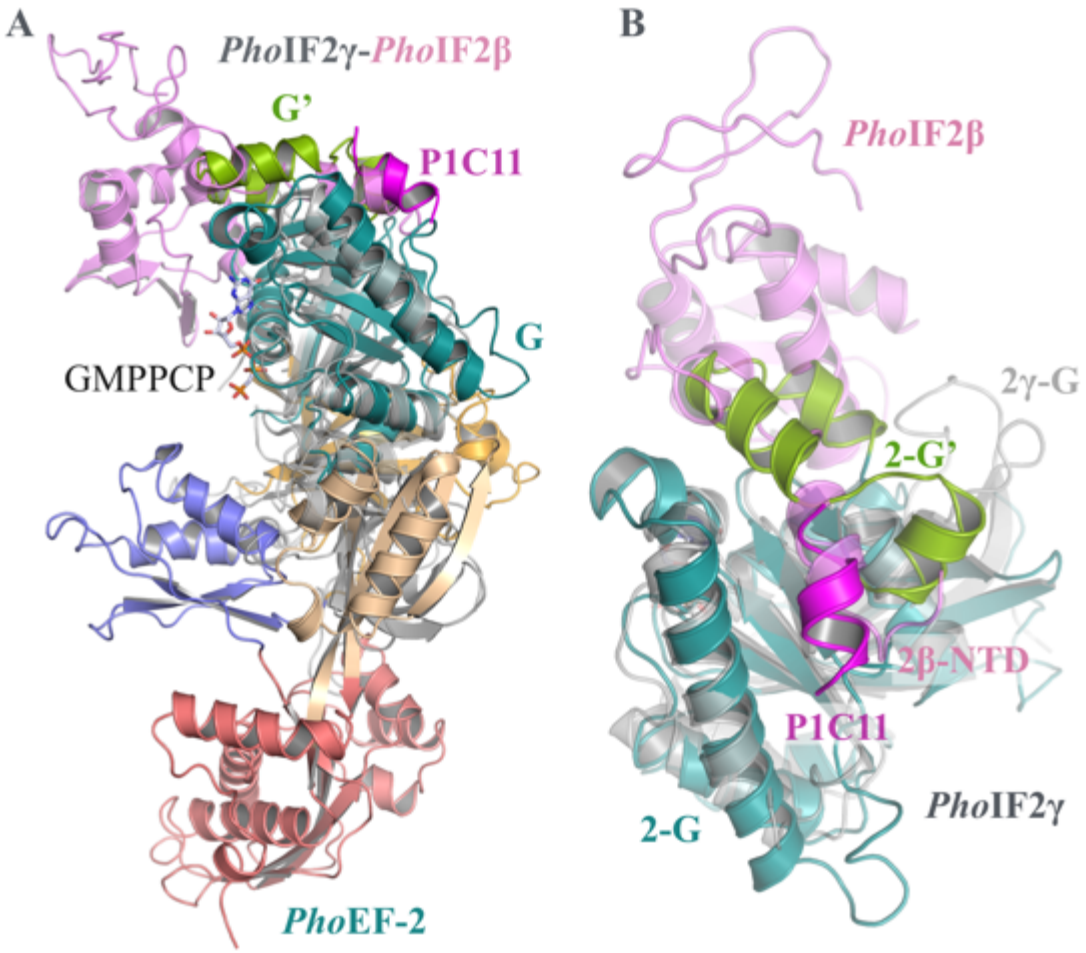

Figure 4-8. Structural comparison between aIF2γ-aIF2β complex from *Pyrococcus horikoshii* (*Pho*IF2γβ, PDBID: 2D74) and *Pho*EF-2-GMPPCP-P1C11. (**A**) *Pho*IF2γβ superposed on *Pho*EF-2-GMPPCP-P1C11 by arranging domain G. *Pho*IF2γ and *Pho*IF2β are represented by ribbon models and colored gray and pink, respectively. *Pho*EF-2-GMPPCP-P1C11 is shown in the same as using Figure 3-9A. (**B**) Top and closed view of P1 binding groove of *Pho*EF-2-GMPPCP-P1C11 with domain G of *Pho*IF2γ and *Pho*IF2β.

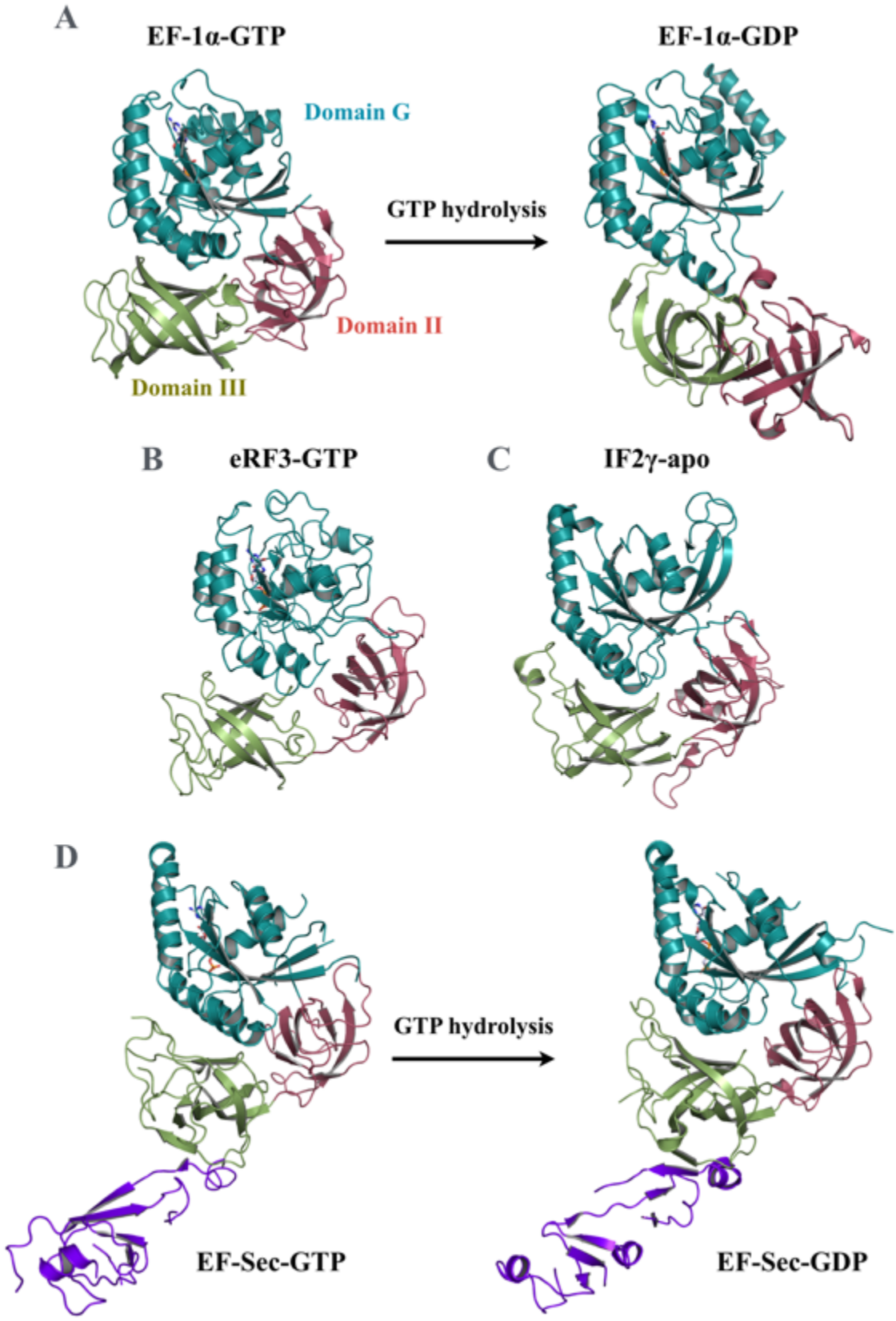
A
EF-1α-GTP
EF-1α-GDP
Domain G
GTP hydrolysis
Domain II
Domain III
B
eRF3-GTP
C
IF2γ-apo
D
GTP hydrolysis
EF-Sec-GTP
EF-Sec-GDP

Figure 4-9. Structures of GTP- and GDP-bound forms of EF-1α, GTP-bound form of RF3, IF2γ-Apo, and GTP- and GDP-bound forms of EF-Sec. The only EF-1α has the different conformation as compared with others. The proteins are represented by ribbon models, and GTP, GMPPCP, and GDP are stick models. The domains G, II, and III of them are colored deep teal, raspberry, olive, respectively and the domain IV of eEF-Sec is colored blue purple The color-coding of the C, N, O, and P atoms of GTP, GMPPCP, and GDP are the same as used in Figures 3-1 and 3-2. (**A**) The conformational change from aEF-1α-GTP to aEF-1α-GDP by GTP hydrolysis. Crystal structures of aEF-1α-GTP from *Aeropyrum pernix* (*Ape*EF-1α-GTP, PDBID: 3VMF) (75) and aEF-1α-GDP from *Sulfolobus solfataricus* (*Sso*EF-1α-GDP, PDBID: 1SKQ) (32). (**B**) Cryo-EM structure of eRF3-GTP from *Saccharomyces cerevisiae* (*Sce*RF3-GTP, PDBID: 4CRN) (76). (**C**) Crystal structure of *Pho*IF2γ-Apo (PDBID: 2D74). (**D**) The conformational change from EF-Sec-GTP to EF-Sec-GDP by GTP hydrolysis. Comparing to aEF-1α, EF-Sec does not change the conformation between GTP-form and GDP-form.

3. The recruitment process

3-1. The recruiting and releasing processes of *Pho*EF-2 by P1 stalk

The most remarkable findings from the present study were the conformational changes that occurred in *Pho*EF-2 around the P1C11 binding groove, not only in response to the presence or absence of P1C11, but also in its different forms (Apo, GTP, and GDP). During the translational cycle, *Pho*EF-2 works through five stages: Apo, GTP-bound, GTP/P1-bound, GDP/P1-bound, and GDP-bound. In this study, we obtained the crystal structures of four of these forms, and modeled the GDP/P1-bound form using MD simulation (Figure 3-14A). A structural comparison then highlighted the conformational changes between the different forms. Taken together, our findings suggest that in response to GTPase recruitment, *Pho*EF-2 works through three states: "closed," "open," and "release" of the P1 binding groove (Figure 4-10). First, the P1 binding groove of *Pho*EF-2-Apo is in a closed state (Figure 4-10A). When GMPPCP binds to *Pho*EF-2, it retains its closed state but the side chain of M219 changes its conformation to make a space in the P1 binding groove (Figure 4-10B). Then, through the interaction with P1C11, the side chains of M167, M168, F205, M219, and F226 rotate to form an open (GTP) state for receiving and binding P1C11 (Figure 4-10C). Following GTP hydrolysis, M168 and F226 retain their open state, while the residues M167, F205, and M219 change to their conformations that is close to the release form, which makes a favorable situation for dissociation of P1 (Figure 4-10D). Then, when *Pho*EF-2-GDP dissociates from the ribosome and P1, the groove is fully changed to a release state (Figure 4-10E). In this state, the side chains of five residues (M167, M168, F205, M219, and F226) return to the closed state conformation, but the main chain of the α-helix (P164–E169) changes to the

conformation that is intermediate between the open and closed states (Figure 4-10E). Finally, after GDP dissociates from *Pho*EF-2, the conformation of the groove returns to the closed state (Figure 4-10A).

3-2. Behaviors of the stalk binding region of elongation factors on ribosome

In the case of EF-G from *Thermus thermophilus* (*Tth*EF-G) which is a homologue of *Pho*EF-2, the complex structures of the *Tth*EF-G-GMPPCP-ribosome (PDBID: 4V9H) (Figure 4-11A) and the *Tth*EF-G-GDP-ribosome (PDBID: 4V5F) (Figure 4-11B) were determined by X-ray crystallography (11, 20). Although both ribosomes of the *Tth*EF-G-ribosome complex change a conformation between the pre-translocational state and the post-translocational state in the translation elongation stage, the domain G of both *Tth*EF-G-GMPPCP (activated form) and *Tth*EF-G-GDP (inactivated form) on their ribosomes hardly changes their conformations, especially, the relationship between GMPPCP or GDP of EF-G and Sarcin/Ricin Loop (SRL) of the large ribosomal subunit is retained (Figure 4-11C). Additionally, both structures show that bacterial stalk L12CTD interacts with the same position of EF-G (Figure 4-11C). This result may support our previous and the present studies (15) that the P1CTD retains the EF-2 throughout its recruitment to the ribosome, the GTP hydrolysis, and the subsequent dissociation from the ribosome.

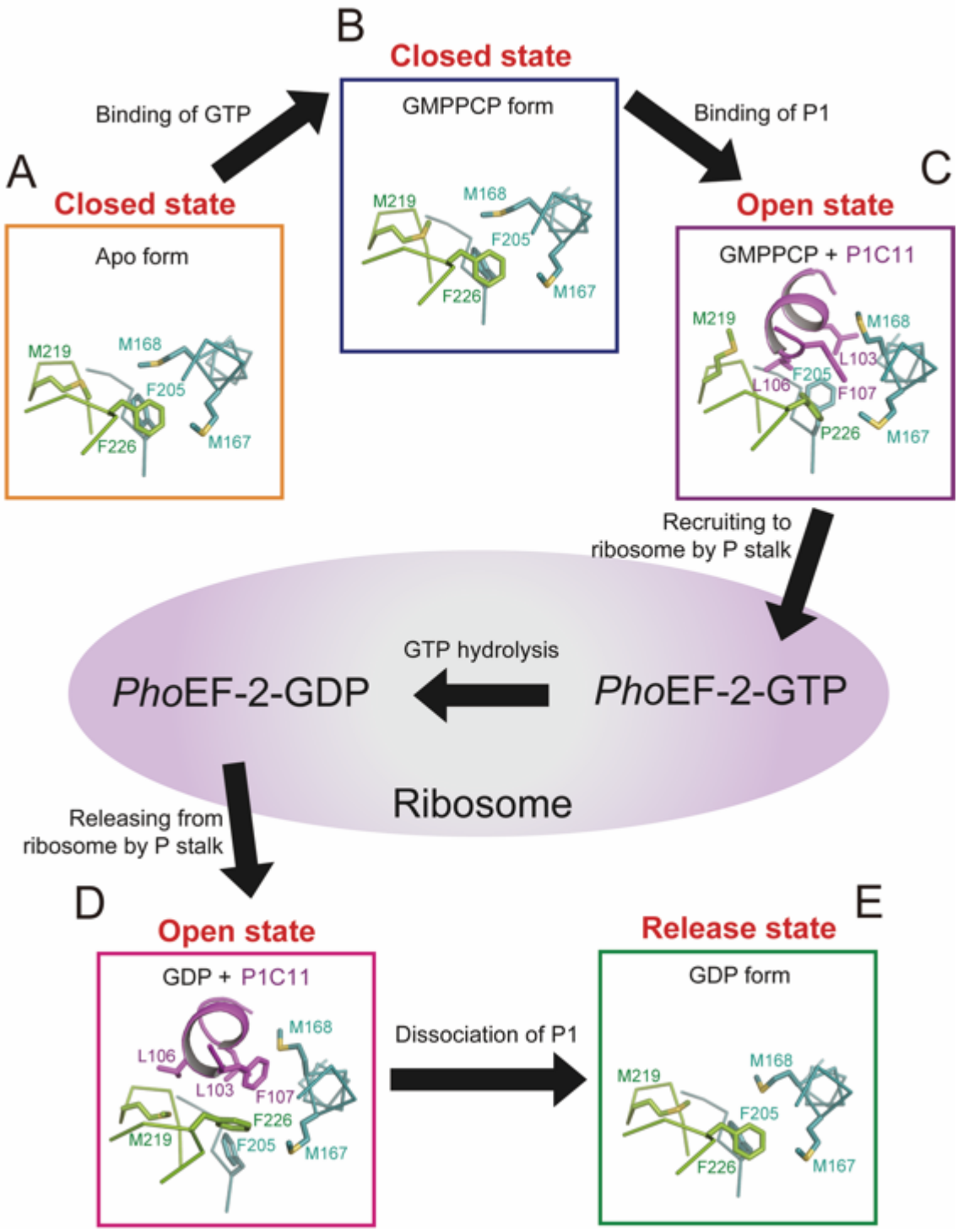
B
Closed state
GMPPCP form
M219
M168
F205
F226
M167
Binding of GTP
Binding of P1
A
Closed state
Apo form
M219
M168
F205
F226
M167
C
Open state
GMPPCP + P1C11
M219
M168
L103
F205
L106
F107
P226
M167
Recruiting to
ribosome by P stalk
GTP hydrolysis
PhoEF-2-GDP
PhoEF-2-GTP
Ribosome
Releasing from
ribosome by P stalk
D
Open state
GDP + P1C11
L106
M168
L103
F107
F226
M219
F205
M167
Dissociation of P1
E
Release state
GDP form
M219
M168
F205
F226
M167

Figure 4-10. The responses of P1-binding groove of *Pho*EF-2 during recruitment and releasing process by P1 stalk. The domain G and subdomain G' of *Pho*EF-2, and P1C11 are shown in colors same as in Figure 3-9. P1C11, *Pho*EF-2 and side chains of residues are represented by ribbon, line and stick models, respectively. (**A**) The "closed" state of P1-binding groove in Apo form of *Pho*EF-2. (**B**) GMPPCP bound *Pho*EF-2 with "closed" state of P1-binding groove. (**C**) The "open" state of the P1-binding groove of GMPPCP bound *Pho*EF-2. When P1C11 binds to *Pho*EF-2-GMPPCP, the side chains of M168 and M219 rotate to an "open" state for receiving P1C11, following which *Pho*EF-2-GMPPCP is recruited to the ribosome. (**D**) The "open" state of the P1-binding groove in GDP-bound *Pho*EF-2. After GTP hydrolysis in the ribosome, the P1-binding groove maintains the "open" state with slight conformational changes. (**E**) The "release" state of the P1-binding groove. When *Pho*EF-2-GDP dissociates from the ribosome and P1 stalk, the groove changes its conformation to a "release" state. Once GDP has dissociated from *Pho*EF-2, the P1-binding groove of *Pho*EF-2-Apo returns to the "closed" state (**A**).

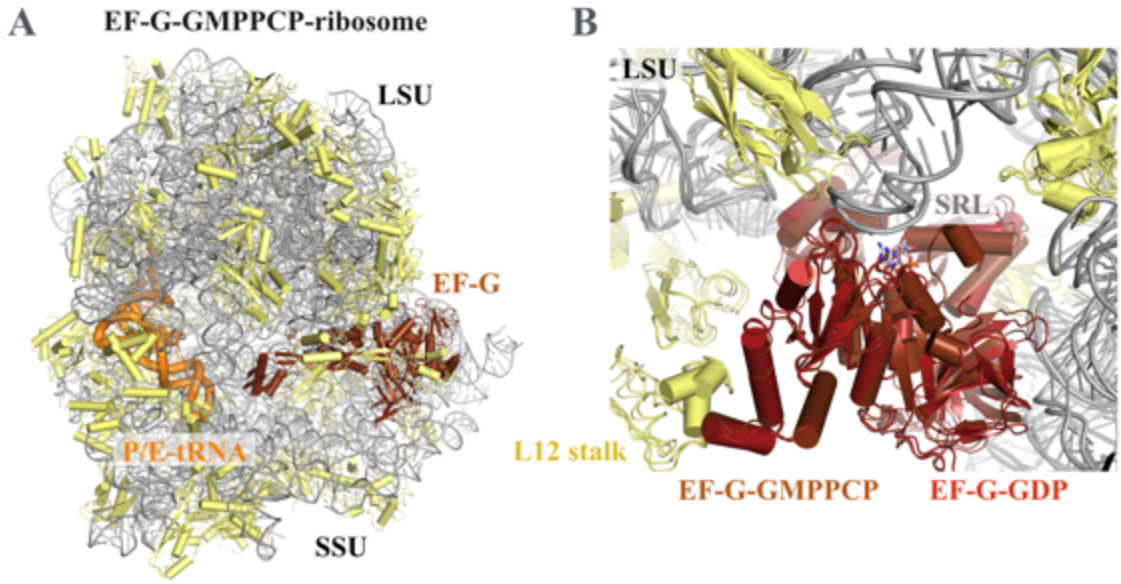

Figure 4-11. Structures of ribosome in complex with EF-G. The ribosomal RNA (rRNA) and proteins are the same as using Figure 4-6. The GMPPCP and GDP are represented by stick models and the C, N, O, and P atoms of GMPPCP are colored pale blue, blue, red, and orange. (**A**) Crystal structure of ribosome complexed with GMPPCP-bound EF-G (ribosome-EF-G-GMPPCP, PDBID: 4V9H) (20). EF-G and P/E-tRNA are represented by ribbon models and colored brown and orange, respectively. (**B**) Closed view of the structural superposition of domain G of EF-G between ribosome-EF-G-GMPPCP and ribosome-EF-G-GDP. Because both structures showed that L12 stalk could be visible, the label of the L12 stalk is indicated.

3-3. *Pho*EF-2 recruiting model with ribosome and P stalk

In the present study, we revealed how aEF-2 is recognized by P1CTD. For best understanding how the P stalk recruits/releases translation factors to/from the sarcin-ricin loop of the ribosome during protein synthesis, the structure of the ribosome with its stalk complex and elongation factor is indispensable. Based on the structures that EF-G or eEF-2 bound on the ribosome (19, 20, 30, 83), we built a model of GTPase recruitment on the ribosome with P0-$[P1]_2[P1]_2[P1]_2$ and *Pho*EF-2-GMPPCP-P1C11 complex to understand the positional relationships between aEF-2, P1CTD, and the ribosome once aEF-2 has been delivered to the ribosome by the P stalk (Figure 4-12). This model showed that the P1CTD binding region of aEF-2 protrudes from the ribosome, indicating that the way in which P1 binds to aEF-2 may facilitate the efficient recruitment without effect of the GTP hydrolysis and conformation changes of aEF-2 on the ribosome. Furthermore, as described above, this study implies that the P1 binding grooves of GTPases are different in position and sequence, but conserve a hydrophobic shape for binding helical P1CTD. Such feature implies that the P1 binding groove of each GTPases may relate to how or where they work on the ribosome because P stalk should hold them during the recruitment cycle; recruitment of GTPase to ribosome, and dissociation of GTPase from ribosome following execution of its function on the ribosome.

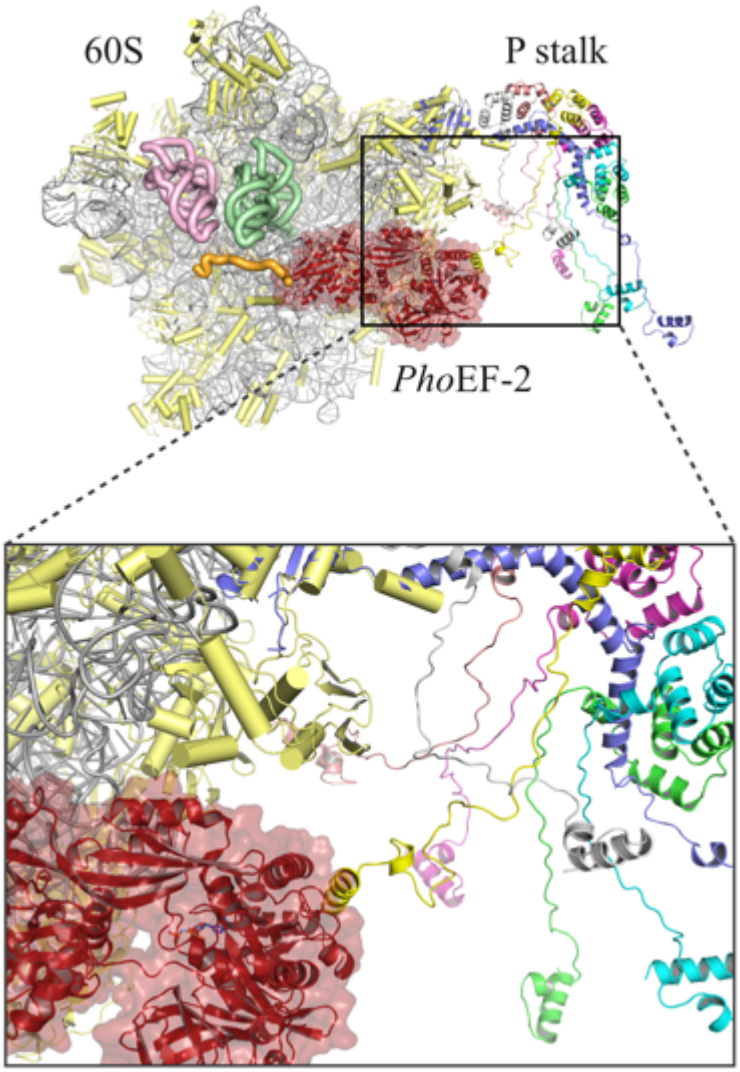

Figure 4-12. A model of aEF-2 recruitment by the ribosomal P stalk on the ribosome. The crystal structures of *Pho*EF-2-GMPPCP-P1C11 and P stalk P0-$[P1]_2[P1]_2[P1]_2$ (PDBID: 3A1Y) (14) are superposed on the large subunit of *Pyrococcus furiosus* ribosome (PDBID: 3J2L, 3J20 and 3J21) (top). The rRNA (gray), ribosomal proteins (yellow), and P stalk are represented in the ribbon model. EF-2 (red) is represented in both the ribbon and surface model. The tRNAs at the E/P site (pink) or P/A site (green), and mRNA (orange) are represented in the ribbon model. A close-up view is shown at the bottom.

CONCLUSION & FUTURE PERSPECTIVE

Our structures of *Pho*EF-2-Apo, *Pho*EF-2-D2-GDP, *Pho*EF-2-GMPPCP, and *Pho*EF-2-GMPPCP-P1C11, and the MD simulated model of *Pho*EF-2-GDP-P1C11 demonstrated the *Pho*EF-2 recognition mechanism of the CTD of P stalk, and the conformational changes of the P1C11-binding groove in each form, providing that in response to the translation cycle, the groove has four states: closed, open (GTP), open (GDP), and release during recruitment and dissociation. However, considering the diverseness of recruitment partners, it is difficult to predict the P1CTD binding grooves of aIF5B and eEF-2 based on a structural comparison with *Pho*EF-2-GMPPCP-P1C11. Therefore, a structural analysis of other P stalk-bound GTPases in the future is indispensable for fully understanding the diverse interactions between GTPases and P stalk. Furthermore, some GTPases that appeared by evolution do not interact with P1, suggesting the reason why the P1CTD cannot recognize them does not only have the advantages of their functions, but also slightly differences of the shape of P1CTD binding groove.

ACCESSION NUMBER

Atomic coordinates and structure factors have been deposited to RCSB Protein Data Bank with the accession numbers 5H7J for the *Pho*EF-2-GMPPCP/*Pho*EF-2-Apo, 5H7K for the *Pho*EF-2-D2-GDP and 5H7L for *Pho*EF-2-GMPPCP-P1C11 complex.

FUNDING

This work was supported by Grant-in-Aid for Scientific Research in a Priority Area (No. 26650013 to MY) and Scientific Research (B) (No. 17H05656 to MY; No. 24370073 to TU) from the Ministry of Education, Culture, Sports, Science and Technology of Japan.

REFERENCES

1. Puglisi,J.D., Blanchard,S.C. and Green,R. (2000) Approaching translation at atomic resolution. *Nat. Struct. Biol.*, **7**, 855–861.

2. Whitford,D. (2013) Proteins John Wiley & Sons.

3. Ramakrishnan,V. and Moore,P.B. (2001) Atomic structures at last: the ribosome in 2000. *Curr. Opin. Struct. Biol.*, **11**, 144–154.

4. Wilson,D.N. and Nierhaus,K.H. (2005) Ribosomal Proteins in the Spotlight. *Critical Reviews in Biochemistry and Molecular Biology*, **40**, 243–267.

5. Ban,N., Nissen,P., Hansen,J., Moore,P.B. and Steitz,T.A. (2000) The complete atomic structure of the large ribosomal subunit at 2.4 A resolution. *Science*, **289**, 905–920.

6. Wimberly,B.T., Brodersen,D.E., Clemons,W.M., Morgan-Warren,R.J., Carter,A.P., Vonrhein,C., Hartsch,T. and Ramakrishnan,V. (2000) Structure of the 30S ribosomal subunit. *Nature*, **407**, 327–339.

7. Ben-Shem,A., Garreau de Loubresse,N., Melnikov,S., Jenner,L., Yusupova,G. and Yusupov,M. (2011) The structure of the eukaryotic ribosome at 3.0 Å resolution. *Science*, **334**, 1524–1529.

8. Armache,J.-P., Anger,A.M., Márquez,V., Franckenberg,S., Fröhlich,T., Villa,E., Berninghausen,O., Thomm,M., Arnold,G.J., Beckmann,R., *et al.* (2013) Promiscuous behaviour of archaeal ribosomal proteins: implications for eukaryotic ribosome evolution. *Nucleic Acids Research*, **41**, 1284–1293.

9. Anger,A.M., Armache,J.-P., Berninghausen,O., Habeck,M., Subklewe,M., Wilson,D.N. and Beckmann,R. (2013) Structures of the human and Drosophila 80S ribosome. *Nature*, **497**, 80–85.

10. Voorhees,R.M., Weixlbaumer,A., Loakes,D., Kelley,A.C. and Ramakrishnan,V. (2009) Insights into substrate stabilization from snapshots of the peptidyl transferase

center of the intact 70S ribosome. *Nature Structural & Molecular Biology*, **16**, 528–533.

11. Schmeing,T.M., Voorhees,R.M., Kelley,A.C., Gao,Y.-G., Murphy,F.V., Weir,J.R. and Ramakrishnan,V. (2009) The crystal structure of the ribosome bound to EF-Tu and aminoacyl-tRNA. *Science*, **326**, 688–694.

12. Helgstrand,M., Mandava,C.S., Mulder,F.A.A., Liljas,A., Sanyal,S. and Akke,M. (2007) The Ribosomal Stalk Binds to Translation Factors IF2, EF-Tu, EF-G and RF3 via a Conserved Region of the L12 C-terminal Domain. *Journal of Molecular Biology*, **365**, 468–479.

13. Diaconu,M., Kothe,U., Schlünzen,F., Fischer,N., Harms,J.M., Tonevitsky,A.G., Stark,H., Rodnina,M.V. and Wahl,M.C. (2005) Structural basis for the function of the ribosomal L7/12 stalk in factor binding and GTPase activation. *Cell*, **121**, 991–1004.

14. Naganuma,T., Nomura,N., Yao,M., Mochizuki,M., Uchiumi,T. and Tanaka,I. (2010) Structural basis for translation factor recruitment to the eukaryotic/archaeal ribosomes. *J. Biol. Chem.*, **285**, 4747–4756.

15. Nomura,N., Honda,T., Baba,K., Naganuma,T., Tanzawa,T., Arisaka,F., Noda,M., Uchiyama,S., Tanaka,I., Yao,M., *et al.* (2012) Archaeal ribosomal stalk protein interacts with translation factors in a nucleotide-independent manner via its conserved C terminus. *Proc. Natl. Acad. Sci. U.S.A.*, **109**, 3748–3753.

16. Bocharov,E.V., Sobol,A.G., Pavlov,K.V., Korzhnev,D.M., Jaravine,V.A., Gudkov,A.T. and Arseniev,A.S. (2004) From structure and dynamics of protein L7/L12 to molecular switching in ribosome. *Journal of Biological Chemistry*, **279**, 17697–17706.

17. Nechifor,R., Murataliev,M. and Wilson,K.S. (2007) Functional Interactions between the G' Subdomain of Bacterial Translation Factor EF-G and Ribosomal Protein L7/L12. *Journal of Biological Chemistry*, **282**, 36998–37005.

18. Nechifor,R. and Wilson,K.S. (2007) Crosslinking of Translation Factor EF-G to Proteins of the Bacterial Ribosome Before and After Translocation. *Journal of Molecular Biology*, **368**, 1412–1425.

19. Gao,Y.-G., Selmer,M., Dunham,C.M., Weixlbaumer,A., Kelley,A.C. and Ramakrishnan,V. (2009) The structure of the ribosome with elongation factor G trapped in the posttranslocational state. *Science*, **326**, 694–699.

20. Tourigny,D.S., Fernández,I.S., Kelley,A.C. and Ramakrishnan,V. (2013) Elongation factor G bound to the ribosome in an intermediate state of translocation. *Science*, **340**, 1235490–1235490.

21. Lee,K.M., Yu,C.W.H., Chiu,T.Y.H., Sze,K.H., Shaw,P.C. and Wong,K.B. (2012) Solution structure of the dimerization domain of the eukaryotic stalk P1/P2 complex reveals the structural organization of eukaryotic stalk complex. *Nucleic Acids Research*, **40**, 3172–3182.

22. Grela,P., Bernadó,P., Svergun,D., Kwiatowski,J., Abramczyk,D., Grankowski,N. and Tchórzewski,M. (2008) Structural relationships among the ribosomal stalk proteins from the three domains of life. *J. Mol. Evol.*, **67**, 154–167.

23. Kavran,J.M. and Steitz,T.A. (2007) Structure of the base of the L7/L12 stalk of the Haloarcula marismortui large ribosomal subunit: analysis of L11 movements. *Journal of Molecular Biology*, **371**, 1047–1059.

24. Emsley,P., Lohkamp,B., Scott,W.G. and Cowtan,K. (2010) Features and development of Coot. *Acta Crystallogr. D Biol. Crystallogr.*, **66**, 486–501.

25. Jin,H., Kelley,A.C. and Ramakrishnan,V. (2011) Crystal structure of the hybrid state of ribosome in complex with the guanosine triphosphatase release factor 3. *Proc. Natl. Acad. Sci. U.S.A.*, **108**, 15798–15803.

26. Zavialov,A.V., Buckingham,R.H. and Ehrenberg,M. (2001) A posttermination ribosomal complex is the guanine nucleotide exchange factor for peptide release factor RF3. *Cell*, **107**, 115–124.

27. Petry,S., Brodersen,D.E., Murphy,F.V., Dunham,C.M., Selmer,M., Tarry,M.J., Kelley,A.C. and Ramakrishnan,V. (2005) Crystal structures of the ribosome in complex with release factors RF1 and RF2 bound to a cognate stop codon. *Cell*, **123**, 1255–1266.

28. Rawat,U.B.S., Zavialov,A.V., Sengupta,J., Valle,M., Grassucci,R.A., Linde,J., Vestergaard,B., Ehrenberg,M. and Frank,J. (2003) A cryo-electron microscopic study of ribosome-bound termination factor RF2. *Nature*, **421**, 87–90.

29. Saito,K., Kobayashi,K., Wada,M., Kikuno,I., Takusagawa,A., Mochizuki,M., Uchiumi,T., Ishitani,R., Nureki,O. and Ito,K. (2010) Omnipotent role of archaeal elongation factor 1 alpha (EF1α in translational elongation and termination, and quality control of protein synthesis. *Proc. Natl. Acad. Sci. U.S.A.*, **107**, 19242–19247.

30. Chen,Y., Feng,S., Kumar,V., Ero,R. and Gao,Y.-G. (2013) Structure of EF-G-ribosome complex in a pretranslocation state. *Nature Structural & Molecular Biology*, **20**, 1077–1084.

31. Roll-Mecak,A., Cao,C., Dever,T.E. and Burley,S.K. (2000) X-Ray structures of the universal translation initiation factor IF2/eIF5B: conformational changes on GDP and GTP binding. *Cell*, **103**, 781–792.

32. Vitagliano,L., Masullo,M., Sica,F., Zagari,A. and Bocchini,V. (2001) The crystal structure of Sulfolobus solfataricus elongation factor 1alpha in complex with GDP reveals novel features in nucleotide binding and exchange. *The EMBO Journal*, **20**, 5305–5311.

33. Jørgensen,R., Ortiz,P.A., Carr-Schmid,A., Nissen,P., Kinzy,T.G. and Andersen,G.R. (2003) Two crystal structures demonstrate large conformational changes in the eukaryotic ribosomal translocase. *Nat. Struct. Biol.*, **10**, 379–385.

34. Kabsch,W. (2010) XDS. *Acta Crystallogr. D Biol. Crystallogr.*, **66**, 125–132.

35. Vagin,A. and Teplyakov,A. (2010) Molecular replacement with MOLREP. *Acta Crystallogr. D Biol. Crystallogr.*, **66**, 22–25.

36. Jørgensen,R., Wang,Y., Visschedyk,D. and Merrill,A.R. (2008) The nature and character of the transition state for the ADP-ribosyltransferase reaction. *EMBO Rep.*, **9**, 802–809.

37. Adams,P.D., Afonine,P.V., Bunkóczi,G., Chen,V.B., Davis,I.W., Echols,N., Headd,J.J., Hung,L.-W., Kapral,G.J., Grosse-Kunstleve,R.W., *et al.* (2010) PHENIX: a comprehensive Python-based system for macromolecular structure solution. *Acta Crystallogr. D Biol. Crystallogr.*, **66**, 213–221.

38. McCoy,A.J., Grosse-Kunstleve,R.W., Adams,P.D., Winn,M.D., Storoni,L.C. and Read,R.J. (2007) Phaser crystallographic software. *J Appl Crystallogr*, **40**, 658–674.

39. Baker,N.A., Sept,D., Joseph,S., Holst,M.J. and McCammon,J.A. (2001) Electrostatics of nanosystems: application to microtubules and the ribosome. *Proceedings of the National Academy of Sciences*, **98**, 10037–10041.

40. Thompson,J.D., Higgins,D.G. and Gibson,T.J. (1994) CLUSTAL W: improving the sensitivity of progressive multiple sequence alignment through sequence weighting, position-specific gap penalties and weight matrix choice. *Nucleic Acids Research*, **22**, 4673–4680.

41. Wieden,H.-J., Mercier,E., Gray,J., Steed,B. and Yawney,D. (2010) A combined molecular dynamics and rapid kinetics approach to identify conserved three-dimensional communication networks in elongation factor Tu. *Biophys. J.*, **99**, 3735–3743.

42. Mercier,E., Girodat,D. and Wieden,H.-J. (2015) A conserved P-loop anchor limits the structural dynamics that mediate nucleotide dissociation in EF-Tu. *Sci Rep*, **5**, 7677–9.

43. Kjeldgaard,M., Nissen,P., Thirup,S. and Nyborg,J. (1993) The crystal structure of elongation factor EF-Tu from Thermus aquaticus in the GTP conformation. *Structure*, **1**, 35–50.

44. Humphrey,W., Dalke,A. and Schulten,K. (1996) VMD: visual molecular dynamics. *J Mol Graph*, **14**, 33–8– 27–8.

45. Biasini,M., Bienert,S., Waterhouse,A., Arnold,K., Studer,G., Schmidt,T., Kiefer,F., Gallo Cassarino,T., Bertoni,M., Bordoli,L., *et al.* (2014) SWISS-MODEL: modelling protein tertiary and quaternary structure using evolutionary information. *Nucleic Acids Research*, **42**, W252–8.

46. Phillips,J.C., Braun,R., Wang,W., Gumbart,J., Tajkhorshid,E., Villa,E., Chipot,C., Skeel,R.D., Kalé,L. and Schulten,K. (2005) Scalable molecular dynamics with NAMD. *J Comput Chem*, **26**, 1781–1802.

47. Foloppe,N. and MacKerell,A.D.,Jr (2000) All-atom empirical force field for nucleic acids: I. Parameter optimization based on small molecule and condensed phase macromolecular target data. *J Comput Chem*, **21**, 86–104.

48. Glykos,N.M. (2006) Software news and updates. Carma: a molecular dynamics analysis program. *J Comput Chem*, **27**, 1765–1768.

49. Yu,J., Zhou,Y., Tanaka,I. and Yao,M. (2010) Roll: a new algorithm for the detection of protein pockets and cavities with a rolling probe sphere. *Bioinformatics*, **26**, 46–52.

50. Chen,Y., Koripella,R.K., Sanyal,S. and Selmer,M. (2010) Staphylococcus aureus elongation factor G--structure and analysis of a target for fusidic acid. *FEBS J.*, **277**, 3789–3803.

51. Li,W., Trabuco,L.G., Schulten,K. and Frank,J. (2011) Molecular dynamics of EF-G during translocation. *Proteins*, **79**, 1478–1486.

52. Dever,T.E., Glynias,M.J. and Merrick,W.C. (1987) GTP-binding domain: three consensus sequence elements with distinct spacing. *Proceedings of the National Academy of Sciences*, **84**, 1814–1818.

53. Kjeldgaard,M., Nyborg,J. and Clark,B.F. (1996) The GTP binding motif: variations on a theme. *FASEB J.*, **10**, 1347–1368.

54. Bartish,G. and Nygård,O. (2008) Importance of individual amino acids in the Switch I region in eEF2 studied by functional complementation in S. cerevisiae. *Biochimie*, **90**, 736–748.

55. al-Karadaghi,S., AEvarsson,A., Garber,M., Zheltonosova,J. and Liljas,A. (1996) The structure of elongation factor G in complex with GDP: conformational flexibility and nucleotide exchange. *Structure*, **4**, 555–565.

56. Mohr,D., Wintermeyer,W. and Rodnina,M.V. (2000) Arginines 29 and 59 of elongation factor G are important for GTP hydrolysis or translocation on the ribosome. *The EMBO Journal*, **19**, 3458–3464.

57. Ito,K., Honda,T., Suzuki,T., Miyoshi,T., Murakami,R., Yao,M. and Uchiumi,T. (2014) Molecular insights into the interaction of the ribosomal stalk protein with elongation factor 1α. *Nucleic Acids Research*, **42**, 14042–14052.

58. Bourne,H.R., Sanders,D.A. and McCormick,F. (1991) The GTPase superfamily: conserved structure and molecular mechanism. *Nature*, **349**, 117–127.

59. Zeidler,W., Schirmer,N.K., Egle,C., Ribeiro,S., Kreutzer,R. and Sprinzl,M. (1996) Limited proteolysis and amino acid replacements in the effector region of Thermus thermophilus elongation factor Tu. *Eur. J. Biochem.*, **239**, 265–271.

60. Dreher,T.W., Uhlenbeck,O.C. and Browning,K.S. (1999) Quantitative assessment of EF-1alpha.GTP binding to aminoacyl-tRNAs, aminoacyl-viral RNA, and tRNA shows close correspondence to the RNA binding properties of EF-Tu. *Journal of Biological Chemistry*, **274**, 666–672.

61. Nilsson,L. and Nygård,O. (1988) Structural and functional studies of the interaction of the eukaryotic elongation factor EF-2 with GTP and ribosomes. *Eur. J. Biochem.*, **171**, 293–299.

62. Skar,D.C., Rohrbach,M.S. and Bodley,J.W. (1975) Limited trypsinolysis of native Escherichia coli elongation factor G. *Biochemistry*, **14**, 3922–3926.

63. Wittinghofer,A., Frank,R. and Leberman,R. (1980) Composition and properties of trypsin-cleaved elongation factor Tu. *Eur. J. Biochem.*, **108**, 423–431.

64. Möller,W., Schipper,A. and Amons,R. (1987) A conserved amino acid sequence around Arg-68 of Artemia elongation factor 1 alpha is involved in the binding of guanine nucleotides and aminoacyl transfer RNAs. *Biochimie*, **69**, 983–989.

65. Nilsson,L. and Nygård,O. (1991) Altered sensitivity of eukaryotic elongation factor 2 for trypsin after phosphorylation and ribosomal binding. *Journal of Biological Chemistry*, **266**, 10578–10582.

66. Murakami,R., Miyoshi,T., Uchiumi,T. and Ito,K. (2016) Crystal structure of translation initiation factor 5B from the crenarchaeon Aeropyrum pernix. *Proteins*, **84**, 712–717.

67. Nomura,T., Nakano,K., Maki,Y., Naganuma,T., Nakashima,T., Tanaka,I., Kimura,M., Hachimori,A. and Uchiumi,T. (2006) In vitro reconstitution of the GTPase-associated centre of the archaebacterial ribosome: the functional features observed in a hybrid form with Escherichia coli 50S subunits. *Biochem. J.*, **396**, 565–571.

68. Fan,X., Zhu,Y., Wang,C., Niu,L., Teng,M. and Li,X. (2016) Structural insights into the interaction of the ribosomal P stalk protein P2 with a type II ribosome-inactivating protein ricin. *Sci Rep*, **6**, 37803.

69. Nissen,P., Thirup,S., Kjeldgaard,M. and Nyborg,J. (1999) The crystal structure of Cys-tRNACys-EF-Tu-GDPNP reveals general and specific features in the ternary complex and in tRNA. *Structure*, **7**, 143–156.

70. Yamamoto,H., Unbehaun,A., Loerke,J., Behrmann,E., Collier,M., rger,J.O.R.B.U., Mielke,T. and Spahn,C.M.T. (2014) Structure of the mammalian 80S initiation complex with initiation factor 5B on HCV-IRES RNA. *Nature Structural & Molecular Biology*, **21**, 1–9.

71. Fernández,I.S., Bai,X.-C., Hussain,T., Kelley,A.C., Lorsch,J.R., Ramakrishnan,V. and Scheres,S.H.W. (2013) Molecular architecture of a eukaryotic translational initiation complex. *Science*, **342**, 1240585–1240585.

72. Zheng,A., Yu,J., Yamamoto,R., Ose,T., Tanaka,I. and Yao,M. (2014) X-ray structures of eIF5B and the eIF5B-eIF1A complex: the conformational flexibility of eIF5B is restricted on the ribosome by interaction with eIF1A. *Acta Cryst (2014). D70, 3090-3098 [doi:10.1107/S1399004714021476]*, **70**, 1–9.

73. Sokabe,M., Yao,M., Sakai,N., Toya,S. and Tanaka,I. (2006) Structure of archaeal translational initiation factor 2 betagamma-GDP reveals significant conformational change of the beta-subunit and switch 1 region. *Proceedings of the National Academy of Sciences*, **103**, 13016–13021.

74. Kobayashi,K., Kikuno,I., Kuroha,K., Saito,K., Ito,K., Ishitani,R., Inada,T. and Nureki,O. (2010) Structural basis for mRNA surveillance by archaeal Pelota and GTP-bound EF1α complex. *Proc. Natl. Acad. Sci. U.S.A.*, **107**, 17575–17579.

75. Kobayashi,K., Saito,K., Ishitani,R., Ito,K. and Nureki,O. (2012) Structural basis for translation termination by archaeal RF1 and GTP-bound EF1α complex. *Nucleic Acids Research*, **40**, 9319–9328.

76. Preis,A., Heuer,A., Barrio-Garcia,C., Hauser,A., Eyler,D.E., Berninghausen,O., Green,R., Becker,T. and Beckmann,R. (2014) Cryoelectron microscopic structures of eukaryotic translation termination complexes containing eRF1-eRF3 or eRF1-ABCE1. *Cell Rep*, **8**, 59–65.

77. Ivanov,A., Mikhailova,T., Eliseev,B., Yeramala,L., Sokolova,E., Susorov,D., Shuvalov,A., Schaffitzel,C. and Alkalaeva,E. (2016) PABP enhances release factor

recruitment and stop codon recognition during translation termination. *Nucleic Acids Research*, **44**, 7766–7776.

78. Roque,S., Cerciat,M., Gaugué,I., Mora,L., Floch,A.G., de Zamaroczy,M., Heurgué-Hamard,V. and Kervestin,S. (2015) Interaction between the poly(A)-binding protein Pab1 and the eukaryotic release factor eRF3 regulates translation termination but not mRNA decay in Saccharomyces cerevisiae. *RNA*, **21**, 124–134.

79. Jerbi,S., Jolles,B., Bouceba,T. and Jean-Jean,O. (2016) Studies on human eRF3-PABP interaction reveal the influence of eRF3a N-terminal glycin repeat on eRF3-PABP binding affinity and the lower affinity of eRF3a 12-GGC allele involved in cancer susceptibility. *RNA Biology*, **13**, 306–315.

80. Gupta,N., DeMong,L.W., Banda,S. and Copeland,P.R. (2013) Reconstitution of selenocysteine incorporation reveals intrinsic regulation by SECIS elements. *Journal of Molecular Biology*, **425**, 2415–2422.

81. Kossinova,O., Malygin,A., Krol,A. and Karpova,G. (2014) The SBP2 protein central to selenoprotein synthesis contacts the human ribosome at expansion segment 7L of the 28S rRNA. *RNA*, **20**, 1046–1056.

82. Dobosz-Bartoszek,M., Pinkerton,M.H., Otwinowski,Z., Chakravarthy,S., Söll,D., Copeland,P.R. and Simonović,M. (2016) Crystal structures of the human elongation factor eEFSec suggest a non-canonical mechanism for selenocysteine incorporation. *Nature Communications*, **7**, 12941.

83. Imai,H., Miyoshi,T., Murakami,R., Ito,K., Ishino,Y. and Uchiumi,T. (2015) Functional role of the C-terminal tail of the archaeal ribosomal stalk in recruitment of two elongation factors to the sarcin/ricin loop of 23S rRNA. *Genes Cells*, **20**, 613–624.